Phase transitions in two-dimensional and geophysical turbulence

Marianne Corvellec

École Normale Supérieure de Lyon – Université de Lyon

Laboratoire de Physique

École Doctorale 52 (PHAST)

Doctorat

Physique

Marianne Corvellec

Transitions de phase en turbulence bidimensionnelle et géophysique

---

Thèse dirigée par M. Freddy Bouchet

Présentée et soutenue publiquement le 10 janvier 2012

Après les avis de : M. Julien Barré
M. Hugo Touchette

Devant la commission d'examen formée de :

M. Julien Barré	Rapporteur
M. Freddy Bouchet	Directeur
M. Alessandro Campa	Membre
Mme Bérengère Dubrulle	Membre
M. Peter Holdsworth	Président
M. Hugo Touchette	Rapporteur

Numéro national de thèse : 2012ENSL0705

Résumé

Prédire la statistique des grandes échelles des écoulements turbulents constitue un enjeu important. Pour les équations d'Euler 2D et des modèles analogues d'écoulements géophysiques, une auto-organisation est observée (formation de cyclones/anticyclones, jets intenses). La mécanique statistique d'équilibre des écoulements bidimensionnels s'est avérée fondamentale et pertinente même en présence de forçage et dissipation, dans la limite inertielle. La thèse est motivée par le phénomène de transitions aléatoires entre deux topologies différentes, lié à une bistabilité. Il s'agit de prédire la multiplicité des équilibres d'un écoulement (quasi) bidimensionnel. On développe une classification des transitions de phase, pour des équilibres (statistiques et/ou dynamiques) d'un tel écoulement. Les diagrammes de phase font apparaître la présence générique de points critiques et tricritiques, et des domaines d'inéquivalence d'ensembles statistiques. Dans le cas d'une géométrie annulaire, on décrit les effets de la topographie et de la conservation de deux circulations. Des analogies avec la bistabilité du courant océanique Kuroshio sont proposées à partir de cette étude académique. Enfin, pour le système Euler 2D, on détaille un résultat de mécanique statistique dans l'ensemble énergie–enstrophie : la distribution microcanonique, construite à partir du théorème de Liouville en dimension finie, correspond à la maximisation d'une entropie de mélange de la vorticité.

Mots-clés

Transitions de phase, mécanique statistique, turbulence, auto-organisation, théorie des bifurcations, bistabilité, équations aux dérivées partielles non linéaires, océanographie physique

Title

Phase transitions in two-dimensional and geophysical turbulence

Abstract

A most challenging problem in turbulence is to predict the statistics of flows at the large scales. In the case of the 2D Euler equations and analogous models for geophysical flows, the flow is observed to self-organize: cyclones/anticyclones and intense jets form. Equilibrium statistical mechanics has proven to be fundamental and relevant even in the presence of forcing and dissipation, in the inertial limit. The thesis is motivated by the phenomenon of random transitions between two different topologies. This phenomenon implies bistability. The goal is to predict the multiplicity of equilibria for a (quasi) two-dimensional flow. We develop a classification of phase transitions for the (statistical and/or dynamical) equilibria of this flow. Phase diagrams show critical and tricritical points as well as domains of statistical ensemble inequivalence, all this generically. In the case of an annular geometry, the effects of topography and of conserving two circulations are described. Analogies between the bistability of the ocean current Kuroshio and this academic study are suggested. Lastly, for the 2D Euler system, a statistical-mechanical result in the energy–enstrophy ensemble is detailed: the microcanonical distribution, constructed from Liouville's theorem in finite dimension, corresponds to the maximization of a vorticity-mixing entropy.

Keywords

Phase transitions, statistical mechanics, turbulence, self-organization, bifurcation theory, bistability, nonlinear partial differential equations, physical oceanography

Coordonnées des laboratoires

La thèse a été préparée dans deux laboratoires consécutivement. D'octobre 2008 à août 2010, la thèse a été préparée à l'**Institut Non Linéaire de Nice**, qui était alors l'UMR 6618 CNRS/Université de Nice Sophia Antipolis. De septembre 2010 à janvier 2012, la thèse a été préparée au **Laboratoire de Physique**, UMR 5672 CNRS/ENS de Lyon/Université de Lyon.

Institut Non Linéaire de Nice (INLN)
1361 route des Lucioles
Sophia Antipolis
06560 Valbonne
France

Laboratoire de Physique
Ecole Normale Supérieure de Lyon
46 allée d'Italie
69007 Lyon
France

Mobilité internationale

Pendant la deuxième année de thèse, cinq mois au total ont été passés au **Center for Nonlinear Studies** (CNLS), Los Alamos National Laboratory (LANL), à Los Alamos, NM (Etats-Unis). Ces séjours de recherche à l'étranger ont bénéficié de la subvention "06 RECHERCHE" du Conseil Général des Alpes-Maritimes.

Résumé substantiel

Que ce soit dans la nature ou en laboratoire, différents écoulements turbulents montrent un comportement bistable (ou, plus généralement, multistable). Par exemple, dans les fluides magnétiques en rotation, le champ magnétique dû à l'effet dynamo subit des inversions aléatoires. On trouve de tels fluides magnétiques dans le noyau externe de la Terre (pour la nature) ainsi que dans l'expérience Von Kármán Sodium (pour le laboratoire) [Berhanu et al., 2007, et les références incluses]. Des inversions aléatoires du champ de vitesse sont observées en convection Rayleigh–Bénard (système convectif idéalisé) turbulente, à la fois dans des expériences et dans des simulations numériques [Niemela et al., 2001, Chandra and Verma, 2011, et les références incluses]. Un écoulement bidimensionnel turbulent peut être créé en laboratoire en parcourant électriquement une fine couche horizontale de mercure liquide [Sommeria, 1986]. L'écoulement acquiert une rotation globale moyenne spontanée, et la direction de rotation subit des inversions aléatoires. Une revue récente des inversions de champ dans les écoulements turbulents est donnée par [Gallet et al., 2011].

Des régimes multiples sont décrits pour d'autres écoulements turbulents. Pour l'eau dans un montage Von Kármán, l'écoulement passe d'un état symétrique à deux cellules, globalement sans rotation, à un état asymétrique à une cellule, avec rotation [Ravelet et al., 2004, Ravelet et al., 2008, IV. D]. Une expérience de plaque tournante (écoulement quasi bidimensionnel) montre des transitions entre deux configurations très différentes, l'une étant comme un courant-jet ou "zonale", l'autre étant de trajectoire ondulée ou "bloquée" [Tian et al., 2001]. Cela rappelle le phénomène de "blocage atmosphérique", une oscillation qui se produit dans l'hémisphère nord de la Terre [Kimoto and Ghil, 1993].

Nous venons de mentionner des exemples où les deux régimes dans lesquels le système se trouve alternativement, sont soit qualitativement différents (différentes topologies, différentes symétries), soit d'égale amplitude mais de signes opposés. Soulignons que les régimes identifiés sont persistants : ils durent beaucoup plus longtemps que les temps de transition typiques. Les régimes sont déterminés par les grandes échelles de l'écoulement turbulent en question. On peut voir cela dans l'espace de Fourier comme "seuls les premiers modes entrent en jeu dans la description des régimes". Une interprétation tentante est la suivante : considérons que le comportement bistable est gouverné par un système dynamique de faible dimension, tandis que les transitions sont

dues aux fluctuations turbulentes. Cela dit, il n'y a pas de preuve théorique à l'appui de cette idée.

Dans le deuxième chapitre, nous présentons des calculs analytiques et numériques de diagrammes de phase, pour une grande classe d'états d'équilibre d'écoulements bidimensionnels et géophysiques. Trouver et caractériser les transitions est crucial, puisqu'elles contiennent éventuellement les changements qualitatifs (en termes de structures d'écoulement, en ce qui nous concerne). Dans le contexte de la mécanique statistique d'équilibre, il s'agit de *transitions de phase*. Dans le contexte des systèmes dynamiques, il s'agit de *bifurcations*. Il est important de savoir si les transitions sont continues ou discontinues. Nous utilisons des outils techniques de la théorie (appliquée) des bifurcations, à savoir la réduction de Lyapunov–Schmidt, pour caractériser les transitions de phase (du premier ou du second ordre). Ainsi, nous déterminons le caractère continu ou discontinu des transitions, ce dans un cadre général. La bistabilité est spontanément associée aux transitions discontinues. Le deuxième chapitre de la thèse est organisé comme suit :

- Dans la section 2.1, nous présentons le *problème variationnel énergie–circulation microcanonique*. Il s'agit de minimiser une certaine fonctionnelle de Casimir, à énergie et circulation fixées.

- Dans la section 2.3, nous résolvons le problème variationnel dual, non contraint (*problème variationnel énergie–circulation grand canonique*) dans un cas symétrique. Cette symétrie donne une solution qui n'est pas intéressante qualitativement, mais c'est une étape utile à établir dans un cadre plus général, qui contient des situations plus intéressantes.

- Dans la section 2.4, nous résolvons le *problème variationnel énergie–circulation canonique*. Nous mettons en évidence des transitions de phase intéressantes, où la structure de l'écoulement change complètement. Pour des domaines rectangulaires allongés (rapport d'aspect $\tau > \tau_c$), nous retrouvons la transition avec apparition de la structure dipolaire, tandis que pour des domaines proches du carré ($\tau < \tau_c$), nous retrouvons celle du monopole central avec des cellules contrarotatives aux coins [Chavanis and Sommeria, 1996, Venaille and Bouchet, 2009]. La nouveauté ici réside dans le fait de distinguer des transitions continues et des transitions discontinues, selon le signe du quatrième moment de la vorticité. Dans le cas proche du carré, on peut obtenir un diagramme de phase avec trois états (phases) qualitativement différents (stables ou métastables). Nous prétendons que l'ensemble canonique est à considérer pour les applications géophysiques, tel le problème du Kuroshio, puisque les deux régimes de ce courant océanique ont des énergies différentes.

Il apparaît qu'en général, l'ensemble canonique n'est pas équivalent à l'ensemble microcanonique, ce avec un certain intervalle de capacité thermique spécifique négative. Le même résultat est obtenu entre l'ensemble grand canonique et l'ensemble grand microcanonique. Nous retrouvons plusieurs prédictions issues de la classification systématique [Bouchet and Barré, 2005], contribuant ainsi au domaine des systèmes à interactions à longue portée. Ce travail fait l'objet d'un article de revue [Corvellec and Bouchet, 2011a] ainsi que d'une courte publication dans les actes d'une conférence [Corvellec and Bouchet, 2011b].

Dans le troisième chapitre, nous étendons les résultats au cas d'un domaine 2-connexe. Par exemple, le domaine considéré est un canal périodique, ou bien un anneau. Ces topologies sont pertinentes dans le cadre des problèmes d'océanographie, quand le domaine considéré est soit une bande de latitude, soit un bassin (océanique) avec une île. C'est aussi la géométrie des expériences de plaque tournante. Nous considérons une relation linéaire entre vorticité potentielle et fonction courant. Les résultats de [Venaille and Bouchet, 2009] sont génériques, mais la connexité double amène une nouvelle quantité conservée, car la circulation est conservée le long de chaque composante connexe du bord. Ainsi, les diagrammes de phase peuvent être parcourus dans une dimension supplémentaire. Dans une certaine gamme de paramètres, on a deux équilibres qualitativement différents, de part et d'autre d'une ligne de transition de phase du premier ordre. L'un des équilibres est très influencé par la topographie : les lignes de courant suivent approximativement les isolignes de topographie. L'autre structure d'écoulement a une contribution azimuthale/zonale beaucoup plus forte. Nous rappelons qu'une analogie géophysique peut être proposée à partir de ces deux états : il y a le "blocage atmosphérique" et aussi les "méandres" du Kuroshio (voir plus haut). Nous avons donc un résultat très intéressant en vue de la compréhension de la bistabilité, dans les écoulements géophysiques turbulents.

Dans le quatrième chapitre, nous détaillons un résultat issu de [Bouchet and Corvellec, 2010] sur les mesures de probabilité invariantes pour les équations d'Euler 2D. La détermination de mesures invariantes est motivée par le fait qu'elles vivent souvent sur des attracteurs. Quand seuls les invariants quadratiques d'Euler 2D (l'énergie et l'enstrophie) sont pris en compte, nous proposons un calcul explicite qui montre que la mesure microcanonique correspond à la maximisation d'une entropie de champ moyen. Les outils techniques utilisés font intervenir la continuation analytique dans l'évaluation d'une intégrale complexe.

Contents

Chapter 1

Introduction

Contents

1.1 Motivation: bistability

Whether in nature or in the laboratory, a variety of turbulent flows display a bistable (or, more generally speaking, multistable) behaviour. For example, magnetic fluids undergoing rotation show random reversals in the magnetic field due to dynamo effect. Such magnetic fluids are the Earth's outer core (in nature) and liquid sodium in a Von Kármán setup (in the laboratory). We are referring to the VKS (Von Kármán Sodium) experiment [Berhanu et al., 2007, and references therein]. Random reversals in the velocity field are observed in turbulent Rayleigh–Bénard convection (RBC), an idealized convective system, in both experiments and numerical simulations [Niemela et al., 2001, Chandra and Verma, 2011, and references therein]. Such a phenomenon is referred to as 'flow reversal'. A two-dimensional turbulent flow can be obtained by driving electrically a horizontal layer of liquid mercury [Sommeria, 1986]. This flow is seen to acquire a spontaneous mean global rotation, and the rotation direction undergoes random reversals. A recent review of field reversals in turbulent flows is given in [Gallet et al., 2011].

Multiple regimes are reported for other turbulent flows. For water in a Von Kármán setup, the flow is seen to transition from a two-cell symmetric globally non-rotating flow to a one-cell asymmetric globally rotating flow [Ravelet et al., 2004, Ravelet et al., 2008, IV. D]. This flow is three-dimensional axisymmetric. [Ahlers, 2006] reviews the experimental results in RBC for two-dimensional systems of large extent (thin horizontal fluid layer). Bifurcations from disordered states to organized structures (convective patterns: rolls, hexagons, squares) are investigated; this corresponds to the onset of convection. Bifurcations from hexagons to rolls are also reported. With a much larger vertical-to-horizontal aspect ratio for the volume of fluid (cell), two different flow structures are reported to be possible for certain values of the control parameters: either one roll, or two rolls in the height of the cell [Chillá et al., 2004, and references therein]. A transition between the two flows is observed experimentally. Tilting the cell (with respect to horizontal) may lead to the loss of stability of the two-roll flow. In a turbulent Taylor–Couette experiment, transitions between an axisymmetric flow and an azimuth-dependent flow are observed [Mujica and Lathrop, 2005]. The latter flows are three-dimensional. A rotating tank experiment (quasi two-dimensional flow) shows transitions between two different flow patterns, one being jet-like or 'zonal', the other being wavy or 'blocked' [Tian et al., 2001]. They are remindful of atmospheric blocking, an oscillation taking place notably in the Earth's Northern Hemisphere [Kimoto and Ghil, 1993].

We have mentioned examples where the two regimes, in which the system alternatively finds itself, are either qualitatively different (different topologies, different symmetries), or just equal and opposite of each other. We emphasize that the identified regimes (equivalently referred to as flow patterns, flow structures) are long-lived: they persist over time scales much larger than the typical transition time. We elaborate on the picture of bistability with transitions in the next section (section 1.2). The regimes are determined by the large scales of the turbulent flow in question —think of this in Fourier space as "only the lowest modes come into play in the description of the regimes". An appealing interpretation is the following: consider that the bistable behaviour is governed by a low-dimensional dynamical system, while the transitions are due to the turbulent fluctuations. Yet there is no theoretical proof for this idea. For now, let us describe in more detail a few selected bistable systems.

Magnetohydrodynamics. We mention the VKS experiment (Von Kármán Sodium), which generates a turbulent flow of liquid sodium in a cylinder, between two counter-rotating disks [Berhanu et al., 2007, and references therein]. A magnetic field is generated by dynamo effect. This system has two distinct

interesting features. On the one hand, it displays bistability between two qualitatively different states, i.e., a stationary dynamo and an oscillatory one. Both regimes can be obtained for a certain range of forcing [Berhanu et al., 2009] and spontaneous transitions from one to the other are not observed (stability with respect to the turbulent fluctuations). This bistability corresponds to a subcritical bifurcation (see subsection 1.2). On the other hand, magnetic field reversals, i.e., spontaneous transitions between a stationary field and its opposite are observed (figure 1.1). This is remindful of the geomagnetic field reversals, as revealed by paleomagnetic studies. Indeed, given a solution of the equations of magnetohydrodynamics, its opposite is also solution.

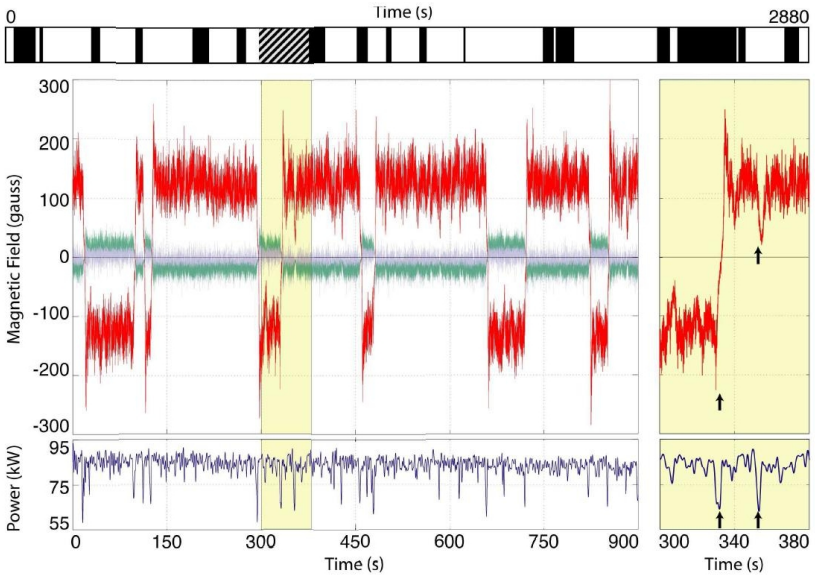

Figure 1.1: Time series for all three components of the magnetic field in the turbulent dynamo from [Berhanu et al., 2007]. The largest component is the azimuthal one. Transitions are irregular and sharp. Right: detail of the time series.

Hydrodynamics. We come back to other interesting results with turbulent flows in a Von Kármán setup, when the fluid is not magnetic (water or water-glycerol mixtures). The multistability of these experimental flows is investigated in [Ravelet et al., 2004, Cortet et al., 2010] and others. Depending on the forcing, the flow takes different symmetries: one regime is perfectly symmetric, with two recirculation cells separated by a shear layer; another one with two recirculation cells is asymmetric; the last regime is fully asymmetric, with only one cell. Whatever the bifurcation diagrams for these states, fluctuations may or may not cause transitions from one branch to the other.

Although turbulent flows are out-of-equilibrium systems, the coexistence of multiple states has to be a property of the equilibrium system as well; we discuss this in the next section. Hence, the relevance of an equilibrium statistical analysis cannot be discarded. Indeed, the coherent structures observed in stationary turbulent flows, namely, vortices in 2D and vorticity thin tubes in 3D, correspond to an alignment of vorticity along velocity (Beltrami flow) [Monchaux et al., 2006, and references therein]. These Beltrami flows are recovered by the equilibrium statistical theory of [Leprovost et al., 2006], for 3D axisymmetric turbulent flows, in an attempt to understand the regimes identified in, for instance, [Ravelet et al., 2004]. The steady states of the inviscid equations (axisymmetric Euler equations) are characterized by two functions (say, F and G), relating streamfunction, angular momentum, and azimuthal velocity. Interestingly enough, the steady states of the Von Kármán flow seem to be described as equilibrium states, although forcing and dissipation are responsible for selecting the specific functions F and G [Monchaux et al., 2006].

Fast-rotating tank experiments. Experiments with fluid in a rotating annulus, using a forcing mechanism, enable to produce a zonal (azimuthal) jet subject to the Coriolis force. Then, observations made on these experimental systems can shed light on atmospheric and oceanic phenomena. On interannual time scales, the Northern Hemisphere atmosphere experiences 'blocking': large anticyclones form, blocking and deflecting the nearly zonal flow (following latitude circles) [Weeks et al., 1997]. Analogous configurations are observed in the Pacific ocean, off Japan (see next paragraph, 'Kuroshio path'). In fast-rotating tanks equipped with ridges at the bottom (mimicking topography), flow patterns similar to 'zonal' and 'blocked' states are observed. In addition, transitions between the two states are found in a certain range of forcings (tank rotation and pumping rate) [Weeks et al., 1997, Tian et al., 2001]. In the blocked state, streamlines tend to follow topography contours.

Recently, our collaborators Mani Mathur and Joël Sommeria found (at least) two qualitatively different states in a similar experiment, where the control parameters are the rotation of the tank Ω_t and the rotation of a forcing ring Ω_r (measured in the tank's rotating frame). This ring lies at the surface of the fluid (water). One state shows a propagating wave, while the other shows a standing wave (figure 1.2). The colour scale gives the value of the azimuthal mean (radially averaged) velocity. A propagating state is recognized when lines of a given colour go across the entire azimuthal range: a certain structure travels azimuthally. A standing state is almost time-invariant, so points of a given colour remain at the same azimuth over time.

Spontaneous transitions between the two states are not observed, but when Ω_t is varied, while keeping Ω_r constant, hysteresis is reported: the transition

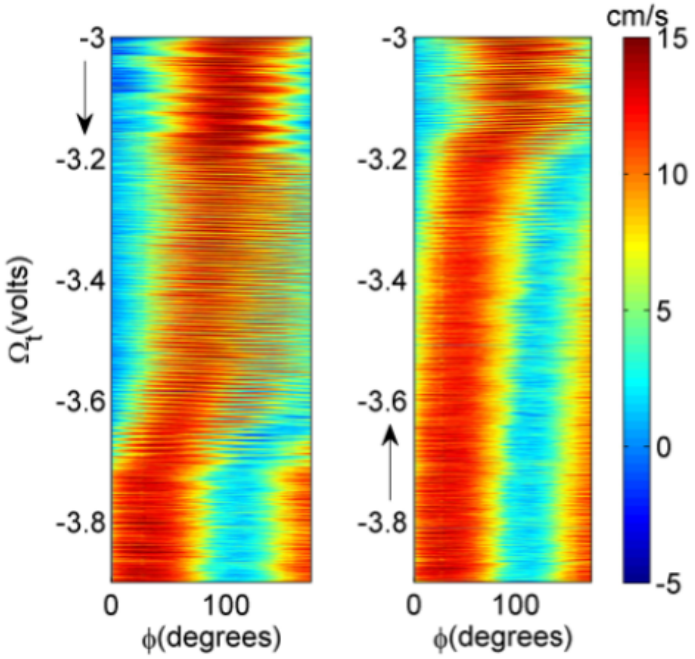

Figure 1.2: Hovmöller diagrams of the azimuthal velocity, with azimuth ϕ on the x axes and tank angular velocity Ω_t —which is varied linearly in time— on the y axes. Left: Ω_t is increased with time. Right: Ω_t is decreased with time. Calibration to physical units: 3 V $\leftrightarrow$ 0.4409 s^{-1}, 4 V $\leftrightarrow$ 0.5764 s^{-1}. $\Omega_t < 0$ means counter-clockwise rotation. The relative rotation of the forcing ring is kept constant: $\Omega_r = 0.79$ s^{-1}. There is a bistable range: -3.7 V $< \Omega_t < -3.2$ V. Figure by Mani Mathur (private communication, 2011).

from propagating to standing flow, when increasing Ω_t (in magnitude), occurs at $\Omega_t \approx -3.7$ V (equivalent units), but the transition from standing to propagating flow, when decreasing Ω_t, occurs at $\Omega_t \approx -3.2$ V (figure 1.2). The empirical relationship between voltage and frequency is such that 3.2 V corresponds to about 0.45 s^{-1} and 3.7 V to about 0.52 s^{-1}. The negative value of Ω_t indicates counter-clockwise rotation. Therefore, $\Omega_t \in [-3.7, -3.2]$ V is a range of bistability. Remark that there is a third state: when increasing Ω_t from -3 V to about -3.2 V, there is another kind of standing state. Hysteresis is reported also when Ω_r is varied, at fixed Ω_t.

Flows in fast-rotating tanks are quasi two-dimensional. Like large-scale flows in atmospheres and oceans, their dynamics can be modeled by the barotropic quasi-geostrophic equations (see section 1.3). In a numerical simulation of these with stochastic forcing, in a periodic channel, Eric Simonnet found transitions between a monopolar flow (state I) and a dipolar one (state II). Figure 1.3 visualizes many of these transitions occurring in time.

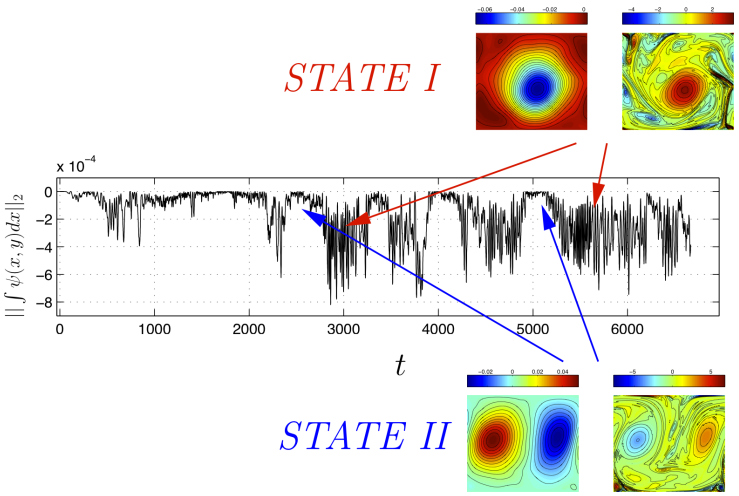

Figure 1.3: Time series for a relevant order parameter —zero for a perfect dipole, clearly nonzero for a monopole-like flow. The insets show the streamfunction field (right) and the vorticity field (left). Several transitions between the two states are seen to occur irregularly. Figure by Eric Simonnet (private communication, 2011).

Kuroshio path. The Kuroshio current is the western boundary current of the north Pacific ocean (figure 1.4). In this respect, it is analogous to the Gulf Stream in the north Atlantic ocean. The Kuroshio Extension forms an eastward mid-basin jet in the north Pacific ocean. The Kuroshio is seen to

oscillate between an intense jet-like (zonal) state and a weaker meandering (blocked) state.

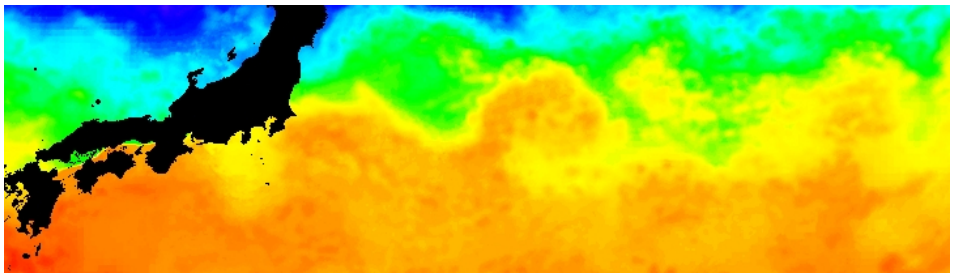

Figure 1.4: Sea surface temperature of the Pacific ocean east of Japan, on February 18, 2009; New Generation Sea Surface Temperature from infrared radiometers (AVHRR, MODIS), data from JAXA (Japan Aerospace Exploration Agency). The color gradient shows the path of the current. The yellow bulge south of Japan shows the large meander: the Kuroshio is then in its 'blocked' state. The Kuroshio Extension shows a meandering path as well, with eddies alongside.

Each state can be characterized quantitatively by the mean distance of the Kuroshio axis from the Japanese coast (Kuroshio path index): this quantity is low for the zonal state, high for the blocked state. The Kuroshio axis is given by a relevant isotherm (figure 1.4). Transitions from one to the other occur over a few months, while a given state persists for a few years and up to a decade [Schmeits and Dijkstra, 2001, and references therein]. To account for this multiplicity of equilibria, [Charney and Flierl, 1981] consider the stationary solutions of the barotropic quasi-geostrophic equations (see next section). The key ingredient is an irregular (non-zonal, sinusoidal) coastline, acting as an equivalent topography. In a bifurcation analysis, they find two stable branches, corresponding to low and high 'sinusoidalities', respectively, of the flow, in a region of the bifurcation diagram. The bifurcation (control) parameter is the mean velocity of the flow.

[Qiu and Miao, 2000] run an ocean general circulation model with realistic coastlines and bottom topography, driven by observed monthly wind stress: they find a time variability for the Kuroshio path close to the observed one (figure 1.5). Unlike the authors, who invoke a 'self-sustained internal oscillation', [Schmeits and Dijkstra, 2001] relate this result to the existence of multiple equilibria, for the steady states of the (forced and dissipated) dynamics.

Climate models. To investigate equilibrium climate states, idealized coupled (ocean–atmosphere–sea ice) models are used —notably, the MIT General

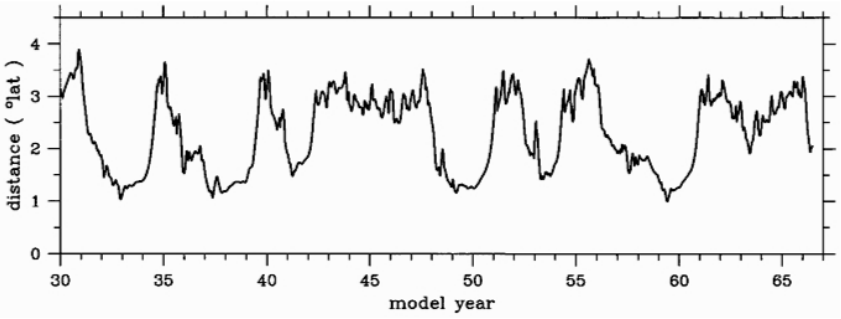

Figure 1.5: Timeseries of the Kuroshio path index, from a numerical simulation of a two-layer primitive-equation model, with climatological forcing, by [Qiu and Miao, 2000]. The two regimes are well identified over annual time scales.

Circulation Model[1]. A climate state is defined by the size of the ice cap covering an Earth-like planet, i.e., by the latitude of the ice edge. The coldest climate is a fully ice-covered state ('snowball'), while the warmest climate is a state with no ice. The forcing corresponds to the flux of solar energy. Less solar forcing, i.e., cooling, leads to more ice cover and, hence, more reflection of radiation, resulting in more cooling. The equivalent can be said for warming; that is the ice–albedo feedback. Extensions of EBMs (energy balance models) happen to support multiple stable equilibrium states: for a given solar forcing, both a moderate climate (high-latitude ice edge) and a much colder climate (mid-latitude ice edge) solve the models [Rose and Marshall, 2009]. There, a solution is said to be stable as long as the ice-edge latitude is an increasing function of solar forcing. Thus, the coexistence of two stable equilibria shows as the equilibrium curve splitting into two branches, in the ice edge–solar forcing diagram. One branch is called the 'cooling branch' and the other the 'warming branch', referring to the path taken by the ice edge in the numerical integrations (hysteresis loop). Coming next is the question of whether complex (realistic) coupled climate models also support multiple (stable) equilibria. Clearly, this question is key to climate change issues.

1.2 Bistability and phase transitions

As we have just described, the motivation for this thesis lies in the observed bistability of turbulent flows, whether geophysical or experimental. Bistability is well-defined in the context of dynamical systems. It is the coexistence,

[1] http://mitgcm.org/ Accessed January 5, 2012.

for some control parameter value (or range thereof), of two stable equilibria. In other words, the bifurcation diagram —order parameter versus control parameter— displays two stable branches whose respective domains overlap. So, when we speak of 'bistability', we assume the existence of multiple (here, two) attractors for a certain dynamical system. A less committing term may be 'bimodality'. Also, to consider a description in terms of bifurcations within reach, we wish to be able to capture the bistability in a dynamical system restricted to very few dimensions.

To this day, there exists no theory explaining the bistability or bifurcations, which a turbulent system is subject to in general. Also, the attractors are not easy to determine. In our particular framework of two-dimensional and geophysical turbulence, we propose a theory for predicting the equilibrium states. The qualitative changes undergone by a flow structure are understood as phase transitions. This implies an equilibrium statistical-mechanical approach for describing the large-scale structures of (quasi) two-dimensional turbulence. We introduce this approach in section 1.4. To justify the equilibrium approach, we first show, in section 1.3, that the dynamics of the large scales is essentially inertial. The persistent large-scale structures arise from self-organization and, because of the very high number of degrees of freedom, this phenomenon of self-organization should be explained statistically. We detail our results in section 1.5.

To keep it simple at first, instead of a 'bifurcation diagram', we may just speak of an input–output diagram: say a system is subject to a certain forcing (input), then it has a certain response (output). In the case of bistability, the input–output diagram contains a hysteresis loop. Notice that bistability cannot be achieved without nonlinearity in the dynamical equations. Although we restrict our considerations to bistability, the discussion could, of course, be extended to the general case of multistability, with however many outputs for a given input (and however high orders of nonlinearity).

We have the following picture in mind: one stable equilibrium is fully symmetric, corresponding to zero output (base state), and the other stable equilibrium is non-symmetric, corresponding to a finite output (bifurcated state). Besides, the bifurcated state exists as its equal and opposite version. Bifurcation theory gives a suitable framework to account for the coexistence of these three states over a certain range of input: it is the situation of a subcritical pitchfork bifurcation.

This simple picture cannot be applied straightforwardly to turbulent flows, where there is no such input (varying external parameter). Let us still use the terms 'base state' and 'bifurcated state' in this context. In a fully turbulent flow, symmetries should be preserved; when reversals of the bifurcated state

occur (transitions from the bifurcated state to its opposite), the symmetry can be considered recovered in a statistical sense [Gallet et al., 2011]. In this thesis, we work on flows with infinite Reynolds number (purely inertial limit), showing how their study is relevant to real flows with high, but finite, Reynolds number. Transitions can occur only if the system is out of equilibrium: there is either enough intrinsic noise due to turbulence, or some stochastic forcing. The presence of rapid transitions implies that the multistability is a property of the system at equilibrium (no forcing). By 'rapid', we mean of duration much less than the residence time (time spent at/around either equilibrium).

Statistical equilibria are particular stationary states of the dynamics, so they are dynamical equilibria. We discuss both interpretations (statistical and dynamical) of the steady states presented in this work. Phase transitions occur when their existence or stability change. In a first-order (discontinuous) phase transition, a stable equilibrium and a metastable one exchange their stabilities. In a second-order (continuous) phase transition, a stable equilibrium becomes unstable, while two stable equilibria show up. Bistability is associated with discontinuous transitions, and hence, straightforwardly with first-order phase transitions. Second-order phase transitions can be relevant to the out-of-equilibrium system though. In any case, it is crucial to know whether a qualitative change corresponds to a continuous or discontinuous phase transition. We carry out a systematic classification of the phase transitions.

Note that beyond the geophysical motivation, the interest of a classification of phase transitions is also theoretical. Notably, two-dimensional flows are long-range interacting systems[2]. The nice thing about these systems is that theoretical results for one of them is relevant and useful to the others. So our results extend to other systems with long-range interactions.

1.3 Inertial theory

Experimental and geophysical fluids, whose motion is turbulent and quasi two-dimensional, display persistent large-scale structures. The natural equations governing this type of motion are the two-dimensional Navier–Stokes equations. Scale analysis shows that the motion of the large scales is dominated by the advective term, also called *inertial* term; forcing and dissipation terms are small with respect to the inertial term. We refer to this limit as inertial. We say that the flows self-organize, precisely because the large-scale structures are not at all determined (say, linearly) by some external forcing.

[2]For a definition of 'long-range interacting systems', please see foonote 1 on page 62.

At zeroth order in the inertial limit (viscosity goes to zero, then linear friction goes to zero), the 2D Navier–Stokes equations reduce to 2D Euler equations. If topography is included in the model, we have instead the (inviscid) barotropic quasi-geostrophic equations. Then, in this inertial limit, the attractors of the dynamics are expected to be found near a set of steady states of the inviscid equations. We wish to predict the large scales of (quasi) two-dimensional turbulence as equilibria of the inviscid equations. These equilibria can be given either a *statistical-mechanical (thermodynamical) interpretation* or a *dynamical interpretation*. We explain this in the next section.

Naturally, this conservative theory ignores all effects due to forcing and dissipation, which are present in any real flow. Still, a recent work showed that the inertial description of equilibria is fundamental and relevant even in the presence of forcing and dissipation [Bouchet and Simonnet, 2009]. Phase transitions are found out of equilibrium: in two-dimensional flows, the large-scale flow undergoes random transitions between two different topologies, which are determined from equilibrium statistical mechanics. Thus, the equilibrium theory appears predictive for out-of-equilibrium transitions. This is related to the fact that attractors of 2D stochastic Navier–Stokes are close to the attractors of 2D Euler. Interestingly enough, this kind of phase transitions is a very usual phenomenon in inertial flows [Venaille and Bouchet, 2009].

We introduce the systems under study, namely the 2D Euler equations, and the barotropic quasi-geostrophic equations. Both are 2D equations of the motion, expressing the advection of vorticity and potential vorticity, respectively. The barotropic quasi-geostrophic equations serve as a simple model for the motion of atmospheric or oceanic flows. We derive it in appendix A. In this model, the two-dimensionality of the motion comes from three approximations: hydrostatic approximation, smallness of vertical scales with respect to horizontal scales, and geostrophic approximation (balance between the Coriolis force and the pressure gradient). The barotropic quasi-geostrophic model is also relevant to the description of experimental flows, such as the approximation of fluid dynamics when three-dimensional motion is constrained by a strong transverse field (e.g., rotation) or takes place in geometries of small (vertical-to-horizontal) aspect ratio.

It should be noted that the large scales of geophysical flows are highly turbulent. This suggests that we should consider the inertial limit of the dynamical equations to describe them. We are left with a system at equilibrium (no forcing, no dissipation). We have the transport of a scalar quantity q by an incompressible two-dimensional velocity $\mathbf{u}$:

$$\frac{\partial q}{\partial t} + \mathbf{u} \cdot \nabla q = 0 \; ; \quad \mathbf{u} = \mathbf{e}_z \times \nabla \psi \; ; \quad q = \Delta \psi + h. \tag{1.1}$$

The 2D velocity $\mathbf{u}$ is solenoidal, i.e., its divergence is zero and its curl is nonzero. A streamfunction ψ (defined up to an additive constant) can thus be introduced. The vorticity $\nabla \times \mathbf{u}$ only has a vertical component. We denote this scalar vorticity by $\omega = (\nabla \times \mathbf{u}) \cdot \mathbf{e}_z = \Delta\psi$. Unless otherwise specified, we complement the elliptic equation $q = \Delta\psi + h$ with impermeability boundary conditions: $\psi = 0$ on $\partial\mathcal{D}$, where $\mathcal{D}$ is a simply connected domain. h is interpreted as a topography (see appendix A). If $h = 0$, $q = \omega$ is just the vorticity, and (1.1) reduce to the 2D Euler equations. If $h \neq 0$, $q = \omega + h$ is the potential vorticity (PV) and (1.1) are the barotropic quasi-geostrophic equations.

We wish to determine the final state(s) of the system. It is readily noted that any state verifying a functional relationship between (potential) vorticity and streamfunction is a steady state of (1.1)[3]. Thus, there are an infinity of steady states. How can we determine which ones are stable? Since q is a field, (1.1) has an infinite number of degrees of freedom (continuous system). A deterministic approach would then be unrealistic. Then, we turn to statistical mechanics. Rather than describing fine-grained structures (exact fields), equilibrium statistical theories of two-dimensional turbulent flows predict —assuming ergodicity— the final organization of the flow at a coarse-grained level: a mixing entropy is maximized, under the constraints that all the flow invariants be indeed conserved [Miller, 1990, Robert, 1991, Robert and Sommeria, 1991].

1.4 State of the art: statistical-mechanical approach

In this section, we give the state of the art regarding equilibrium statistical mechanics approaches in two-dimensional turbulence. The first attempts to build statistical hydrodynamics date back to [Onsager, 1949]. There, the continuous vorticity field was approximated by a multitude of singular vortices (point-vortex model). Other finite-dimensional approximations of a continuous vorticity have been considered [Kraichnan and Montgomery, 1980]. A statistical mechanics for the actual continuous vorticity was derived by [Robert, 1990, Robert, 1991] and [Robert and Sommeria, 1991], and independently by [Miller, 1990]. This statistical–mechanical theory is referred to as the Miller–Robert–Sommeria theory (MRS theory, for short).

[3]The term $\mathbf{u} \cdot \nabla q$ cancels if and only if $\mathbf{u}$ and q are orthogonal. Since $\mathbf{u}$ is orthogonal to the gradient of ψ, we demand equivalently that ∇q and $\nabla\psi$ be collinear, i.e., that q be a function of ψ.

1.4.1 Miller–Robert–Sommeria theory

The MRS theory predicts and describes the self-organisation of two-dimensional turbulent flows as a purely inertial process. Actually, the MRS theory determines a statistical equilibrium for the 2D Euler system; assuming ergodicity, the final state of the system is that statistical equilibrium. A statistical mechanics description entails the definition of microscopic configurations versus macroscopic ones.

Assume, just to get the idea, that the vorticity takes values in a finite discrete set. Consider an initial vorticity field in a given domain: it consists of a certain number of 'vorticity patches', each patch having uniform vorticity. As time increases, turbulence (advection) makes the boundaries between patches more and more filamented in space. Then, the final state displays very fine-grained (small-scale) structures. This exact (fine-grained) vorticity field is a certain *microscopic state*.

We are not interested in the exact vorticity field with its very small scales, but precisely in the large-scale structures. Let $\rho(\sigma, \mathbf{r})$ be the probability density to observe the vorticity value σ at point $\mathbf{r}$. We have the local average (coarse-grained) vorticity

$$\bar{\omega}(\mathbf{r}) = \int \mathrm{d}\sigma \ \sigma\rho(\sigma, \mathbf{r}), \tag{1.2}$$

where the integral is taken over all vorticity values (levels). The local probability density ρ defines a *macroscopic state*.

The area of each vorticity patch is conserved by the dynamics. So is the total kinetic energy of the system. The small-scale structures, which can be seen as fluctuations around the coarse-grained field, do not contribute to this energy [Robert and Sommeria, 1991]. The accessible microstates have prescribed value of the energy and prescribed vorticity level distribution. As a statistical-mechanical theory, the MRS theory determines the most probable macrostate, i.e., the one for which the corresponding microstates are the most numerous.

The number of microstates corresponding to a given ρ is quantified by a mixing entropy. Therefore, the statistical equilibrium (equilibria, possibly) is the solution of a variational problem, namely the maximisation of the mixing entropy, under the constraints of fixed energy and fixed vorticity distribution. This is analogous to the *microcanonical problem* of usual statistical mechanics.

Let us now recall the prediction of the MRS theory at a more technical level. The probability density ρ verifies the normalization condition

$$N[\rho](\mathbf{r}) = \int \mathrm{d}\sigma \ \rho(\sigma, \mathbf{r}) = 1, \tag{1.3}$$

for every point $\mathbf{r}$ of the spatial domain $\mathcal{D}$. Let us express the conserved quantities. The vorticity distribution writes

$$\mathcal{A}[\rho](\sigma) = \int_{\mathcal{D}} \mathrm{d}\mathbf{r}\ \rho(\sigma, \mathbf{r}). \tag{1.4}$$

It is conserved, since the dynamics simply reorder the initial 'infinitesimal vorticity patches'. The kinetic energy is computed from the coarse-grained field:

$$\mathcal{E}[\bar{\omega}] = -\frac{1}{2} \int_{\mathcal{D}} \mathrm{d}\mathbf{r}\ \bar{\omega}\bar{\psi}, \tag{1.5}$$

where the average streamfunction $\bar{\psi}$ is such that $\Delta\bar{\psi} = \bar{\omega}$. A mean-field approximation is made: $\mathcal{E}[\bar{\omega}] = \mathcal{E}[\omega]+$ fluctuation terms, which are neglected.

The mixing entropy of vorticity levels is

$$\mathcal{S}[\rho] = -\int_{\mathcal{D}} \mathrm{d}\mathbf{r} \int_{-\infty}^{+\infty} \mathrm{d}\sigma\ \rho(\sigma, \mathbf{r}) \log \rho(\sigma, \mathbf{r}). \tag{1.6}$$

It can be proven to be proportional to the logarithm of the number of microstates corresponding to the macrostate ρ (Boltzmann's entropy formula). Then, the MRS microcanonical variational problem writes

$$\sup_{\{\rho \,|\, N[\rho]=1\}} \left\{ \mathcal{S}[\rho] \mid \mathcal{E}[\bar{\omega}] = E,\ \mathcal{A}[\rho] = \gamma \right\}, \tag{1.7}$$

where $\gamma(\sigma)$ denotes a prescribed vorticity distribution. Let us assume that the Lagrange multiplier rule applies. If ρ is a solution to (1.7), then there exist β and $\mu(\sigma)$ such that $(\rho, \beta, \mu(\sigma))$ is a critical (actually, stationary) point for the functional $\mathcal{G}(\beta, \{\mu\}) = \mathcal{S} - \beta\mathcal{E} - \int \mathrm{d}\sigma\ \mu(\sigma)\mathcal{A}$. These critical points verify

$$\delta\mathcal{S} - \beta\delta\mathcal{E} - \int \mathrm{d}\sigma\ \mu(\sigma)\delta\mathcal{A} = 0, \tag{1.8}$$

where first variations are taken with respect to ρ. A critical point of (1.7) is also a critical point of $\mathcal{G}(\beta, \{\mu\})$. By analogy with usual thermodynamics, β represents an 'inverse temperature', $\mu(\sigma)$ a 'chemical potential' associated with the vorticity level σ, and $\mathcal{G}$ the Gibbs free energy. (1.8) is equivalent to

$$-(\log\rho + 1) + \beta\psi\sigma - \mu(\sigma) = 0,$$

leading to

$$\rho(\sigma, \mathbf{r}) = \mathcal{N} \exp(\beta\sigma\bar{\psi}(\mathbf{r}) - \mu(\sigma)), \tag{1.9}$$

with $\mathcal{N}$ a normalization constant such that (1.3) holds. Therefore, from (1.2), the average vorticity and the average streamfunction are related in the following functional way:

$$\bar{\omega} = \mathcal{N} \int \mathrm{d}\sigma\ \sigma \exp(\beta\sigma\bar{\psi} - \mu(\sigma)) =: f_{\beta,\{\mu\}}(\bar{\psi}). \tag{1.10}$$

For instance, for a two-level vorticity distribution, where $\sigma = \{\pm 1\}$ and $\mu(-1) = \mu(1)$, $\bar{\omega}$ is proportional to $\sinh(\beta\bar{\psi})$. The vorticity level distribution determines the form of the functional relationship. Since $\bar{\omega} = \Delta\bar{\psi}$, (1.10) should be solved in $\bar{\psi}$, from which the velocity field can be computed. Statistical equilibria are the critical points (1.10) which are maxima (negative second-order variations): this is the usual statistical-mechanical (thermodynamical) stability.

So we need to know—or choose—the vorticity level distribution, to apply directly the MRS theory. But what was the 'initial' distribution in oceans and atmospheres? We do not know what the vorticity level distribution should be for two-dimensional turbulent flows in general. We can study the statistical equilibria in the case of a two-level vorticity distribution or of any other particular vorticity distribution, provided we can solve (1.10) for the particular form of $f_{\beta,\{\mu\}}$. This way, we have access to particular classes of MRS equilibria. We may check whether these equilibria are relevant, comparing them to structures observed in real flows.

Indeed, throughout the thesis, we consider only certain classes of MRS equilibria. These equilibria are characterized by the form of the function f relating (potential) vorticity and streamfunction. In the next chapter, we take f to be nonlinear, thus considering a very large class of MRS equilibria. The general strategy is to solve variational problems simpler than (1.7), and give an interpretation to their solutions. In the following, we recall a few milestones in this strategy.

1.4.2 Robust invariants

The conservation of vorticity distribution ($\mathcal{A}[\rho] = \gamma$) implies the conservation of an infinite number of so-called *Casimir* functionals

$$\mathcal{C}_s[\omega] = \int_{\mathcal{D}} s(\omega),$$

where s is any integrable function. In this infinite list, which conserved quantities are statistically relevant to the large-scale equilibrium? Or, maybe, more relevant than others? To answer this question, phenomenological arguments are invoked [Majda and Wang, 2006]. It is readily noted that when considering a truncation of (1.1) in Fourier space, only the linear and quadratic invariants survive. The linear invariant $\int_{\mathcal{D}} \omega$ is called the circulation. The quadratic invariant $\int_{\mathcal{D}} \omega^2$ is called the enstrophy. Another quadratic invariant is the kinetic energy (1.5). Vorticity moments $\int_{\mathcal{D}} \omega^n$, for $n \geq 1$, do not survive coarse-graining except for the circulation ($n = 1$). Indeed, given a microscopic field ω and the three operations: a) take it to the power of n, b) coarse-grain

it over $\mathcal{D}$, and c) integrate it over $\mathcal{D}$. We may commute a) and b) without change in the result only for $n = 1$. This leads to the identification of energy and circulation as *robust* (or 'rugged') conserved quantities, in contrast with *fragile* (or 'dissipated') conserved quantities. The term 'dissipated' refers to the interpretation of small-scale (fine-grained) fluctuations being dissipated by a small viscosity [Robert and Sommeria, 1991, section 6].

Therefore, energy and circulation play an important role, as robust invariants. On the contrary, enstrophy is fragile. In the thesis, we enforce the conservation of energy and circulation only. The relationships between various simpler variational problems and the MRS variational problem (1.7) are settled in [Bouchet, 2008] and in [Chavanis, 2009]. Generally speaking, the more constrained the problem, the more difficult it is to solve. Stability in a less constrained problem (say, canonical) implies stability in a corresponding more constrained one (microcanonical). Therefore, results from a less constrained problem (canonical results) give sufficient conditions for stability in a stronger sense (microcanonical stability). This justifies the use of simpler variational problems.

1.4.3 Strong-mixing limit

The simplest non-trivial form for the relationship between vorticity and streamfunction is linear. It is natural to begin with assuming $\omega = \beta\psi$. We drop the bar symbol over the average fields for ease of notation, but we really mean the coarse-grained fields from now on. [Chavanis and Sommeria, 1996] interpret the linear relationship $\omega = \beta\psi$ as arising from a strong-mixing limit. Indeed, the constraint of energy conservation goes against mixing, which would ultimately lead to a trivial (uniform) vorticity field. So $\beta = 0$ means no constraint of energy conservation, and hence, complete mixing. And $\beta \to 0$ means a limit of strong mixing. A Taylor expansion of the exponential with small argument $\pm\beta\psi$ (considering the two-level distribution, for simplicity) gives ω proportional to $\beta\psi$ at lowest order.

It is noted that the linear relationship $\omega = \beta\psi$ is recovered from another variational problem, where the enstrophy (domain-averaged squared vorticity) is minimized and only the constraints of energy and circulation conservation are enforced. This variational problem was initially based upon a selective decay principle [Majda and Wang, 2006]. The study by [Chavanis and Sommeria, 1996] is carried out in a closed simply connected domain, first a rectangle, then a disk. The class of equilibria corresponding to $\omega = \beta\psi$ appears to show monopoles, dipoles, and other intermediate structures, depending on aspect ratio (domain geometry) and on a single parameter containing energy and circulation. Systematic phase diagrams can be

constructed.

1.4.4 Canonical treatment of the fragile invariants

Later, [Venaille and Bouchet, 2009] showed that invoking a 'strong-mixing limit' was not needed. Neither a 'minimum-enstrophy principle'. It is enough to consider the following: the infinity of invariants which are not included in the variational problem are treated canonically. Thus, restricting ourselves to linear ω–ψ relationships does not give access to all the statistical equilibria, for sure, but it can be seen as a low-order description. The systematic description of phase diagrams for steady states of Euler 2D with linear ω-ψ relation is a great achievement. In the next chapter, we investigate the robustness of this linear description in the low-energy limit.

1.5 Results

In chapter 2, we present analytical and numerical computations of phase diagrams, for a large class of equilibrium states of two-dimensional and geophysical turbulent flows. Finding and characterizing transitions is crucial, because they bear the possibly interesting qualitative changes (in flow structures, as far as we are concerned). In the equilibrium statistical-mechanical context, we deal with phase transitions. In the dynamical system context, we deal with bifurcations. It is important to know whether the transitions are continuous or discontinuous. We used technical tools of applied bifurcation theory, namely, Lyapunov–Schmidt reduction, to characterize the phase transitions (first-order or second-order). Thus, we determine the continuous or discontinuous nature of phase transitions in a general framework.

Bistability is more straightforwardly associated with discontinuous transitions, as already discussed. Chapter 2 is organized as follows:

- In section 2.1, we introduce the *microcanonical energy–circulation variational problem*. It is about minimizing a certain Casimir functional, at fixed energy and fixed circulation.

- In section 2.3, we solve the unconstrained dual variational problem (*grand canonical energy–circulation variational problem*) in a symmetric case. This symmetry yields a solution, which is not most interesting qualitatively, but helps set the general framework for the other (more promising) derivations.

- In section 2.4, we solve the *canonical energy–circulation variational problem*. We find interesting phase transitions, where the flow structure

completely changes. For elongated rectangular domains (aspect ratio $\tau > \tau_c$) we recover the showing up of a dipolar structure, while for square-like domains ($\tau < \tau_c$) we recover that of a central monopole with counter-circulating cells at the corners [Chavanis and Sommeria, 1996, Venaille and Bouchet, 2009]. The novelty here is to distinguish between a continuous transition and a discontinuous one, depending on the sign of the quartic moment of the vorticity. In the square-like case, we can be in the presence of three qualitatively different states (stable or metastable). We wish to emphasize that the canonical ensemble may be relevant to geophysical applications, such as the Kuroshio, since the two regimes of this ocean current have different energies.

We find that the canonical ensemble is not equivalent to the microcanonical ensemble, with a range of negative specific heat. The same holds between the grand canonical ensemble and the grand microcanonical ensemble. We recover many predictions of the systematic classification by [Bouchet and Barré, 2005], thus feeding the field of long-range interacting systems. This work is the topic of a long journal article [Corvellec and Bouchet, 2011a] and of a short proceedings paper [Corvellec and Bouchet, 2011b].

In chapter 3, we extend the results of [Venaille and Bouchet, 2009] to the case of a doubly connected domain. For instance, the domain is a periodic channel or an annulus. This kind of topology is relevant to many problems in oceanography, when the domain is either a latitude band, or a basin with an island. It also corresponds to the geometry of rotating-tank experiments. So, we consider a linear relationship between PV and streamfunction. The results found in [Venaille and Bouchet, 2009] are generic, but the double-connectedness brings in a new conserved quantity, as the circulation is conserved along each connected piece of boundary. Thus, the phase diagrams can be explored in an additional dimension. In a certain range of parameters, two qualitatively different equilibria are identified, on either side of a first-order phase transition line. One is topography-dominated: streamlines roughly follow topography contours. The other flow structure has a much stronger azimuthal/zonal contribution. We point out that these two states have geophysical analogues, as in atmospheric 'blocking' or in the Kuroshio 'meanders' (see section 1.1). This is a very interesting result for our understanding of bistability in turbulent geophysical flows.

In chapter 4, we focus on a result of [Bouchet and Corvellec, 2010] about invariant probability measures of the 2D Euler equations. The determination

of invariant measures is motivated by the fact that they usually live on attractors. When only the quadratic invariants (energy and enstrophy) are taken into account, we give an explicit computation showing that the microcanonical measure corresponds to the maximization of a mean-field entropy. The technical tools involve analytic continuation for the evaluation of a complex integral.

Chapter 2

Complete theory of low-energy phase diagrams for stable steady states of 2D turbulence

Contents

In geophysical turbulent flows, it is customary to have two or more attractors. In the inertial limit, i.e., when the advection time is much less than the spin-up time[1], the attractors are concentrated near a set of steady states of

[1]The 'spin-up' time, also called 'spin-down' time, is the typical time it takes for a system to reach an equilibrium state in the presence of friction [Pedlosky, 1987]. If there is large-scale linear (Rayleigh) friction, spin-up time is the time scale given by the friction coefficient.

the inviscid equations. Steady states of two-dimensional and quasi-geostrophic turbulence are characterized by a functional relationship between (potential) vorticity q and streamfunction ψ. Statistical-mechanical approaches can be used to select stable states among these equilibria. Note that statistical (thermodynamical) stability implies dynamical stability. A particular class of equilibria is characterized by linear (or affine) q–ψ relations. Phase diagrams for the latter equilibrium states have been computed analytically and numerically by several authors, such as [Chavanis and Sommeria, 1996, Venaille and Bouchet, 2009, Naso et al., 2010]. In this chapter, we consider a small nonlinearity in the q–ψ relationship, and investigate its effect on the phase diagrams. We find that the 'linear' results are not generic: the structure of phase diagrams is completely changed by this small perturbation. In particular, we find additional occurrences of statistical ensemble inequivalence. Interesting phase transitions are reported, with tricritical or critical points in the relaxed ensembles, and spinodal points in the constrained ensembles. We get a general theory for the phase diagrams of quasi 2D turbulence in the limit of low energy: the sign of the nonlinearity determines the type of phase transition (continuous or discontinuous). We discuss phase diagrams which display (two or more) qualitatively different states, because we wish to relate these states to the (two) regimes given by the bistability of real and experimental flows.

2.1 General considerations

We consider the barotropic quasi-geostrophic equations:

$$\partial_t q + \mathbf{u}\cdot\nabla q = 0\,; \quad \mathbf{u} = \mathbf{e}_z \times \nabla\psi\,; \quad q = \Delta\psi + h, \tag{2.1}$$

where $\mathbf{u}$ denotes the (two-dimensional) velocity field, ψ the streamfunction (defined up to a constant), q the potential vorticity (PV), and h an equivalent topography. We consider a rectangular domain $\mathcal{D} = \{(x,y) \in [0,\sqrt{\tau}] \times [0,1/\sqrt{\tau}]\}$ of area unity ($|\mathcal{D}| = 1$) and aspect ratio $\tau \geq 1$. The boundary condition is that of no normal flow (free slip), implying ψ is constant on $\partial\mathcal{D}$; without loss of generality, we may take $\psi_{|\partial\mathcal{D}} = 0$. If $h = 0$, (2.1) are just the 2D Euler equations. Without loss of generality, we take h such that $\int_{\mathcal{D}} h = 0$. For two fields q_1 and q_2, the L^2 scalar product is denoted by $\langle q_1 q_2\rangle := \int_{\mathcal{D}} q_1 q_2$.

The inviscid dynamics (2.1) corresponds to a limit of infinite Reynolds number. But in 2D turbulence, unlike in 3D turbulence, there is no direct energy cascade (energy cascading towards smaller and smaller scales) [Kraichnan, 1967]. The reason for having self-organization in 2D turbulent

flows lies in the long-range interacting nature of these systems. The long-rangedness of interactions may be thought of in terms of infinitesimal PV patches: the interaction between one another is nonvanishing as their distance in space goes to infinity. Although the number of degrees of freedom is infinite in a turbulent flow, the formation of large-scale structures indicates that just a few effective degrees of freedom should be enough to characterize the flow.

In this chapter, we describe a class of equilibria of (2.1), and the phase transitions which they undergo, through scalar bifurcation equations. The stability of the above-mentioned equilibria can be established statistically (thermodynamically) and dynamically. In the first chapter, section 1.4, we have described the MRS theory, which predicts the statistical equilibria of 2D turbulence in terms of a functional relationship between PV and streamfunction: $q = f(\psi)$. Then, from (2.1), it can be seen that statistical equilibria are particular steady states of the dynamics. Computing the MRS equilibrium states is a difficult task though, because an infinite number of conserved quantities is involved. Simpler problems —taking into account only a few conserved quantities— were shown to give access to some classes of MRS equilibria [Bouchet, 2008].

An example of using statistical mechanics for predicting and describing real turbulent flows can be found in [Bouchet and Simonnet, 2009, and references therein]. There, $h = 0$ and (2.1) reduces to the 2D Euler equations. Bifurcations between stable steady solutions of 2D Euler are found to occur when varying the aspect ratio of the domain, the nonlinearity of $f(\psi)$, or the energy. This suggests that a general theory of phase transitions for 2D and geophysical flows should be looked for —it is not available at the present day. Only instances of such phase transitions have been reported in the literature. Note that key results regarding statistical ensemble inequivalence, including a case of nonlinear equation $q = f(\psi)$, were presented in [Ellis et al., 2002]. In this chapter, we present new analytical results on phase transitions related to the nonlinearity of $f(\psi)$. It appears that phase transitions can be characterized through the bifurcation analysis of scalar equations, acting as normal forms.

2.2 Variational problem

We have seen (section 1.4) that the MRS statistical equilibrium is obtained by maximizing a mixing entropy, under the constraints of energy conservation and vorticity distribution conservation. We have argued that the kinetic energy and the circulation (domain-averaged PV) are invariants which play an

important role. Then, we consider the simpler variational problem[2]

$$C_s(E,\Gamma) = \min_q \left\{ \int_{\mathcal{D}} s(q) \mid \mathcal{E}[q] = E\,, \mathit{\Gamma}[q] = \Gamma \right\}. \tag{2.2}$$

The function $s(q)$ is assumed strictly convex. In thermodynamics, the microcanonical problem is a two-constraint variational problem where the thermodynamical potential to be maximized is called the entropy. We can draw an analogy with (2.2), where our Casimir functional $\int_{\mathcal{D}} s(q)$ acts as the opposite of an entropy. We recall the expressions of

$$\mathcal{E}[q] = -\frac{1}{2}\int_{\mathcal{D}} \psi(q-h) \quad \text{energy, and}$$
$$\mathit{\Gamma}[q] = \int_{\mathcal{D}} q \quad \text{circulation.}$$

So we call (2.2) microcanonical, in analogy with usual thermodynamics. Note that this variational problem corresponds to (CVP) in [Bouchet, 2008] (see this reference about the relationship between the solutions to our variational problem and the actual MRS statistical equilibria). For given values of the constraints E and Γ, the q fields solving (2.2) are microcanonically stable equilibria. This is a sufficient condition for their dynamical stability [Arnol'd, 1966]. Indeed, let us consider a functional which is conserved by the dynamics. This can be a linear combination of a Casimir functional and of the energy functional ('energy–Casimir functional'). The point is the following: if the system lies at a nondegenerate extremum of this invariant, then it cannot go away from this point.

In this paper, we restrict our attention to even functions $s(q)$. Indeed, there are many situations where the $q \mapsto -q$ symmetry applies. If q is a solution to (2.1), then $-q$ is also a solution to (2.1). In real flows, the $q \mapsto -q$ symmetry could be broken by a nonsymmetric forcing or by a nonsymmetric initial distribution (of PV). Say

$$s(q) = \frac{1}{2}q^2 - \sum_{n\geq 2} \frac{a_{2n}}{2n} q^{2n}. \tag{2.3}$$

Assuming that the Lagrange multiplier rule applies (q regular enough), there exists a couple $(\beta,\gamma) \in \mathbb{R}^2$ such that solutions of (2.2) are critical points of

$$\mathcal{G}[q] = \int_{\mathcal{D}} s(q) + \beta\mathcal{E}[q] + \gamma\mathit{\Gamma}[q]. \tag{2.4}$$

[2]The minimization is taken over the coarse-grained fields: $q(\mathbf{r}) = \int \mathrm{d}\sigma\ \sigma\rho(\sigma,\mathbf{r})$. As announced at the beginning of subsection 1.4.3, page 16, we have (abusively?) dropped the bar symbol characterizing coarse-grained fields.

We call this functional the Gibbs free energy, in analogy with usual thermodynamics. The variational problem dual to (2.2), i.e.,

$$G(\beta,\gamma) = \min_q \left\{ \mathcal{G}[q] = \int_{\mathcal{D}} s(q) + \beta\mathcal{E}[q] + \gamma\Gamma[q] \right\}, \tag{2.5}$$

is referred to as the grand canonical variational problem. Because it is relaxed (unconstrained), it is more easily tractable.

β and γ are the Lagrange multipliers associated with the energy and circulation constraints, respectively. For all couples (β,γ), minima $G(\beta,\gamma)$ are also minima $C_s(E(\beta,\gamma),\Gamma(\beta,\gamma))$. But some minima $C_s(E,\Gamma)$ may correspond to critical points of (2.4) which are not minima of (2.4). These are classical results (see any textbook on convex optimization). When $E(\beta,\gamma)$ and $\Gamma(\beta,\gamma)$ do not span their entire accessible range ($E \in \mathbb{R}_+$, $\Gamma \in \mathbb{R}$), as (β,γ) is varied, the microcanonical ensemble and the (dual) grand canonical ensemble are said to be inequivalent. Then, some microcanonical solutions are not obtained as grand canonical solutions. This feature is typical of long-range interacting systems. In short-range interacting systems, the different statistical ensembles are used interchangeably, because they are usually equivalent.

It is natural to begin with the study of the convexity of $\mathcal{G}[q]$ (2.4). Indeed, it is readily noted that if $\mathcal{G}[q]$ is strictly convex, it has a unique critical point, which is then the (unique) solution of (2.2). Since $\Gamma[q]$ is a linear form, it is sufficient to investigate the convexity of the Helmholtz free energy functional $\mathcal{F}[q] = \int_{\mathcal{D}} s(q) + \beta\mathcal{E}[q]$. Since $\mathcal{E}[q]$ is convex, $\mathcal{F}[q]$ is strictly convex if $\beta \geq 0$.

If $\beta < 0$, we need to study the sign of the second-order variation of $\mathcal{F}$, denoted by $\delta^2\mathcal{F}$, and defined through $\mathcal{F}[q+\delta q]-\mathcal{F}[q] = \delta\mathcal{F}[q]+\frac{1}{2}\delta^2\mathcal{F}[q]+o(\delta q^2)$. We get

$$\delta^2\mathcal{F}[q] = \int_{\mathcal{D}} s''(q)\delta q^2 - \beta \int_{\mathcal{D}} \delta\psi\delta q. \tag{2.6}$$

In appendix 2.5, we recall the classical proof of the Poincaré inequality:

$$\int_{\mathcal{D}} \delta\psi\delta q \geq -\frac{1}{\lambda_1}\int_{\mathcal{D}} \delta q^2,$$

where $-\lambda_1 < 0$ is the greatest (smallest, in absolute value) eigenvalue of the Laplacian on $\mathcal{D}$. Then,

$$\delta^2\mathcal{F}[q] \geq \int_{\mathcal{D}} \left(s''(q) + \frac{\beta}{\lambda_1}\right)\delta q^2 \geq \left(s''_m + \frac{\beta}{\lambda_1}\right)\int_{\mathcal{D}} \delta q^2 \tag{2.7}$$

for $\beta < 0$, where $s''_m := \min_{\mathbf{r}\in\mathcal{D}}\{\min_q s''(q(\mathbf{r}))\}$. So if $\beta > -s''_m\lambda_1$, $\mathcal{F}$ is strictly convex, and so is $\mathcal{G}$. There is a unique solution to (2.5), and hence,

a unique solution to (2.2). The conditions $\beta \geq 0$ and $-s''_m\lambda_1 < \beta < 0$ are the hypotheses for the first and second Arnol'd theorems, respectively, on Lyapunov stability. In both cases, the sufficient condition is that $\delta^2\mathcal{F}$ be positive-definite [Michel and Robert, 1994].

We conclude that, in the grand canonical ensemble, phase transitions may occur only for $\beta \leq -s''_m\lambda_1$, where solutions to (2.5) may cease to be unique or cease to exist.

The critical points of $\mathcal{G}$ are the q fields for which the first-order variation of $\mathcal{G}$ vanish, i.e.,

$$s'(q) - \beta\psi + \gamma = 0. \tag{2.8}$$

Since $s(q)$ is strictly convex, $s'(q)$ is strictly increasing, so its inverse $(s')^{-1}(q)$ is well-defined (and strictly increasing). We have

$$q = (s')^{-1}(\beta\psi - \gamma).$$

From (2.3), the Taylor expansion of $(s')^{-1}$ around 0 reads $(s')^{-1}(x) = x + a_4x^3 + o(x^4)$. Then, the term in a_4 is the lowest-order nonlinear contribution to $(s')^{-1}(x)$.

2.3 Grand canonical solutions

2.3.1 Symmetric case: $\gamma = 0$

In this subsection, we derive the solutions to (2.5) at $\gamma = 0$. We will see that they give us some solutions to (2.2), but not all of them. In this section, we show that the grand canonical ensemble with $\gamma = 0$ is equivalent to the grand microcanonical (only energy-constrained) ensemble if $a_4 \leq 0$. It is not the case if $a_4 > 0$.

We denoted the first (largest-scale) Laplacian eigenmode by e_1. As long as the topography field h is orthogonal to e_1, we find the following results, for the grand canonical ensemble with $\gamma = 0$:

- for $a_4 \leq 0$, there is a second-order phase transition at $\beta = -\lambda_1$: the solution goes continuously from a trivial state (zero energy, uniform vorticity) to a state dominated by e_1;
- for $a_4 > 0$, a_4 small enough, there is a first-order phase transition at $\beta = \beta_c(a_4) \in]-\lambda_1, -\lambda_1 s''_m[$: the solution goes discontinuously from a trivial state ($E = 0$) to a state dominated by e_1 ($E = E_c(a_4) > 0$). The energy range accessible by grand canonical solutions (with $\gamma = 0$) displays a gap $]0, E_c(a_4)[$.

Systems with symmetry display a richer phenomenology of phase transitions, especially regarding second-order phase transitions [Bouchet and Barré, 2005]. It is not surprising to find a second-order phase transition line here, owing to the $q \mapsto -q$ symmetry of $\int_{\mathcal{D}} s(q) + \beta\mathcal{E}[q]$. In the grand microcanonical ensemble with $\gamma = 0$, we find that

- there is no phase transition at low energy (we cannot tell what happens at high energy);
- at nonzero low energy, the solution is a state dominated by e_1 ;
- for $a_4 > 0$, states of lowest energy ($E \in [0, E_{c_2}(a_4)]$) have negative specific heat.

Energies E_c and E_{c_2} will be defined later in the section.

When solving (2.2), the quadratic part of s comes into play at lowest (linear) order in E [Bouchet and Simonnet, 2009]. Therefore, in the low-energy limit, it is the dominant contribution. Also, at lowest order, the solution is along e_1, the largest-scale eigenmode. The next order brings into play the small parameter a_4, referred to as the nonlinearity, for short. We may always write

$$q = Ae_1 + q' \tag{2.9}$$

with $A \in \mathbb{R}$ and $q' \in M_g = \{q' | \langle q' e_1 \rangle = 0\}$. We see q' as a perturbation to the lowest-order solution $\pm Ae_1$, assuming it admits an asymptotic expansion in (powers of) A. This would lead to an asymptotic expansion in A for the Gibbs free energy, i.e., a normal form describing the phase transitions in a neighbourhood of $a_4 = 0$. We expect the symmetries at play to show in this normal form. Through $q = \Delta\psi$, we have $\psi = -\frac{A}{\lambda_1} e_1 + \psi'$, with $\psi' \in M_g$. We may also decompose $h = h_1 e_1 + h'$, with $h' \in M_g$. Let us denote the Gibbs free energy (2.4) with $\gamma = 0$ by $\mathcal{G}_0$.

The idea is to minimize $\mathcal{G}_0$ with respect to q' first, and then with respect to A:

$$\mathcal{G}_0[q] = \mathcal{G}_0[A, q'] = \int_{\mathcal{D}} \left[s(Ae_1 + q') - \frac{\beta}{2}\psi'(q' - h') \right] + \frac{\beta}{2}\frac{A^2}{\lambda_1} - \frac{\beta}{2}\frac{h_1}{\lambda_1} A.$$

The second-order variation of $\mathcal{G}_0$ with respect to q' is

$$\delta^2\mathcal{G}_0[A, q'] = \int_{\mathcal{D}} s''(Ae_1 + q')\delta q'^2 - \beta \int_{\mathcal{D}} \delta\psi' \delta q'. \tag{2.10}$$

It is straightforward to prove a generalization of the Poincaré inequality in the subspace M_g (any $q' \in M_g$ may be written $q' = \sum_{i \geq 2} q_i e_i$), which yields,

for $\beta < 0$, the inequality

$$\delta^2\mathcal{G}_0[A, q'] \geq \left(s_A^g + \frac{\beta}{\lambda_2}\right) \int_{\mathcal{D}} \delta q'^2,$$

where $s_A^g := \min_{\mathbf{r}\in\mathcal{D}}\{\min_{q'} s''(Ae_1 + q'(\mathbf{r}))\}$. Therefore, if $\beta > -s_A^g\lambda_2$, $\mathcal{G}_0$ is convex with respect to q' and we denote by q'_{eq} the unique solution to the minimization problem

$$G_0(A) = \min_{q'} \mathcal{G}_0[A, q'] = \int_{\mathcal{D}} \left[s(Ae_1 + q'_{eq}) - \frac{\beta}{2}\psi'_{eq}(q'_{eq} - h')\right] + \\ + \frac{\beta}{2}\frac{A^2}{\lambda_1} - \frac{\beta}{2}\frac{h_1}{\lambda_1}A. \tag{2.11}$$

For $\beta > -s_A^g\lambda_2$, q'_{eq} is the unique critical point of $\mathcal{G}_0$ with respect to q'. It satisfies

$$\int \big(s'(Ae_1 + q'_{eq}) - \beta\psi'_{eq}\big)\delta q' = 0 \quad \forall\ \delta q' \mid \langle \delta q' e_1\rangle = 0,$$

therefore there exists $\alpha_g \in \mathbb{R}$ such that

$$s'(Ae_1 + q'_{eq}) - \beta\psi'_{eq} = \alpha_g e_1\,. \tag{2.12}$$

We compute the solution to (2.12) perturbatively around $(A, q') = (0, 0)$, in order to obtain an asymptotic expansion for $G_0(A)$ around $A = 0$, and hence determine the type of phase transitions to expect in the vicinity of ($\beta \leq -s''_m\lambda_1\,, a_4 = 0$). Remark that if $a_{2n} \leq 0$ for all $n \geq 2$, then $s''_m = \min_q\{1 - 3a_4q^2 - o(q^3)\} = 1$ and $s''_m \to 1$ as $(a_4, q) \to (0, 0)$; $s(q)$ is said to be strongly convex[3].

We have the Taylor expansion $s'(q) = q - a_4q^3 - a_6q^5 + o(q^6)$. Substituting this expression into (2.12), and projecting (2.12) orthogonally onto M_g (projection of x being denoted by $P(x) := x - \langle xe_1\rangle e_1$), we get

$$q'_{eq} - a_4A^3P(e_1^3) - 3a_4A^2P(e_1^2q'_{eq}) - 3a_4AP(e_1q'^2_{eq}) - a_4P(q'^3_{eq}) + \\ + O(A^5, A^4q'_{eq}, A^3q'^2_{eq}, A^2q'^3_{eq}, Aq'^4_{eq}, q'^5_{eq}) = \beta\psi'_{eq}.$$

At lowest order in the asymptotic expansion of q'_{eq} ($q'_{eq} = q'_0 +$ higher powers of A), we have

$$q'_0 - \beta\psi'_0 = \Delta\psi'_0 - \beta\psi'_0 = a_4A^3P(e_1^3)\,;$$

[3] http://en.wikipedia.org/w/index.php?title=Convex_function&oldid=466661785#Strongly_convex_functions Accessed January 5, 2012.

the linear operator $\mathcal{L}_\beta : \psi' \mapsto \Delta\psi' - \beta\psi'$ is invertible in the subspace M_g for β in the vicinity of $-\lambda_1$. Thus, we get

$$\begin{cases} \psi'_0 = a_4 A^3 \mathcal{L}_\beta^{-1} P(e_1^3) =: \tilde{\psi}'_0 A^3, \\ q'_0 = a_4 A^3 \Delta\mathcal{L}_\beta^{-1} P(e_1^3) =: \tilde{q}'_0 A^3. \end{cases} \tag{2.13}$$

Now, we compute the asymptotic expansion of $G_0(A)$ using this perturbative result: substituting $q'_{eq} = \tilde{q}'_0 A^3 + o(A^3)$ into (2.11), we get

$$\begin{aligned} G_0(A) = -\frac{\beta}{2}\frac{h_1}{\lambda_1}A + \frac{1}{2}\left(1+\frac{\beta}{\lambda_1}\right)A^2 - \frac{a_4}{4}\langle e_1^4\rangle A^4 + \\ - \left[a_4 \int \tilde{q}'_0 e_1^3 + \frac{1}{2}\int \tilde{q}'^2_0 - \frac{\beta}{2}\int \tilde{\psi}'_0 \tilde{q}'_0 + \frac{a_6}{6}\langle e_1^6\rangle\right] A^6 + o(A^6). \end{aligned} \tag{2.14}$$

The parity of $G_0(A)$ is broken by $h_1 \neq 0$. Let us take $h_1 = 0$ until further notice. Note that up to quartic order, only mode e_1 contributes —the perturbation q'_{eq} contributes only from order 6 and up.

2.3.2 Tricritical point in the relaxed ensemble

In the more relaxed ensemble, we can predict the phase diagram in the vicinity of $(\beta, a_4) = (-\lambda_1, 0)$, which is a tricritical point, that is, a point where a second-order phase transition turns into a first-order one. Indeed, we have (2.14)

$$G_0(A) = \frac{1}{2}\left(1+\frac{\beta}{\lambda_1}\right)A^2 - \frac{a_4}{4}\langle e_1^4\rangle A^4 + o(A^5).$$

We can readily relate this expression to the normal form $s_{a,b}(m) = -m^6 - 3bm^4/2 - 3am^2$. This normal form is used in the context of constrained variational problems in [Bouchet and Barré, 2005]. Note that $s_{a,b}(m)$ is to be maximized, and hence, solutions are maximizers there. Then, the identification of coefficients is to be done between $s_{a,b}$ and $-G_0$. The typical behavior of $s_{a,b}$ and the associated transition lines are shown on Fig. 6 of this reference, reproduced below (our figure 2.1).

If $a > 0$ and $b > 0$, then $s_{a,b}$ is concave and there is only one maximizer, namely $m = 0$. We can see that $m = 0$ is always a critical point. The other possible critical points are such that $m^4 + bm^2 + a = 0$. For $b \geq 0$, a pair of maxima appears as a becomes negative, hence the second-order phase transition at $(a = 0, b \geq 0)$. A pair of minima and a pair of (local) maxima appear as $|b| \geq 2\sqrt{a}$ in the quarter plane $(a \geq 0, b \leq 0)$. There is a first-order phase transition when these maxima reach $s_{a,b}(m = 0) = 0$ as a and b decrease. It is found to occur for $16a = 3b^2$.

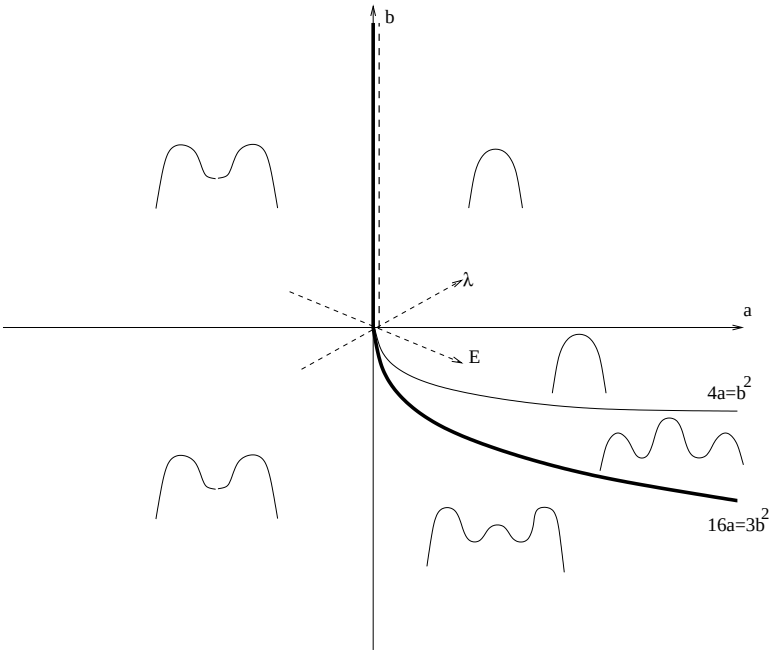

Figure 2.1: The 'canonical' tricritical point is at $(a, b) = (0, 0)$. The curve $(4a = b^2, b < 0)$ corresponds to the appearance of three local maxima. The bold curve $(16a = 3b^2, b < 0)$ is a first-order phase transition line. The bold-dashed curve is a second-order phase transition line. Here, 'canonical' simply refers to a relaxed ensemble with respect to a constrained one. Figure from [Bouchet and Barré, 2005].

Parameters a and b are identified with $(1+\frac{\beta}{\lambda_1})/6$ and $-a_4\langle e_1^4\rangle/6$ respectively. Therefore, $(\beta, a_4) = (-\lambda_1, 0)$ is a tricritical point in the grand canonical ensemble with $\gamma = 0$. The normal form sketched in the various areas of the phase diagram (Figure 2.1) should be identified with the opposite of $G_0(A)$. Critical points near $A = 0$ are found to be $A_0 = 0$ for all (β, a_4); in addition,

$$A_\pm = \pm\sqrt{\frac{\beta+\lambda_1}{\lambda_1 a_4\langle e_1^4\rangle}} + o\left(\left(1+\frac{\beta}{\lambda_1}\right)^{3/2}\right) \tag{2.15}$$

are critical points when $\beta + \lambda_1$ and a_4 have the same sign.

- For $\beta > -\lambda_1$, A_0 is a local minimum.
- For $\beta < -\lambda_1$ and $a_4 < 0$, $\{A_\pm\}$ are local minima originating from symmetry-breaking: there is a second-order phase transition at $(\beta = -\lambda_1, a_4 < 0)$.
- For $\beta > -\lambda_1$ and $a_4 > 0$, $\{A_\pm\}$ are local maxima. Then, minima far away from $A = 0$ have to exist, for $G_0(A)$ has a lower bound, owing to the convexity of $s(q)$. These, say, 'nonlocal' minima cannot be obtained perturbatively.
- For $\beta < -\lambda_1$ and $a_4 > 0$, A_0 is a local maxima; it is the only critical point obtained perturbatively. Solutions have to be the above-mentioned nonlocal minima. So there has to be a first-order phase transition at $\beta > -\lambda_1$, where the solution jumps from A_0 to the 'nonlocal' minima.

Since we also know (see section 2.1) that A_0 is the only solution for $\beta > -\lambda_1 s_m''$, the first-order phase transition is a line $\beta_c(a_4 > 0)$ such that $\beta_c(a_4) \in]-\lambda_1, -\lambda_1 s_m''(a_4)[$.

2.3.3 Ensemble inequivalence

We now argue that ensembles are equivalent for $a_4 \leq 0$. For $a_4 \leq 0$ ($b \geq 0$ in figure 2.1), relaxed and constrained ensembles are equivalent. The entire range of admissible energies ($E \geq 0$) is spanned by grand canonical solutions (with $\gamma = 0$), and $C_s(E)$ is convex. We recover the picture predicted in [Bouchet and Barré, 2005] (see bottom left-hand corner in figure 2.2). For $\beta \geq -\lambda_1$ ($a \geq 0$ in figure 2.1), the solution is on the ($E = 0$) axis. As $\beta \leq -\lambda_1$ ($a \leq 0$) decreases, the energy of the solutions increases and $C_s(E)$ increases with larger and larger slope (equal to $|\beta| = -\beta$). The caloric curve $\beta(E)$ is then monotonically decreasing. We have

$$\beta = -\frac{\partial C_s}{\partial E}.$$

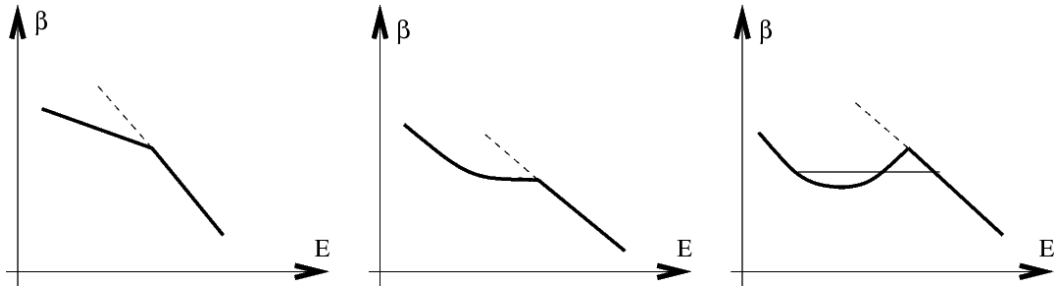

Figure 2.2: Caloric curves $\beta(E)$ as b changes sign. Lhs: $b > 0$, $\beta(E)$ is strictly decreasing. Centre: $b = 0$, $\beta(E)$ is monotonically decreasing. Rhs: $b < 0$, $\beta(E)$ is not monotonic, it is increasing on a certain interval. Figure extracted from [Bouchet and Barré, 2005].

Ensembles are inequivalent for $a_4 > 0$. For $a_4 > 0$ ($b < 0$ on Figure 2.1), relaxed and constrained ensembles are not equivalent. Keep in mind that our argument is valid for small nonlinearity. Let us denote by E_c the energy of the nontrivial (nonlocal) minima at the first-order phase transition (at $\beta = \beta_c$). For $E > E_c$, this pair of nonlocal minima are the solution to the relaxed (dual) problem. In the relaxed ensemble (grand canonical with $\gamma = 0$), for $a_4 > 0$, there is no solution in the energy range $]0, E_c[$.

For $E \in]0, E_c[$, solutions to the constrained problem are given by the critical points of $\mathcal{G}_0$ for which the energy continuously increases from 0 to E_c. Let E_{c_2} be the energy of the critical points (of $\mathcal{G}_0$, but just think of the normal form G_0) as they turn from local maxima into 'nonlocal' minima (then, $\beta := \beta_{c_2}$). Therefore, our statistical equilibria are the local maxima of G_0 for $E \in]0, E_{c_2}[$ (as β increases from $-\lambda_1$ to β_{c_2}). The statistical equilibria are the 'nonlocal' minima for $E \in]E_{c_2}, E_c[$ (as β decreases from β_{c_2} to β_c). The picture is that of the bottom right-hand corner of Figure 2.2, although the initial decrease of $\beta(E)$ shown there is absent in our case: our caloric curve $\beta(E)$ is increasing on $]0, E_{c_2}[$ and decreasing for $E \geq E_{c_2}$ (Figure 2.7). There are 'grand microcanonically' metastable equilibria (dashed line on Figure 2.2) corresponding to the local trivial minimum, for $(-\lambda_1 \leq \beta \leq \beta_c, E = 0)$.

To sum up, $C_s(E)$ has an inflexion point at $E = E_{c_2}$. $C_s(E)$ is convex only for $E \geq E_{c_2}$. Inside the inequivalence range $]0, E_c[$, $C_s(E)$ is concave for $E \in]0, E_{c_2}[$. Thus, states of energy $E \in]0, E_{c_2}[$, for $a_4 > 0$, have negative $-\partial\beta/\partial E$. The latter quantity is called the specific heat in analogy with usual thermodynamics.

2.3.4 Example

For the sake of illustration, we give an explicit example in this subsection. We carry out computations numerically, using a method of continuation, namely pseudo-arclength continuation (see appendix B). Our continuation parameters are the control parameters, β and a_4. We consider the example of a function $s(q)$ such that

$$s'(q) = \left(\frac{1}{3} - 2a_4\right)\tanh^{-1}(q) + \left(\frac{2}{3} + 2a_4\right)\sinh^{-1}(q)$$

with $a_4 \in [-1/3\,, 1/6]$ so that $s(q)$ is convex, as required, in a square domain ($\tau = 1$). The bound $a_4 = 1/6$ corresponds to $q = \sinh(\beta\psi)$ (two-level PV distribution, as mentioned in subsection 1.4.1, page 15), while $a_4 = -1/3$ corresponds to $q = \tanh(\beta\psi)$ (three-level PV distribution). We have $a_6 = a_4/4 - 7/60$.

We solve $\Delta\psi = (s')^{-1}(\beta\psi)$ (2.8) in ψ, that is, we compute the critical points of $\mathcal{G}_0$. Thinking of A as an order parameter, there is a fold bifurcation at $\beta = \beta_{c_2}(a_4)$. Pseudo-arclength continuation is well-suited for computing solution branches which undergo such bifurcations. Because of the parity symmetry, we may restrict our study to the domain $A \geq 0$. For a given $a_4 > 0$, A_+ (2.15) is the local maximum. If we increase β from $-\lambda_1^+$ up to β_{c_2}, we can bifurcate into the 'nonlocal' minimum of $G_0(A)$.

In a square domain $\mathcal{D}$, $\lambda_1 = 2\pi^2 \approx 19.7392$ and $e_1(x, y) = 2\sin(\pi x)\sin(\pi y)$. We start at $(\beta, a_4) = (-\lambda_1 + 0.006, 0.015)$ with solution guess

$$\psi = -\frac{A_+}{\lambda_1} e_1.$$

Let us denote by A_{comp} the scalar product of the (computed) solution q with mode e_1. $|A_{\text{comp}} - A_+|$ must scale like A_+^3. We check that we caught the proper solution branch by verifying this scaling relation. Figure 2.3 shows A_{comp} as a function of β, displaying the expected fold bifurcation.

We show the value of G_0 as a function of β on Figure 2.4. The first-order phase transition ($\beta = \beta_c$) is found as $G_0(A \neq 0)$ vanishes.

We compute the line $\beta_c(a_4)$ for $a_4 > 0$ using continuation on β and on a_4. Just like $16a = 3b^2$ is the first-order phase transition for the normal form $s_{a,b}$ (Figure 2.1), we recover the scaling

$$a_4 \sim \left(1 + \frac{\beta}{\lambda_1}\right)^{1/2}$$

on the first-order phase transition line, as shown Figure 2.5. The phase diagram in the grand canonical ensemble ($\gamma = 0$) is shown Figure 2.6.

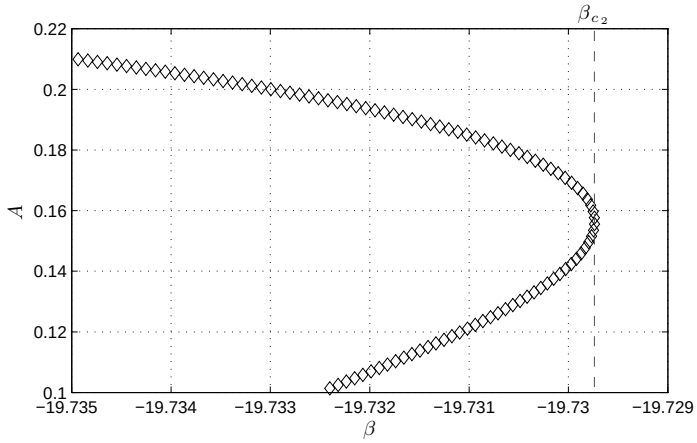

Figure 2.3: For positive nonlinearity ($a_4 > 0$), the normal form $G_0(A)$ has an inflection point at $\beta = \beta_{c_2}$ (two critical points appear). This shows as a fold (saddle-node) bifurcation in $A(\beta)$. We show here the numerical computation, using a pseudo-arclength continuation algorithm (appendix B), of $A(\beta)$ for $a_4 = 0.015$.

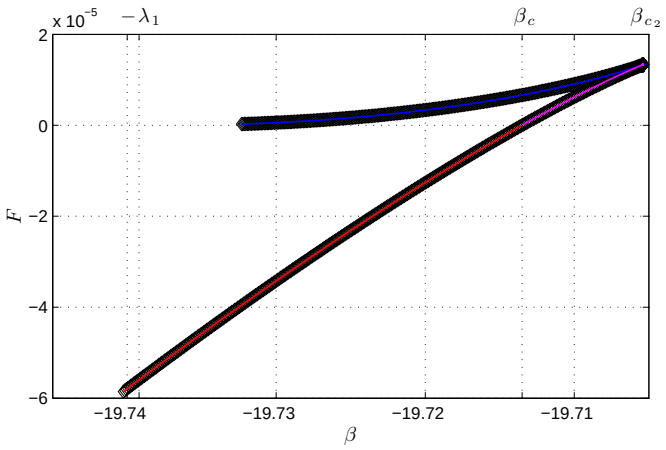

Figure 2.4: Here, we visualize the inflection point of $G_0(A) = F(A)$ at $\beta = \beta_{c_2}(a_4)$ in a way other than in figure 2.3. We plot $G_0(\beta)$ for $a_4 = 0.030$. The crossing of $G_0 = 0$ enables to determine the grand microcanonically stable equilibria (with $\gamma = 0$): decreasing β, at the crossing, the grand microcanonically metastable equilibrium (local minimum) at $A \neq 0$ exchanges its stability with the minimum at $A = 0$ ($G_0(0) = 0$).

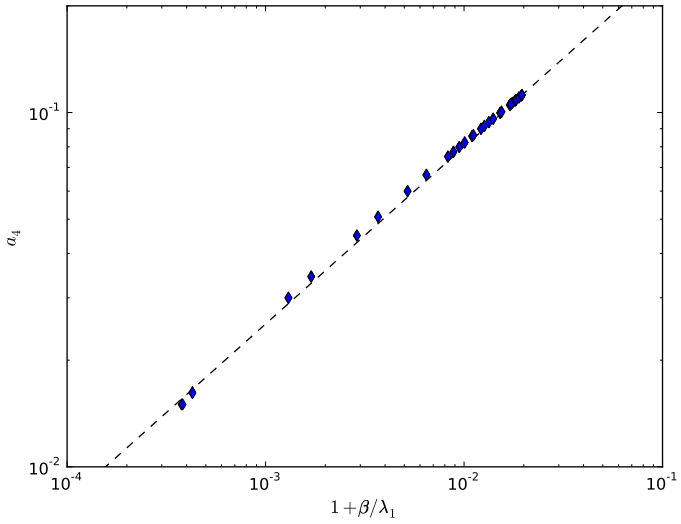

Figure 2.5: We verify a scaling relation between parameters β and a_4. We plot $\log(a_4)$ as a function of $\log(1 + \beta_c(a_4)/\lambda_1)$. The cyan and blue points, almost superimposing, are upper and lower bounds respectively, for the first-order phase transition line. The sets of points are well fitted by a straight line of slope 1/2.

2.3.5 General case: $\gamma \neq 0$ or $h_1 \neq 0$

We discuss the effect of having topography not orthogonal to the largest-scale mode e_1, and of having $\gamma \neq 0$: this is the general case for the grand canonical problem. Then, the normal form reads

$$G(A) = \left(\langle e_1\rangle\gamma - \frac{\beta}{2}\frac{h_1}{\lambda_1}\right) A + \frac{1}{2}\left(1 + \frac{\beta}{\lambda_1}\right) A^2 - \frac{a_4}{4}\langle e_1^4\rangle A^4 + \\ + O(A^3\gamma, A^6, A^3\gamma^3, A^4\gamma^2).$$

We see that the effect is that of breaking the $A \mapsto -A$ symmetry of $G(A)$, which is a normal form for the grand canonical potential (to be minimized). We may take $h_1 = 0$ without loss of generality, because the effect of $h_1 \neq 0$ is qualitatively encompassed by $\gamma \neq 0$.

Since the second-order phase transition we had originated from the $A \mapsto -A$ symmetry, we lose it in the general case $\gamma \neq 0$. Therefore, the tricritical point is lost. We are left with a critical point, when the first-order phase transition survives. It does so for small enough $|\gamma|$. It simply gets shifted in phase diagram (β, a_4): now, β_c depends on both a_4 and γ. We illustrate this, at given small $a_4 > 0$, in figure 2.6. In the grand canonical ensemble, we have a triple point in phase diagram (β, γ).

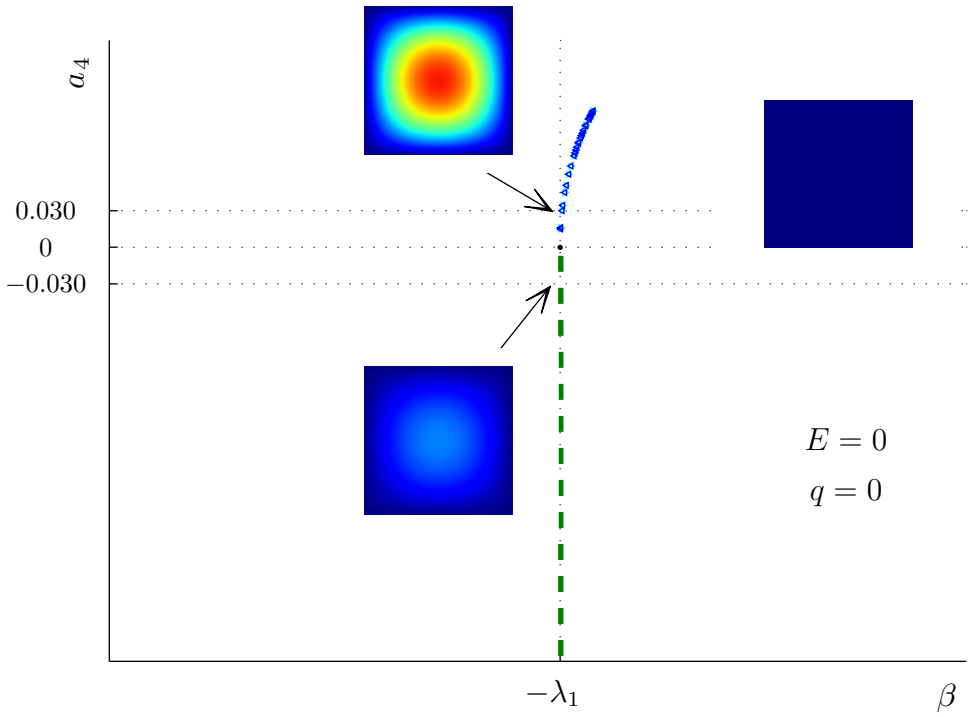

Figure 2.6: Phase diagram in the vicinity of the (grand canonical, $\gamma = 0$) tricritical point. The tricritical point is represented by the black dot at $(-\lambda_1, 0)$. The second-order phase transition is represented by the green dashed line at $(-\lambda_1, a_4 < 0)$. The first-order phase transition, at $(\beta_c(a_4), a_4 > 0)$, lies between the light blue dot series and the dark blue dot series (computed numerically). Insets show vorticity fields at $(\beta_c - (0.006 \pm 0.001), 0.030)$ and at $(-\lambda_1 - (0.006 \pm 0.001), -0.030)$; color scale ranges from 0 to 0.6 (from blue to red). As the phase transition line is crossed (from right to left), the flow acquires a structure. In the case of positive nonlinearity a_4, the change in configuration is abrupt (first-order phase transition). In the case of negative nonlinearity a_4, it is gradual (second-order phase transition).

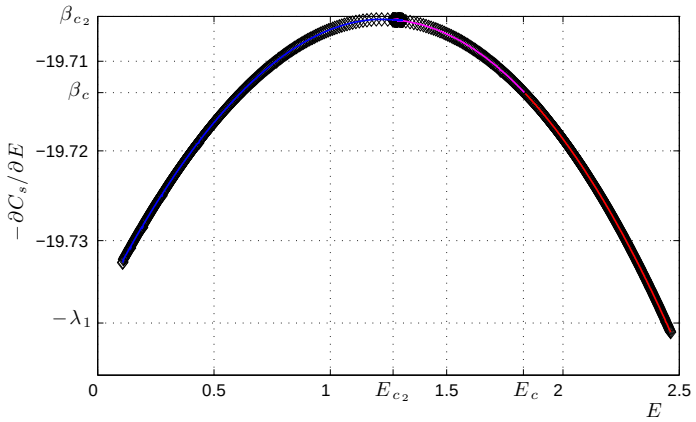

Figure 2.7: We plot the caloric curve $\beta(E)$ for $a_4 = 0.030$, to show ensemble inequivalence and negative specific heat. The relaxed and constrained ensembles are equivalent for $E \geq E_c$. In the range $0 < E < E_{c_2}$, the caloric curve is increasing, which means we have negative specific heat $-\partial\beta/\partial E = \partial^2 C_s/\partial E^2$.

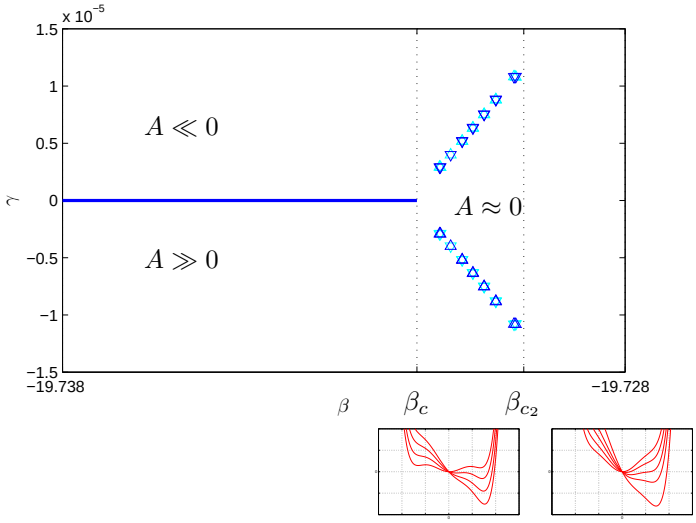

Figure 2.8: Phase diagram in dual space (β, γ) at $a_4 = 0.015$, displaying a first-order transition line at $\gamma = 0$ up to $\beta_c > -\lambda_1$, splitting into two first-order transition lines ($\gamma \mapsto -\gamma$ symmetry) for $\beta \in]\beta_c, \beta_{c_2}[$ (insets below the phase diagram show sketches of a sixth-order normal form for $G(A)$, when $a_4 > 0$: different curves on each diagram correspond to $\gamma = \{-0.001, -0.01, -0.02, -0.03, (-0.05)\}$ from top to bottom, when looked at in domain $A \geq 0$; lhs is for $-\lambda_1 < \beta < \beta_c$, rhs is for $\beta_c < \beta < \beta_{c_2}$). Values of A for the solution states are shown in the different regions of dual space.

2.4 Canonical solutions

We now consider the canonical variational problem:

$$F(\beta,\Gamma)=\min_{q}\left\{\mathcal{F}[q]=\int_{\mathcal{D}}s(q)+\beta\mathcal{E}[q]\mid \mathit{\Gamma}[q]=\Gamma\right\}. \tag{2.16}$$

It is the problem of minimizing the Helmholtz free energy with fixed circulation Γ. In the linear case ($a_4 = 0$), the constrained canonical problem was transformed into a tractable equivalent unconstrained problem [Venaille and Bouchet, 2009], for which the independent variables reduce to the set $\{q_i\}_{i\geq 2}$. This trick is still relevant here: since

$$\Gamma=\sum_i q_i\langle e_i\rangle\,, \tag{2.17}$$

we may decompose

$$q=\frac{\Gamma}{\langle e_1\rangle}e_1+\sum_{i\geq 2}q_i\left(e_i-\frac{\langle e_i\rangle}{\langle e_1\rangle}e_1\right)=:\frac{\Gamma}{\langle e_1\rangle}e_1+q_c\,, \tag{2.18}$$

so as to consider the minimization of $\mathcal{F}$ with respect to q_c:

$$\min_q\{\mathcal{F}[q]\mid \mathit{\Gamma}[q]=\Gamma\}=\min_{q_c}\left\{\mathcal{F}\left[\frac{\Gamma}{\langle e_1\rangle}e_1+q_c\right]\right\}. \tag{2.19}$$

Let $M_c=\{q_c,\text{ determined by }\{q_i\}_{i\geq 2}|\langle q_c\rangle=0\}$. M_c is a subspace complementary to the line spanned by e_1. M_c is a subspace orthogonal to 1. Canonical solutions live in M_c.

Note

$$s_\Gamma:=\min_{\mathbf{r}\in\mathcal{D}}\left\{\min_{q_c\in M_c}s''\left(\frac{\Gamma}{\langle e_1\rangle}e_1+q_c\right)\right\},$$

and consider $\delta^2\mathcal{F}$, the second-order variation of $\mathcal{F}$ with respect to q_c. In appendix 2.6, we prove a generalization of the Poincaré inequality in the subspace M_c, leading to $\delta^2\mathcal{F}\geq(s_\Gamma+\beta/\lambda_c)\langle\delta q_c^2\rangle$. We have introduced $\lambda_c:=\min\{\lambda_*,\lambda_1'\}$, corresponding to the vanishing of the quadratic part of $\mathcal{F}[\Gamma e_1/\langle e_1\rangle+q_c]$ (denoted by $\mathcal{Q}_\mathcal{F}$) at $\beta=-\lambda_c$. The space M_c is a direct sum of the subspace generated by eigenmodes of zero domain average, $\{e_i'\}_{i\geq 1}$, and the subspace generated by all the other modes. In the former subspace, $\mathcal{Q}_\mathcal{F}$ vanishes at $\beta=-\lambda_1'$ along e_1'. In the latter subspace, $\mathcal{Q}_\mathcal{F}$ vanishes at $\beta=-\lambda_*$ along e_*, where λ_* is the smallest value of $-\beta$ such that

$$\hat{f}(\beta)=-\sum_{i\geq 1}\frac{\lambda_i\langle e_i\rangle^2}{\lambda_i+\beta}=0. \tag{2.20}$$

The interested reader can find details about the above function in [Chavanis and Sommeria, 1996]. Anyhow, there are no phase transitions in the canonical ensemble for $\beta > -s_\Gamma \lambda_c$.

First of all, we restrict our study to the case of zero circulation ($\Gamma = 0$), bringing symmetry to our system. As noted earlier, systems with symmetries are well known to display a richer phenomenology of phase transitions.

2.4.1 Zero-circulation canonical solutions

Throughout this section, $\Gamma = 0$. We just showed that there is a unique trivial solution for $\beta > -s_{\Gamma=0}\lambda_c$. Keep in mind that $s_{\Gamma=0}$ depends on a_4. In particular, $s_{\Gamma=0} = 1$ if $a_{2n} \leq 0$ for all $n \geq 1$ (2.3). In the linear case ($a_4 = 0$), the solution is $q = 0$ at zero energy ($\beta > -\lambda_c$) and $q = \pm A e_c$ at $\beta = -\lambda_c$, $A > 0$ varying like the square root of E.

We introduce the mode e_c as follows: we refer to the case $\lambda_c = \lambda_* < \lambda_1'$ as case **i)**, and to the case $\lambda_c = \lambda_1' < \lambda_*$ as case **ii)**, consistently with [Venaille and Bouchet, 2009]. Likewise, the corresponding neutral direction of $\mathcal{Q}_\mathcal{F}$, denoted by e_c, is $e_c = \mathcal{N} e_*$ in case **i)**, and $e_c = e_1'$ in case **ii)**. $\mathcal{N}$ is simply a normalization factor (see appendix 2.7). Note that e_* gives the actual neutral direction of $\mathcal{Q}_\mathcal{F}$: $\mathcal{Q}_\mathcal{F}[e_*] = 0$ at $\beta = -\lambda_*$, i.e., e_* is actually proportional to the vorticity field at $(\beta = -\lambda_*, a_4 = 0)$ in case **i)**. We have $e_* = \Delta\psi_*$, where ψ_* was first introduced in [Chavanis and Sommeria, 1996].

In the weakly nonlinear case (small $|a_4|$), we obtain phase diagrams in the vicinity of $(\beta = -s_{\Gamma=0}\lambda_c, a_4 = 0)$ which are qualitatively the same as in section 2.3:

- for $a_4 \leq 0$, there is a second-order phase transition at $\beta = -s_{\Gamma=0}\lambda_c = -\lambda_c$: the solution goes continuously from a trivial state (zero energy, uniform vorticity) to a state dominated by e_c;
- for $a_4 > 0$, a_4 small enough, there is a first-order phase transition at $\beta = \beta_c(a_4) \in]-\lambda_c, -\lambda_c s_{\Gamma=0}[$: the solution goes discontinuously from a trivial state ($E = 0$) to a state dominated by e_c ($E = E_c(a_4) > 0$). The energy range accessible by canonical solutions (with $\Gamma = 0$) displays a gap $]0, E_c(a_4)[$.

In appendix 2.7, we give the technical details of this derivation. Because we linearize (2.8), it is natural to recover the same critical values and neutral directions as in the linear case ($a_4 = 0$), which was investigated by [Chavanis and Sommeria, 1996, Venaille and Bouchet, 2009].

We decompose $q = A e_c + \tilde{q}$, with $\tilde{q}$ a canonical solution such that $\langle \tilde{q} e_c \rangle = 0\}$, and introduce $F(A) = \min_{\tilde{q}|\langle \tilde{q} e_c \rangle = 0} \mathcal{F}[A, \tilde{q}]$. F has to be invariant under

$A \mapsto -A$, since $\pm A e_c$ are the two degenerate 'linear' solutions, and $s(q)$ is an even function. We find the following normal forms for describing the phase diagrams in each case, in the limits of low energy (small $|A|$):

i)

$$F(A) = \frac{1}{2}\frac{\langle e_*^2\rangle}{\langle e_*^2\rangle + 1}\left(s''(0) + \frac{\beta}{\lambda_*}\right)A^2 - \frac{\langle e_*^4\rangle}{(\langle e_*^2\rangle + 1)^2}\frac{a_4}{4}A^4 + o(A^5); \quad (2.21)$$

ii)

$$F(A) = \frac{1}{2}\left(s''(0) + \frac{\beta}{\lambda_1'}\right)A^2 - \frac{a_4}{4}\langle e_1'^4\rangle A^4 + o(A^5). \quad (2.22)$$

The prefactor of the quadratic term vanishes at $\beta = \beta_c := -s_{\Gamma=0}\lambda_c$, that of the quartic term at $a_4 = 0$. Since $s_{\Gamma=0} = 1$ for $a_4 = 0$, we have a tricritical point at $(\beta = -\lambda_c\,, a_4 = 0)$. Again, we refer the reader to section 2.3 and references therein for a general description of tricritical points.

Thus, results in the microcanonical ensemble (with $\Gamma = 0$) will be deduced the same way as in section 2.3: for $a_4 \leq 0$, no singularity of $C_s(E)$; for $a_4 > 0$, canonical spinodal point, negative specific heat for the lowest-energy states.

Because we are ultimately interested on the stable flow configurations, we describe qualitatively the modes at play. From (2.20), λ_* has to be found in the interval $]\lambda_1'', \lambda_2''[$. We use the notation λ_i'' (resp. λ_i') for the eigenvalue associated with eigenmode e_i'' (resp. e_i') such that $\langle e_i''\rangle \neq 0$ (resp. $\langle e_i'\rangle = 0$). We have $\lambda_1 = \lambda_1''$ and

$$e_1(x,y) = e_1''(x,y) = 2\sin(\pi x/\sqrt{\tau})\sin(\pi y\sqrt{\tau})$$

so that $\langle e_1\rangle \neq 0$. This eigenmode came into play in the grand canonical problem (section 2.3). It has the structure of a monopole. We have $e_2(x,y) = e_1'(x,y) = 2\sin(2\pi x/\sqrt{\tau})\sin(\pi y\sqrt{\tau})$ so that $\langle e_1'\rangle = 0$. This eigenmode has the structure of a dipole. It comes into play in the canonical problem in case **i)**. The mode e_* has zero domain average. In a square, it has a central monopole with counter-rotating cells at the corners (see Figure 2.10).

2.4.2 Low-circulation canonical solutions

For circulation Γ, the expression of the 'linear' solution ($a_4 = 0$) is

$$q(\beta > -\lambda_c, \Gamma) = -\frac{\Gamma}{\hat{f}(\beta)}\sum_{i\geq 1}\frac{\lambda_i''\langle e_i''\rangle}{\lambda_i'' + \beta}e_i'',$$
$$q(\beta = -\lambda_c, \Gamma) = -\frac{\Gamma}{\hat{f}(\beta)}\sum_{i\geq 1}\frac{\lambda_i''\langle e_i''\rangle}{\lambda_i'' + \beta}e_i'' \pm Ae_c, \quad (2.23)$$

where $\hat{f}(\beta)$ was defined in (2.20). We can see that a nonzero circulation will introduce a symmetry breaking into (2.21)–(2.22). We consider a small circulation $|\Gamma|$, for the description to remain close to the zero-circulation case. Also, this is required by the low-energy limit and the vicinity of $\beta = \beta_c$. Because of the $A \mapsto -A$ symmetry breaking, due to $\Gamma \neq 0$, the second-order phase transition disappears, leaving a phase diagram with a critical point.

Let us consider the phase space (β, a_4). Right to the first-order phase transition line, the solution is a weak monopole (the amplitude A of e_c is very close to 0). As the first-order phase transition line is crossed, $|A|$ jumps to a larger value, giving a different structure to the solution flow. For example, in case **ii)**, the transition to a dipolar contribution is abrupt in the upper half-plane, while it is smooth in the lower half-plane, with a canonical metastable state showing up (local minimum). The phase diagram for case **ii)** is shown Figure 2.9.

Figure 2.10 shows a schematic phase diagram for case **i)**. Equilibrium states of the left-hand side have different topologies, depending on the relative contributions of the monopole and e_*. The contribution of the monopole is determined by $|\Gamma|$, that of e_* by $|A|$. For certain values of Γ, there is a region in the left-hand-side neighbourhood of $(\beta, a_4) = (-\lambda_*, 0)$ where the two contributions have the same order of magnitude, yielding a tripolar structure for the equilibrium states. At large $|A|$ (i.e., very negative β, at given a_4), only e_* contributes to the structure of the equilibrium states.

2.4.3 Low-circulation microcanonical solutions

For $a_4 > 0$, the canonical first-order transition now takes place between two nontrivial states, both having nonzero energy. This shows in the caloric curve $\beta(E)$, with a decreasing part of $\beta(E)$ at lowest energies, before reaching the inequivalence range and the negative–heat-capacity states (see bottom right-hand corner of Figure 2.2). The picture is that of Figure 2 from [Bouchet and Barré, 2005], with a convexification singularity for $C_s(E)$.

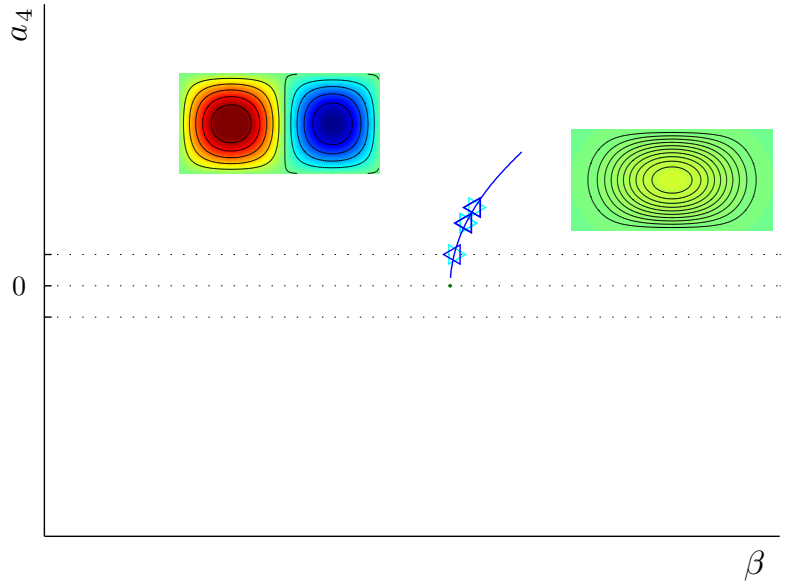

Figure 2.9: Phase diagram in the canonical ensemble (circulation equal to 0.01) for a rectangle of aspect ratio 2 (case **ii)**). The blue curve plots $a_4 = 0.13\sqrt{\lambda_1' + \beta}$; the 0.13 prefactor was chosen so as to fit the three first-order phase transition points computed from numerical continuation. This first-order phase transition line ends at a second-order phase transition point —green dot at $(-\lambda_1', 0)$. Insets show vorticity fields at $(\beta_c^-, 0.030)$ and at $(\beta_c^+, -0.030)$; color scale ranges from -0.5 to 0.5 (from blue to red); the black contours are ten iso-vorticity lines on each plot.

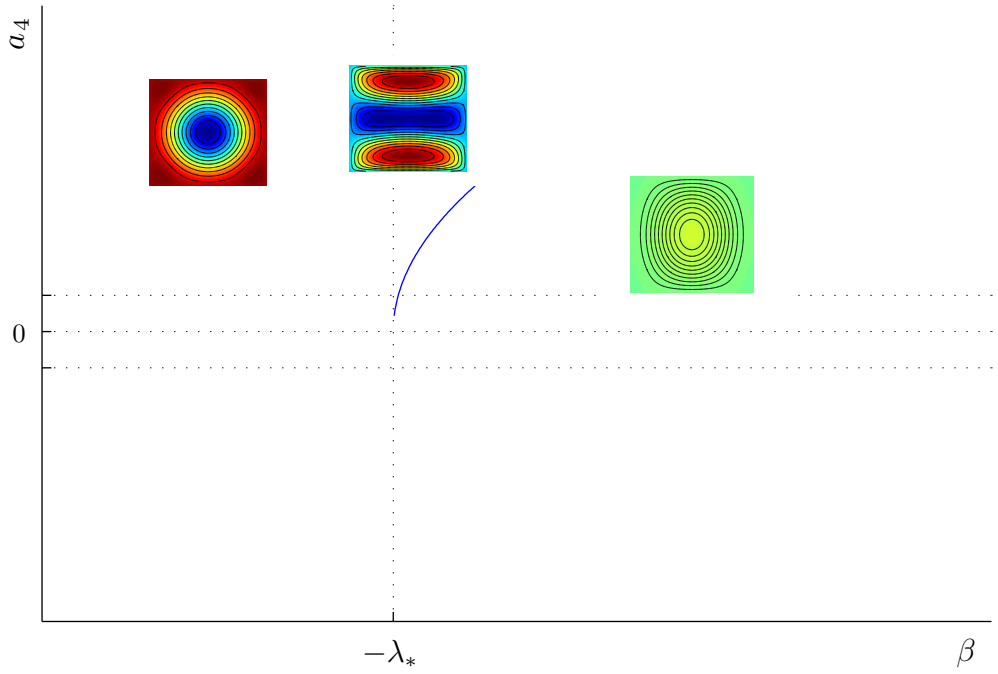

Figure 2.10: Schematic phase diagram in the canonical ensemble for a rectangle of aspect ratio 1.1 (case **i)**). The blue curve represents the first-order phase transition line. This first-order phase transition line ends at a (microcanonical) critical point, which is located above and close to the point $(-\lambda_*, 0)$. Insets show vorticity fields. The color scale shows negative (resp. positive) values in blue (resp. red); the black contours are ten iso-vorticity lines on each plot. From left to right: equilibrium dominated by e_*; equilibrium consisting of equivalent contributions from e_* and the low-circulation monopole; low-circulation monopole.

2.5 Appendix: Poincaré inequality

Let us introduce the orthonormal Laplacian eigenbasis $\{e_i(\mathbf{r})\}_{i\geq 1}$, i.e.,

$$\Delta e_i(\mathbf{r}) = -\lambda_i e_i(\mathbf{r}), \quad \int_{\mathcal{D}} e_i e_j = \delta_{ij}, \quad 0 < \lambda_1 < \lambda_2 < \dots, \tag{2.24}$$

with $e_i = 0$ on $\partial\mathcal{D}$ for all $i \geq 1$. All fields may be decomposed in this basis:

$$\begin{aligned} \delta\psi(\mathbf{r}) &= \sum_i \delta\psi_i e_i(\mathbf{r}), \\ \delta q(\mathbf{r}) &= \delta(\Delta\psi(\mathbf{r}) + h(\mathbf{r})) = \delta\Delta\psi(\mathbf{r}) = -\sum_i \lambda_i \delta\psi_i e_i(\mathbf{r}) \\ &= \sum_i \delta q_i e_i(\mathbf{r}). \end{aligned} \tag{2.25}$$

Therefore,

$$\int_{\mathcal{D}} \delta\psi\delta q = -\sum_i \frac{\delta q_i^2}{\lambda_i} \geq -\frac{1}{\lambda_1}\sum_i \delta q_i^2 = -\frac{1}{\lambda_1}\int_{\mathcal{D}} \delta q^2.$$

2.6 Appendix: Poincaré inequality in the canonical ensemble

In this appendix, we prove a generalization of the Poincaré inequality to the case with fixed circulation, i.e., in the subspace M_c.

Let $\tilde{q} \in M_c$. Then, $\delta\tilde{q} = \sum_{i\geq 2} \delta q_i \big(e_i - \frac{\langle e_i\rangle}{\langle e_1\rangle} e_1\big)$ and $\delta\tilde{\psi} = -\sum_{i\geq 2} \delta q_i \big(\frac{e_i}{\lambda_i} - \frac{\langle e_i\rangle}{\langle e_1\rangle}\frac{e_1}{\lambda_1}\big)$. We have

$$\begin{aligned} \int_{\mathcal{D}} \delta\tilde{q}^2 &= \sum_{i\geq 2} \delta q_i^2 + \frac{1}{\langle e_1\rangle^2}\sum_{i,j\geq 2} \langle e_i\rangle\langle e_j\rangle \delta q_i \delta q_j, \\ -\beta\int_{\mathcal{D}} \delta\tilde{\psi}\delta\tilde{q} &= \beta\sum_{i\geq 2} \frac{\delta q_i^2}{\lambda_i} + \frac{\beta}{\lambda_1\langle e_1\rangle^2}\sum_{i,j\geq 2} \langle e_i\rangle\langle e_j\rangle \delta q_i \delta q_j. \end{aligned}$$

Now,

$$\begin{aligned} \int_{\mathcal{D}} \delta\tilde{q}^2 - \beta\int_{\mathcal{D}} \delta\tilde{\psi}\delta\tilde{q} = &\sum_{i\geq 1} \left(1 + \frac{\beta}{\lambda_i'}\right) \delta q_i'^2 + \\ &+ \sum_{i,j\geq 2} \left[\delta_{ij}\left(1 + \frac{\beta}{\lambda_i''}\right) + \left(1 + \frac{\beta}{\lambda_1''}\right)\frac{\langle e_i''\rangle\langle e_j''\rangle}{\langle e_1\rangle^2}\right] \delta q_i'' \delta q_j'' \end{aligned}$$

is positive definite if and only if $\beta > -\min\{\lambda_1', \lambda^*\} = -\lambda_c$. See (2.20) for a definition of λ_*.

Since $-\beta \int_{\mathcal{D}} \delta\tilde{\psi}\delta\tilde{q} \geq -\beta/\beta \int_{\mathcal{D}} \delta\tilde{q}^2$ for all $\beta \in [-\lambda_c\,, 0[$, then the best (greatest) lower bound that we can obtain is

$$-\beta \int_{\mathcal{D}} \delta\tilde{\psi}\delta\tilde{q} \geq \frac{\beta}{\lambda_c} \int_{\mathcal{D}} \delta\tilde{q}^2.$$

2.7 Appendix: Lyapunov–Schmidt reduction

In this appendix, we derive the phase diagram for the canonical solutions at zero circulation. Consider the following canonical variational problem (let us drop the $\mathcal{D}$ subscript in the integral notation):

$$\min_q = \left\{ \int s(q) - \frac{\beta}{2} \int q\psi \mid \int q = 0 \right\}.$$

A critical point is q such that

$$\int s'(q)\delta q - \beta \int \psi\delta q = 0 \text{ for all } \delta q \in \mathcal{Q} \text{ such that } \int \delta q = 0,$$

or, equivalently, using the Lagrange multiplier rule,

$$\tilde{f}(q, \gamma; \beta) := \begin{cases} \tilde{f}_1(q, \gamma; \beta) = s'(q) - \beta\psi + \gamma = 0, \\ \tilde{f}_2(q, \gamma; \beta) = \int q = 0, \end{cases} \tag{2.26}$$

where $\gamma \in \mathbb{R}$ is the Lagrange parameter associated with the conservation of (zero) circulation.

The system (2.26) is to be solved in the variables (q, γ), while the bifurcation parameter is $\beta \in \mathbb{R}$. Let us denote the variable by $X = (q, \gamma)$ and the variable space by E. Please do not get this notation mixed up with the energy, which we never mention in this appendix. $\tilde{f}$ maps $E \times \mathbb{R}$ into E. For any $\beta \in \mathbb{R}$, we have the trivial solution $X = 0$. We want to determine the bifurcations, which the system may undergo, from this trivial solution.

For a bifurcation to occur, the Jacobian matrix of (2.26) has to become singular, i.e., there must exist a nontrivial vector $u_c = (q_c, \gamma_c) \in E$ such that $D_X\tilde{f}(0; \beta)[u_c] = 0$ for a certain $\beta = \beta_c$. We have

$$D_X\tilde{f}(0; \beta)[u_c] = \begin{pmatrix} s''(0)\delta q_c - \beta\delta\psi_c + \delta\gamma_c \\ \int \delta q_c \end{pmatrix} \in E, \tag{2.27}$$

with $\Delta\psi_c = q_c$. Let us endow E with the scalar product $(\cdot|\cdot)$, defined as follows: for $X_k = (q_k, \gamma_k) \in E$, $k = \{1, 2\}$,

$$(X_1|X_2) = \langle q_1 q_2 \rangle + \gamma_1\gamma_2 = \int (q_1 q_2) + \gamma_1\gamma_2. \tag{2.28}$$

A complete orthonormal basis for E is $\{u_i\}_{i\geq 0}$, where $u_0 = (0, 1)$ and $u_i = (e_i, 0)$ for $i \geq 1$. $D_X\tilde{f}(0;\beta)$ is self-adjoint since

$$\begin{aligned}(X_1|D_X\tilde{f}(0;\beta)[X_2]) &= \int q_1(s''(0)\delta q_2 - \beta\delta\psi_2 + \delta\gamma_2) + \gamma_1 \int \delta q_2 \\ &= s''(0)\langle q_1\delta q_2\rangle - \beta\langle q_1\delta\psi_2\rangle + \langle q_1\delta\gamma_2\rangle + \langle\gamma_1\delta q_2\rangle \\ &= (D_X\tilde{f}(0;\beta)[X_1]|X_2),\end{aligned}$$

so $D_X\tilde{f}(0;\beta)$ may be diagonalized in $\{u_i\}_{i\geq 0}$, and its eigenvalues are real. The equalities $\langle q_1\delta q_2\rangle = \langle q_2\delta q_1\rangle$, $\langle q_1\delta\psi_2\rangle = \langle q_2\delta\psi_1\rangle$, and so on, come from the Euclidean-ness of E. Indeed, let $k = \{1, 2\}$ and $q_k = \sum_i q_{k,i}e_i$. The tangent vector $\delta q_k = \sum_i \delta q_{k,i}e_i$ is along q_k, so for all $i \geq 1$, $\delta q_{k,i} = a_k q_{k,i}$. Now, $a_1 = a_2$ because q_1 and q_2, belonging to the same space, must be mapped onto their tangent space with the same coefficient. Decomposing the variables in the Laplacian eigenbasis $\{e_i\}_{i\geq 1}$,

$$\delta q = \sum_{i\geq 1} \delta q_i e_i \ ; \quad \delta\psi = -\sum_{i\geq 1} \frac{\delta q_i}{\lambda_i} e_i \ ; \quad \delta\gamma = \delta\gamma \sum_{i\geq 1} \langle e_i\rangle e_i, \tag{2.29}$$

it is readily seen that u_c is either along $(e'_i, 0)$ at $\beta = -s''(0)\lambda'_i$, or along $(e_*, 1)$ at $\beta = -s''(0)\lambda_*$. Indeed, we identify

$$\delta q_i = -\delta\gamma \frac{\lambda_i\langle e_i\rangle}{s''(0)\lambda_i + \beta} \quad \text{for all } i \geq 1,$$

and we require

$$\langle\delta q\rangle = \sum_{i\geq 1} -\delta\gamma \frac{\lambda_i\langle e_i\rangle^2}{s''(0)\lambda_i + \beta} = \frac{\delta\gamma}{s''(0)} \hat{f}\left(\frac{\beta}{s''(0)}\right) = 0,$$

where the $\hat{f}$ function is that of (2.20). We have noted

$$e_* := -\sum_{i\geq 1} \frac{\lambda_i\langle e_i\rangle}{s''(0)\lambda_i - \lambda_*} e_i.$$

Note again that δX belongs to the tangent space of E, but E is Euclidean, so $\{X \in E \mid \delta X = au_c, a \in \mathbb{R}\} = \{X \in E \mid X = au_c, a \in \mathbb{R}\}$.

The first bifurcation, and hence, phase transition, to occur is found at $\beta_c = -s''(0)\lambda_c$ (considering a decreasing β). Let $u_c = \mathcal{N}(e_*, 1)$ in case **i)**, $u_c = (e_1', 0)$ in case **ii)**. $\mathcal{N}$ is the normalization factor $(\langle (e_*)^2 \rangle + 1)^{-1/2}$.

Let us denote the operator $D_X \tilde{f}(0; \beta_c)$ by J. J maps E into E. Let E_c be the null space (kernel) of J. It is the subspace generated by u_c; it is 1-dimensional in E (it is a line). Let us show that the range of J is orthogonal to E_c. This is the case if and only if $(Y|u_c) = 0$ for any Y in the range of J.

i) Let us show that

$$\langle (s''(0)\delta q - \beta_c \delta\psi + \delta\gamma)e_* \rangle + \langle \delta q \rangle = 0.$$

Let ψ_* be the vector such that $\Delta\psi_* = e_*$ and $\psi_* = 0$ on $\partial\mathcal{D}$. We have $\langle \psi e_* \rangle = \langle q\psi_* \rangle$ (straightforward when decomposing in the Laplacian eigenbasis), so

$$\langle (s''(0)\delta q - \beta_c \delta\psi + \delta\gamma)e_* \rangle + \langle \delta q \rangle = \langle (s''(0)e_* - \beta_c \delta\psi_* + 1)\delta q \rangle = 0. \tag{2.30}$$

Indeed, the last parenthesed term is the first component of Ju_c ($Ju_c = 0$).

ii) Let us show that

$$\langle (s''(0)\delta q - \beta_c \delta\psi + \delta\gamma)e_1' \rangle = 0.$$

We have $\beta_c = -s''(0)\lambda_1'$, so

$$\langle (s''(0)\delta q - \beta_c \delta\psi + \delta\gamma)e_1' \rangle = \left\langle \left(s''(0)e_1' + \frac{\beta_c}{\lambda_1'} e_1' \right) \delta q \right\rangle = 0.$$

Therefore, the kernel of J is orthogonal to the range of J. We can then apply classical bifurcation theorems [Chow and Hale, 1982]. Let E_1 be the orthogonal complementary subspace to E_c in E (E_1 is the range of J). There exist $\tilde{X}(A, \beta) \in E_1$ ($A \in \mathbb{R}$) such that $\tilde{X}(0, \beta_c) = 0$ and $\frac{\partial \tilde{X}}{\partial A}(0, \beta_c) = 0$, so that we may decompose the variable X as follows:

$$X = X(A, \beta) = Au_c + \tilde{X}(A, \beta) = Au_c + \big(\tilde{q}(A, \beta), \tilde{\gamma}(A, \beta)\big). \tag{2.31}$$

We will also use the notation $\tilde{\psi}$ for the vector in $\mathcal{Q}$ such that $\Delta\tilde{\psi} = \tilde{q}$. Besides, there exists a projector $Q : E \to E_1$, $QX = X - (X|u_c)u_c$ such that $Q\tilde{f}(X; \beta) = Q\tilde{f}(Au_c + \tilde{X}; \beta) = 0$ for all $A, \beta \in \mathbb{R}$. Now,

$$\tilde{f}(Au_c + \tilde{X}; \beta) = Q\tilde{f}(Au_c + \tilde{X}; \beta) + (\tilde{f}(Au_c + \tilde{X}; \beta)|u_c)u_c$$

so the bifurcation problem (2.26) is equivalent to (reduces to) the scalar problem

$$h(A,\beta) := (\tilde{f}(Au_c + \tilde{X}(A,\beta);\beta)|u_c) = 0$$

(Liapunov–Schmidt reduction). From the normalization of u_c, we have $f(Au_c + \tilde{X};\beta) = h(A,\beta)u_c$. Explicitly, this writes

i)

$$\begin{cases} s'(A\mathcal{N}e_* + \tilde{q}) - \beta(A\mathcal{N}\psi_* + \tilde{\psi}) + A\mathcal{N} + \tilde{\gamma} = \mathcal{N}h(A,\beta)e_*, \\ \int A\mathcal{N}e_* + \tilde{q} = \mathcal{N}h(A,\beta); \end{cases} \tag{2.32}$$

ii)

$$\begin{cases} s'(Ae_1' + \tilde{q}) + \beta(\dfrac{A}{\lambda_1'}e_1' - \tilde{\psi}) + \tilde{\gamma} = h(A,\beta)e_1', \\ \int Ae_1' + \tilde{q} = 0. \end{cases} \tag{2.33}$$

We may notice that for $(A,\tilde{X},h)$ solution, $(-A,-\tilde{X},-h)$ is also a solution, so that h and $\tilde{X}$ are odd in A. Therefore $\frac{\partial^2 h}{\partial A^2}$ and $\frac{\partial^2 \tilde{X}}{\partial A^2}$ are also odd in A, and so on.

We know that F is even in A. We have $F(A=0)=0$, so the lowest order of F is quadratic. We determine the successive coefficients (of each power of A) in F from its successive derivatives w.r.t. A, evaluated at $A=0$. Because $\langle \tilde{q}e_c\rangle = 0$, we also have $\langle \frac{\partial \tilde{q}}{\partial A}e_c\rangle = 0$, and so on with all the derivatives with respect to the scalar A. All these properties lead to drastic simplifications in the computation of $\frac{\mathrm{d}^2F}{\mathrm{d}A^2}(A=0)$ and $\frac{\mathrm{d}^4F}{\mathrm{d}A^4}(A=0)$, leaving us with (2.21)-(2.22).

Bifurcation-wise, it is shown that

$$h(0,\beta_c) = 0, \quad \frac{\partial h}{\partial A}(0,\beta_c) = 0, \quad \frac{\partial^2 h}{\partial A^2}(0,\beta_c) = 0,$$

but

$$\frac{\partial^3 h}{\partial A^3}(0,\beta_c) \neq 0; \quad \operatorname{sgn}\left(\frac{\partial^3 h}{\partial A^3}(0,\beta_c)\right) = -\operatorname{sgn}(a_4).$$

Therefore, the bifurcation will be determined (qualitatively) by the cubic nonlinearity of h in A (corresponding to the quartic nonlinearity of F in A, in the present paper). The sign of a_4, i.e., the parameter for the nonlinearity in the $q-\psi$ relationship, determines the type of bifurcation at play:

- If $a_4 < 0$, the pitchfork bifurcation is supercritical, giving a second-order phase transition.

– If $a_4 > 0$, the pitchfork bifurcation is subcritical, giving a first-order phase transition (the higher-order nonlinearities yielding nontrivial branches beyond $\beta = \beta_c$, at $\beta < \beta_c$).

Chapter 3

Statistical equilibria over topography in a channel

Contents

3.1 Introduction

In this chapter, we consider the linear relationship of the previous chapter (q–ψ relationship), in the case of a doubly connected domain. For instance, the domain is a periodic channel, or it is an annulus. This kind of topology is relevant to many problems in oceanography, when the domain is either a latitude band, or a basin with an island. It also corresponds to the geometry of rotating-tank experiments, such as in [Tian et al., 2001]. We take the topography to be nonzero, with variations in the zonal (or longitudinal, or azimuthal) direction.

In section 3.2, we specify the boundary conditions for this problem: we use the model proposed by [McWilliams, 1977]. The double-connectedness of the domain brings in a new conserved quantity, the circulation (of velocity) being conserved along each connected piece of boundary. We thus have two different conserved circulations, referred to as inner and outer circulations (we explicit the naming convention in the next section). Their sum is the total circulation Γ. One of the two circulations, say, the outer one, is absorbed into the boundary condition, appearing as an external control parameter Γ_1.

Thus, we extend the results of [Venaille and Bouchet, 2009] to the case of a doubly connected domain. It appears that a nonzero Γ_1 breaks the $\Gamma \mapsto -\Gamma$ symmetry of the system. Because the phase transitions predicted in simply connected domains (chapter 2) are generic, their existence and nature are not affected by the value of Γ_1. We find that the $\Gamma \mapsto -\Gamma$ symmetry breaking leads to a loss of stability of some of the metastable states (in the canonical ensemble, maybe not in the microcanonical one). Nonzero topography, although preserving the $\Gamma \mapsto -\Gamma$ symmetry, is shown to have the same effect on these canonically metastable equilibria.

For Γ_1 in a certain range, two qualitatively different equilibria are identified, on either side of a first-order phase transition line. One is topography-dominated: streamlines roughly follow topography contours. The other flow structure has a much stronger azimuthal/zonal contribution. Such states have geophysical analogues, as in atmospheric 'blocking' or in the Kuroshio 'meanders'. We recall that the bistability displayed by the Kuroshio —between a meandery state and a jet-like state— is a major motivation for our studies. To conclude, we propose a picture for the relevance of (inviscid) statistical equilibria to real (viscous) flows.

3.2 Barotropic quasi-geostrophic equations in a channel or annulus

The problem has the same governing equations as usual. We still consider the barotropic quasi-geostrophic model, in the inertial limit of no dissipation nor forcing:

$$\frac{\partial q}{\partial t} + \mathbf{u} \cdot \nabla q = 0. \tag{3.1}$$

As in the previous chapter, let all quantities be nondimensional. Again, the streamfunction ψ is introduced so that the geostrophic velocity field $\mathbf{u} = \mathbf{e}_z \times \nabla\psi$. The potential vorticity reads $q = \Delta\psi + h$, with h an equivalent topography.

Now, $\mathcal{D}$ is a doubly connected domain. We denote its boundary by $\partial\mathcal{D} = \partial\mathcal{D}_1 \cup \partial\mathcal{D}_2$. Let us focus on the following two simplest doubly connected domains:

– The zonal channel $\mathcal{D} = \{(x, y) \in [0, L_x[\times[0, L_y]\}$, with L_x-periodicity in x; the aspect ratio is $\tau := L_x/L_y \geq 1$; $\partial\mathcal{D}_1$ is the northern boundary ($y = L_y$), $\partial\mathcal{D}_2$ the southern boundary ($y = 0$). The zonal (or longitudinal) direction is along x.

– The annulus $\mathcal{D} = \{(r, \theta) \in [R_1, R_2] \times [0, 2\pi[\}$; an equivalent aspect ratio can be defined as $\pi(R_1 + R_2)/(R_2 - R_1) > \pi$; $\partial\mathcal{D}_1$ is the inner boundary ($r = R_1$), $\partial\mathcal{D}_2$ the outer boundary ($r = R_2$). This domain is represented on Figure 3.1.

Because the flow is inviscid, the boundary condition is just the kinematic condition of no normal velocity, i.e., the free-slip boundary condition:

$$\begin{cases} \psi = \psi_1(t) & \text{on } \partial\mathcal{D}_1, \\ \psi = \psi_2(t) & \text{on } \partial\mathcal{D}_2. \end{cases} \tag{3.2}$$

The difference $\psi_2 - \psi_1$ is the net zonal/azimuthal transport[1] at a given time. We restrict our attention to the rigid-lid case (see appendix A), so our stream-function is defined only up to a function of time [Graef and Müller, 1996]. Let us take $\psi_2 = 0$ for all times. We now show that ψ_1 can be determined from the circulation constraint.

Without loss of generality, we take h such that $\int_{\mathcal{D}} h = 0$, so the circulation

$$\Gamma = \int_{\partial\mathcal{D}} \mathbf{u} \cdot \mathrm{d}\mathbf{l} = \int_{\partial\mathcal{D}} \mathrm{d}l \ (\nabla\psi \cdot \mathbf{n}) = \int_{\mathcal{D}} \Delta\psi = \int_{\mathcal{D}} q.$$

$\mathbf{n}$ denotes the outward vector element normal to the integration contour and $\mathbf{l}$ is defined by $\mathbf{l} = \mathbf{e}_z \times \mathbf{n}$. The scalar element $\mathrm{d}l$ runs along $\partial\mathcal{D}$ in the positive direction (see Figure 3.1).

Γ is the total circulation; the circulations along $\partial\mathcal{D}_1$ and $\partial\mathcal{D}_2$, respectively, Γ_1 and Γ_2, are defined in the most natural way:

$$\Gamma_1 = \oint_{\partial\mathcal{D}_1} \mathrm{d}l \ (\nabla\psi \cdot \mathbf{n}) \ ; \quad \Gamma_2 = \oint_{\partial\mathcal{D}_2} \mathrm{d}l \ (\nabla\psi \cdot \mathbf{n}) \ ; \quad \Gamma = \Gamma_1 + \Gamma_2.$$

As in chapter 2, steady states of (3.1) verify

$$q = \Delta\psi + h = f(\psi), \tag{3.3}$$

where f may be any function. In this chapter, we restrict our attention to the case of f linear. Then, the elliptic equation (3.3) with nonhomogeneous Dirichlet boundary conditions (3.2) (with $\psi_2 = 0$) has a unique solution, which

[1] This is readily seen in the Cartesian co-ordinate system of the zonal channel, where $\mathbf{u} = (u_x, u_y) = (-\frac{\partial\psi}{\partial y}, \frac{\partial\psi}{\partial x})$. We have

$$\psi_2 - \psi_1 = -\int_0^{L_y} \mathrm{d}y \ \frac{\partial\psi}{\partial y} = \int_0^{L_y} \mathrm{d}y \ u_x.$$

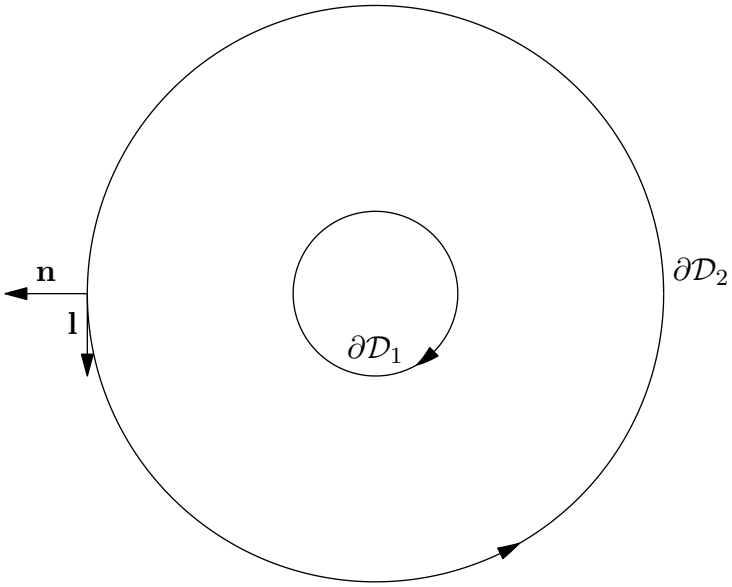

Figure 3.1: Annular geometry for $\mathcal{D}$, showing the inner boundary $\partial\mathcal{D}_1$ and outer boundary $\partial\mathcal{D}_2$ with their respective positive orientations (arrows). The relative positions of the outward normal $\mathbf{n}$ and tangent vector $\mathbf{l}$ are also shown.

can be computed analytically [Courant and Hilbert, 1953, on the vibrating membrane]. Solving (3.3) is equivalent to solving

$$q = \Delta\psi' + h = f(\psi', \psi_1), \tag{3.4}$$

with

$$\psi' = 0 \quad \text{on } \partial\mathcal{D},$$

where $\psi = \psi' + \psi_1\tilde{y}$ and $\tilde{y}$ is a meridional/radial coordinate such that $\Delta\tilde{y} = 0$, $\tilde{y} = 0$ on $\partial\mathcal{D}_2$, and $\tilde{y} = 1$ on $\partial\mathcal{D}_1$. Explicitly, we have

- for the zonal channel, $\tilde{y} = y/L_y$;
- for the annulus, $\tilde{y} = (\log r - \log R_2)/(\log R_1 - \log R_2)$.

The transport ψ_1 has to be determined from conservation laws. We have conservation of total circulation,

$$\frac{\mathrm{d}\Gamma}{\mathrm{d}t} = 0.$$

The additional constraint is provided by the conservation of circulation along each connected piece of boundary, which is a theorem in the shallow water model [Pedlosky, 1987, 3.5]. We have

$$\frac{\mathrm{d}\Gamma_1}{\mathrm{d}t} = 0, \tag{3.5}$$

and we treat Γ_1 as an external parameter. We arbitrarily use Γ_1 to set the boundary conditions.

Let us consider specifically the zonal channel domain, in order to give explicit expressions. Through (3.5), we have

$$\psi_1 = \psi_1(\psi', \Gamma_1) = \frac{1}{\tau}\left(\Gamma_1 - \int_0^{L_x} \mathrm{d}x\ \frac{\partial \psi'}{\partial y}(x, L_y)\right),$$

where τ is the aspect ratio L_x/L_y. From this discussion, we conclude that ψ (or, equivalently, ψ' and ψ_1) is uniquely determined from the knowledge of q and Γ_1.

3.3 Expression of energy

We devote a subsection to the expression of energy because the double-connectedness of the domain brings some subtleties into play. The kinetic energy reads

$$\mathcal{E}[\psi] = \frac{1}{2}\int_{\mathcal{D}} |\nabla\psi|^2 = \frac{1}{2}\int_{\partial\mathcal{D}} \mathrm{d}l\ \psi(\nabla\psi\cdot\mathbf{n}) - \frac{1}{2}\int_{\mathcal{D}} \psi\Delta\psi,$$

where use has been made of the divergence theorem. We obtain the energy as a functional of q parameterized by Γ_1:

$$\mathcal{E}_{\Gamma_1}[q] = \frac{\Gamma_1}{2}\psi_1(q,\Gamma_1) - \frac{1}{2}\int_{\mathcal{D}} (q-h)\,\psi(q,\Gamma_1). \tag{3.6}$$

We decompose the different fields in the Laplacian eigenbasis $\{e_i\}_{i\geq 1}$ —for all $i,j\geq 1$, $\Delta e_i = -\lambda_i e_i$, $\langle e_i e_j\rangle = \int_{\mathcal{D}} e_i e_j = \delta_{ij}$, and $e_i = 0$ on $\partial\mathcal{D}$. We use

$$\begin{aligned} q &= \sum_i q_i e_i, \\ h &= \sum_i h_i e_i, \\ \psi' &= \sum_i \psi_i e_i = \sum_i \frac{h_i - q_i}{\lambda_i} e_i, \end{aligned}$$

to express ψ_1 as a function of q parameterized by Γ_1:

$$\psi_1(q,\Gamma_1) = \frac{\Gamma_1}{\tau} - \frac{1}{\tau}\sum_i \frac{h_i - q_i}{\lambda_i}\int_0^{L_x} \mathrm{d}x\ \left.\frac{\partial e_i}{\partial y}\right|_{y=L_y}.$$

In the above and in the following, we consider the channel geometry. Then, from (3.6),

$$\begin{aligned}\mathcal{E}_{\Gamma_1}[q] =& \frac{\Gamma_1^2}{2\tau} - \frac{\Gamma_1}{2\tau}\sum_i \frac{h_i - q_i}{\lambda_i}\int_0^{L_x} \mathrm{d}x \left.\frac{\partial e_i}{\partial y}\right|_{y=L_y} + \\ &+ \frac{1}{2}\sum_i \frac{(q_i-h_i)^2}{\lambda_i} - \frac{\Gamma_1}{2L_x}\sum_i (q_i - h_i)\langle y e_i\rangle + \\ &- \frac{\Gamma_1}{2L_x}\sum_{i,j}\langle y e_i\rangle (q_i - h_i)\frac{q_j - h_j}{\lambda_j}\int_0^{L_x}\mathrm{d}x \left.\frac{\partial e_j}{\partial y}\right|_{y=L_y}.\end{aligned}$$

For ease of notation, let us introduce

$$C_i := \int_0^{L_x} \mathrm{d}x \left.\frac{\partial e_i}{\partial y}\right|_{y=L_y}$$

for all $i \geq 1$. Remark that considering nonzero values of Γ_1 brings in a bunch of additional terms, both linear and quadratic in q. The particular case $\Gamma_1 = 0$ amounts to considering a simply connected domain: then, computations and phase diagrams are those found in [Venaille and Bouchet, 2009].

The other functionals at play have no explicit dependence on Γ_1:

$$\begin{aligned}\frac{1}{2}\langle q^2\rangle =& \frac{1}{2}\sum_i q_i^2, \\ \mathit{\Gamma}[q] =& \sum_i q_i \langle e_i\rangle\end{aligned}$$

express the lowest-order (quadratic) part of $\int_{\mathcal{D}} s(q)$ and the circulation, respectively. In the following, we restrict ourself to $s(q) = q^2/2$, yielding a linear q–ψ relationship.

3.4 Variational problem

The microcanonical variational problem

$$C_{s,\Gamma_1}(E,\Gamma) = \min_q \left\{ \int_{\mathcal{D}} s(q) \mid \mathcal{E}_{\Gamma_1}[q] = E\,, \mathit{\Gamma}[q] = \Gamma \right\} \tag{3.7}$$

has now parameterization by Γ_1 (through energy). We purposefully consider an irregular enough topography, i.e., with no L_x-periodicity in x in the channel case, with θ-dependence in the annulus case. This way, there are nonvanishing h_i for nonzonal e_i modes. Also, there is no conservation of linear or angular momentum, in spite of the symmetry of $\mathcal{D}$.

As in chapter 2, we begin with the grand canonical variational problem, i.e., the problem of minimizing $\mathcal{G}_{\Gamma_1}[q] = \int_{\mathcal{D}} s(q) + \beta\mathcal{E}_{\Gamma_1}[q] + \gamma\mathit{\Gamma}[q]$. Constant terms do not affect the minimization. So, for convenience, we write directly the first-order variations of $\mathcal{G}_{\Gamma_1}[q]$:

$$\begin{aligned}\delta\mathcal{G}_{\Gamma_1} = &\sum_i q_i\delta q_i + \beta\frac{\Gamma_1}{2\tau}\sum_i \frac{C_i}{\lambda_i}\delta q_i + \\ &+ \beta\sum_i \frac{(q_i - h_i)}{\lambda_i}\delta q_i - \beta\frac{\Gamma_1}{2L_x}\sum_i \langle ye_i\rangle\delta q_i + \\ &- \beta\frac{\Gamma_1}{2L_x}\sum_{i,j}\langle ye_i\rangle\frac{C_j}{\lambda_j}\left(q_i\delta q_j - h_i\delta q_j - h_j\delta q_i\right) + \\ &+ \gamma\sum_i \langle e_i\rangle\delta q_i\end{aligned}$$

Factorizing,

$$\begin{aligned}\delta\mathcal{G}_{\Gamma_1} = &\sum_{i,j} q_i\delta q_j\left[\delta_{ij}\left(1 + \frac{\beta}{\lambda_i}\right) - \beta\frac{\Gamma_1}{2L_x}\frac{C_j}{\lambda_j}\langle ye_i\rangle\right] + \\ &+ \sum_{i,j}\delta q_j\left[\delta_{ij}\left(\beta\frac{\Gamma_1}{2\tau}\frac{C_i}{\lambda_i} - \beta\frac{h_i}{\lambda_i} - \beta\frac{\Gamma_1}{2L_x}\langle ye_i\rangle + \gamma\langle e_i\rangle\right) + \right. \\ &\left. + \beta\frac{\Gamma_1}{2L_x}h_i\left(\frac{C_j}{\lambda_j}\langle ye_i\rangle + \frac{C_i}{\lambda_i}\langle ye_j\rangle\right)\right]. \qquad (3.8)\end{aligned}$$

$\mathcal{G}_{\Gamma_1}$ has a unique minimizer if and only if its quadratic part is positive definite. We notice that the quadratic part of $\mathcal{G}_{\Gamma_1}[q]$ is diagonal in the subspace generated by eigenmodes orthogonal to y ($\{e_i\}_{i\geq 1}$ such that $\langle ye_i\rangle = 0$). The eigenmodes are

$$e_{(k_1,k_2)}(x,y) \propto \cos\left(2\pi k_1\frac{x}{L_x}\right)\sin\left(\pi k_2\frac{y}{L_y}\right), \qquad (3.9)$$

where k_1 (wavenumber in the x direction) and $k_2 \neq 0$ (wavenumber in the y direction) are integers. We use interchangeably the collective index i and the couple (k_1, k_2) in the notation, depending on what is more convenient.

We distinguish between eigenmodes orthogonal to y and the other ones. The former are such that $k_1 \neq 0$ in (3.9). The latter are such that $k_1 = 0$ in (3.9). From now on, for ease of notation, k_1 is always nonzero when it appears in $e_{(k_1,k_2)}$ —otherwise, we write $e_{(0,k_2)}$. So we have $\langle ye_{(k_1,k_2)}\rangle = 0$ and $\langle ye_{(0,k_2)}\rangle \neq 0$. When only modes $e_{(0,k_2)}$ contribute to the streamfunction or PV field, the flow is purely zonal. We also have $C_{(0,k_2)} \propto (-1)^{k_2}$ and $C_{(k_1,k_2)} = 0$ otherwise.

Eigenvalues are given by

$$\lambda_{(k_1,k_2)} = \pi^2 \left(4\frac{k_1^2}{L_x^2} + \frac{k_2^2}{L_y^2} \right).$$

The smallest eigenvalue is $\lambda_{(0,1)}$. In the subspace generated by $\{e_{(k_1,k_2)}\}$, the quadratic part of $\mathcal{G}_{\Gamma_1}[q]$ is positive definite as long as $\beta > -\lambda_{(1,1)}$. In the subspace generated by $\{e_{(0,k_2)}\}$, the quadratic part of $\mathcal{G}_{\Gamma_1}[q]$ vanishes along a certain nontrivial direction $\hat{e} = \sum_{i\geq 1} \hat{e}_i e_i$ at a certain value $\beta = \hat{\beta}$ such that, for all $i \geq 1$,

$$\hat{e}_i \left(1 + \frac{\hat{\beta}}{\lambda_i} \right) - \hat{\beta} \frac{\Gamma_1}{2L_x} \langle y e_i \rangle \sum_{j\geq 1} \frac{C_j}{\lambda_j} \hat{e}_j = 0$$

Multiplying by C_i/λ_i and summing over i, we get

$$g(\hat{\beta}) := \sum_{i\geq 1} \frac{C_i \langle y e_i \rangle}{1 + \lambda_i/\hat{\beta}} - \frac{2L_x}{\Gamma_1} = 0. \tag{3.10}$$

We notice that in our analysis Γ_1 has to be nonzero. This is not an issue, as the case $\Gamma_1 = 0$ is handled by the simple-connected analysis. In the subspace generated by $\{e_{(0,k_2)}\}$, the quadratic part of $\mathcal{G}_{\Gamma_1}[q]$ is positive definite if $\beta > \hat{\beta}$, where $\hat{\beta}$ is the first (highest) zero of the function $x \mapsto g(x)$ (3.10). Therefore, $\mathcal{G}_{\Gamma_1}[q]$ has a unique minimum if $\beta > \max\{\hat{\beta}, -\lambda_{(1,1)}\}$. Then, there are no phase transitions in the grand canonical ensemble.

To solve the canonical variational problem

$$F_{\Gamma_1}(\beta, \Gamma) = \min_q \left\{ \int_{\mathcal{D}} s(q) + \beta \mathcal{E}_{\Gamma_1}[q] \, , \mathit{\Gamma}[q] = \Gamma \right\}, \tag{3.11}$$

we resort to the same trick as [Venaille and Bouchet, 2009], namely, we use

$$q_1 = \frac{1}{\langle e_1 \rangle} \left(\Gamma - \sum_{i\geq 2} \langle e_i \rangle q_i \right)$$

to include the circulation constraint. Note that eigenmodes orthogonal to y and eigenmodes orthogonal to 1 are the same. Again, the quadratic part of the functional $\mathcal{F}_{\Gamma_1}[q] = \int_{\mathcal{D}} s(q) + \beta \mathcal{E}_{\Gamma_1}[q]$ is diagonal in the subspace generated by $\{e_{(k_1,k_2)}\}$ and much trickier in the subspace generated by $\{e_{(0,k_2)}\}$, where the total space is deprived of the direction $e_{(0,k_2)}$. In the former, it is positive definite as long as $\beta > -\lambda_{(1,1)}$. In the latter, it vanishes along a certain nontrivial direction $e_* = \sum_{i\geq 2} e_i^* e_i$ at a certain value $\beta = \beta_*$ such that, for all

$i \geq 2$,

$$e_i^* \left(1 + \frac{\beta_*}{\lambda_i}\right) + \frac{\langle e_i \rangle}{2\langle e_1 \rangle^2} \left(1 + \frac{\beta_*}{\lambda_1}\right) \sum_{j \geq 2} \langle e_j \rangle e_j^* + \\ - \beta_* \frac{\Gamma_1}{2L_x} \langle y e_i \rangle \sum_{j \geq 2} \frac{C_j}{\lambda_j} e_j^* + \beta_* \frac{\Gamma_1}{2L_x} \langle y e_1 \rangle \frac{\langle e_i \rangle}{\langle e_1 \rangle} \sum_{j \geq 2} \frac{C_j}{\lambda_j} e_j^* + \\ + \beta_* \frac{\Gamma_1}{2L_x} \frac{\langle e_i \rangle}{\langle e_1 \rangle} \frac{C_1}{\lambda_1} \sum_{j \geq 2} \langle y e_j \rangle e_j^* = 0.$$

From this complicated relation, it is difficult to exhibit an explicit expression for β^*. We simply argue that if $\beta_* > -\lambda_{(1,1)}$, there is a first-order phase transition which is interesting in the presence of topography. We sketch how it is interesting in the next section. This first-order phase transition, described in [Venaille and Bouchet, 2009], is robust with respect to $\Gamma_1 \neq 0$ and $h \neq 0$. Note that this phase transition is observed when varying the circulation.

From (3.8), we can see what the critical points look like. We see that nonzero Γ_1 gives (only) zonal contributions. So does the term in $\gamma \langle e_i \rangle$. On the contrary, the term in h_i gives nonzonal term due to the nonzonal topography.

3.5 Bistability in the presence of topography

We assume $\beta_* > -\lambda_{(1,1)}$. This can be satisfied by adapting the aspect ratio of the domain. For $\beta = \beta_*$, $\mathcal{F}_{\Gamma_1}[q]$ has a unique minimum if the linear part of $\mathcal{F}_{\Gamma_1}[q]$ vanishes. Say it does at $\Gamma = \Gamma^*$. The value Γ^* is zero for $\Gamma_1 = 0$ and $h = 0$. The first-order phase transition appears as a positive jump in $\partial\gamma/\partial\Gamma$, when plotted versus Γ: γ jumps from a negative finite value to the opposite at $\Gamma = \Gamma^* = 0$. In the bounded annular geometry (R_2 cannot go to infinity), for $\Gamma_1 = 0$, we are always in the case $\beta_* > -\lambda_{(1,1)}$ (see appendix C).

For $\Gamma_1 \neq 0$, Γ^* can be found quite far from zero. The symmetry breaking due to $\Gamma_1 \neq 0$ and $h \neq 0$ can lead to qualitatively different states on either side of the first-order phase transition line. Indeed, the values of γ on the left of Γ^* and on the right of Γ^* are no more equal and opposite. We can have one with large absolute value and the other with small absolute value. Then, if irregular topography is present, the term in h_i can have the same magnitude as the zonal terms when $|\gamma|$ is small —'blocked' state, and it can be largely dominated when $|\gamma|$ is large —zonal state. Note that the terms in Γ_1 also give zonal contributions.

As discussed in the first chapter of this thesis, first-order phase transitions are naturally thought to be related to bistability. Here, we have sketched

a possible scenario for observed bistable behaviours, where flows alternately follow topography contours and go straight (i.e., in the zonal direction).

3.6 Interpretation for real flows

Real flows are viscous and, hence, have zero velocity at every point of their domain boundaries. The value of their total and partial circulations should always be zero then: $\Gamma = \Gamma_1 = \Gamma_2 = 0$. We argue that the inviscid picture can be relevant in the following framework: the domain $\mathcal{D}$ we have just considered for the inviscid dynamics can be identified with the real domain where boundary layers are subtracted (see Figure 3.2).

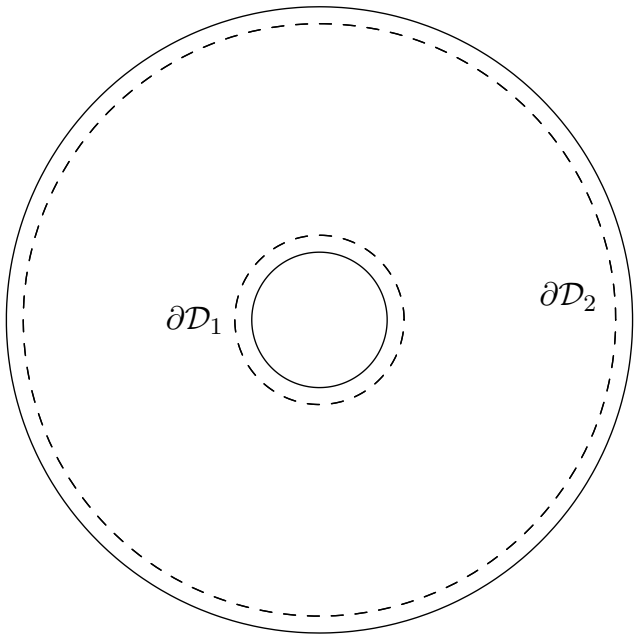

Figure 3.2: We propose a picture for applying inviscid results to real (viscous) flows. The dashed line is the boundary $\partial\mathcal{D}_1 \cup \partial\mathcal{D}_2$ considered so far (for inviscid flows), the solid line is the boundary for a real flow. Between the solid and dashed lines are the boundary layers; between the two dashed lines, the velocity profile compares with that of an inviscid fluid.

Chapter 4

Energy–enstrophy microcanonical measures of the 2D Euler equations

Contents

The Liouville theorem provides a Hamiltonian dynamical system with a natural invariant measure. Starting from finite-dimensional approximations (truncations) of the 2D Euler equations, for which a Liouville theorem is valid, we define the microcanonical measure as a limit measure, where the dimension (truncation order) goes to infinity. When only the energy and enstrophy invariants are taken into account, we give an explicit computation showing that the microcanonical measure corresponds to the maximization of a mean-field entropy. Energy–enstrophy measures were first investigated in the '70s by Kraichnan, in the canonical ensemble, and without considering the limit of an infinite number of degrees of freedom. In this chapter, we derive explicitly the microcanonical measure: it is the physically relevant one, for it

takes into account the invariants as explicit constraints. The results found in the microcanonical ensemble are different from those in the canonical one. This inequivalence of statistical ensembles is typical of long-range interacting systems[1]. The 2D Euler equations form a long-range interacting system.

4.1 General considerations

This chapter aims at describing rigorous results in statistical mechanics of 2D flows, in a self-contained manner. It is a companion to the journal paper [Bouchet and Corvellec, 2010]; by shedding more light on a few selected points thereof, the present chapter is intended for the statistical physics and complex systems communities at large, including interested (undergraduate) students. We still consider the 2D Euler equations in vorticity formulation (see chapter 1). These equations approximate the governing equations of the motion for a perfect 2D fluid, the approximation being the non-divergence of velocity. We have a complex dynamical system (in this case, nonlinear dynamics): the small scales are turbulent and disorganized, while the large scales are self-organized. We define the set of microstates as the set of all possible vorticity fields. We use a random field description: the vorticity $\omega(\mathbf{r}, t)$ is seen as a random field. By analogy with random vectors, we take the liberty, for now, of saying that the vorticity is given (or *distributed*) according to a *probability law* —or *probability distribution* in physics-oriented language, or *probability measure* in mathematics-oriented language— denoted by μ. In a strictly formal sense, we thus have the average vorticity $\bar{\omega} = \int \mathrm{d}\mu(\omega)\ \omega = \int \mathrm{d}\omega\ \rho(\omega)\omega$, where $\rho(\omega)$ would be the *density* of μ. In physics-oriented language, ρ would be referred to as the *probability density function*. Note that, in general, μ would be time-dependent. We would have the normalization condition $\int \mathrm{d}\mu(\omega) = \int \mathrm{d}\omega\ \rho(\omega) = 1$. The formal integrals are taken over all possible microstates $\{\omega\}$, i.e., over the phase space.

Throughout the chapter, the derivations are based on finite-dimensional approximations of the field ω, denoted by ω^N, for which the probability measure and density are well-defined. Dynamical quantities, such as the energy and the vorticity moments, can be evaluated from the knowledge of μ. An 'invariant measure of the 2D Euler equations' is a stationary probability measure μ such that the solution $\omega(\mathbf{r}, t)$ at any time $t \geq 0$ is distributed according to μ,

[1] We use the term 'long-range interactions' as in, for instance, [Bouchet and Barré, 2005] and [Campa et al., 2009]: for a system in space dimension D, the interaction potential between particles separated by a distance r goes like $r^{-\alpha}$, as $r \to \infty$, with $\alpha \leq \mathrm{D}$. The interaction is 'non-integrable'. See (4.21), page 72. Long-range interacting systems include self-gravitating systems in astrophysics and some models in plasma physics.

whenever the initial condition $\omega(\mathbf{r}, 0)$ is distributed according to μ. An invariant measure gives all the vorticity field correlators, thus solving the problem of the unclosed hierarchy of equations for the moments of the velocity increments ('structure functions' in turbulence). Thanks to the probability measure tool, the moments can be considered directly in the statistical sense. An invariant measure is then extremely useful to know, when dealing with complex systems such as (2D) turbulence.

Given a dynamical system, a natural invariant measure is not known explicitly, in the general case. In our case (2D Euler equations), we are confronted with a phase space of infinite dimension. The main issue will be the ill-definition of the phase space volume. Again, we shall start with finite-dimensional approximations of the dynamics. We know, from Hamiltonian mechanics, that finite-dimensional canonical[2] Hamiltonian systems have natural invariant measures: they are uniform measures in the phase-space coordinates, called microcanonical measures. That is Liouville's theorem, forming the basis for equilibrium statistical mechanics.

The main physical phenomenon at play, in the 2D Euler equations, is the self-organization into large-scale coherent structures: monopoles, dipoles, and parallel flows for the 2D Euler equations, as seen throughout this thesis. As first guessed by Onsager [Onsager, 1949], the self-organization can be explained by equilibrium statistical mechanics: interactions between an infinite number of degrees of freedom involved should yield a macroscopic behaviour. Because of the long-range interactions between vortices, such an equilibrium is not a trivial state (uniform in space), and depends strongly on the boundary conditions. This explains the formation of vortices and jets.

Let us recall the 2D Euler equations in vorticity formulation. The 2D velocity $\mathbf{u}$ is solenoidal: $\nabla \cdot \mathbf{u} = 0$ and the vorticity $\omega = (\nabla \times \mathbf{u}) \cdot \mathbf{e}_z$ is a nontrivial scalar; $\mathbf{e}_z$ is the usual upward vertical unit vector. The 2D Euler equations take the simple form of a conservation law for the vorticity:

$$\frac{\partial \omega}{\partial t} + \mathbf{u} \cdot \nabla \omega = 0 \; ; \quad \mathbf{u} = \mathbf{e}_z \times \nabla \psi \; ; \quad \omega = \Delta \psi, \tag{4.1}$$

where a streamfunction ψ is introduced. Unless otherwise specified, we complement the equation $\omega = \Delta\psi$ with impermeability boundary conditions: $\psi = 0$ on $\partial\mathcal{D}$, where $\mathcal{D}$ is a simply connected domain. The kinetic energy reads

$$\mathcal{E}[\omega] = \frac{1}{2} \int_{\mathcal{D}} \mathrm{d}\mathbf{r} \; \mathbf{u}^2 = \frac{1}{2} \int_{\mathcal{D}} \mathrm{d}\mathbf{r} \; (\nabla\psi)^2 = -\frac{1}{2} \int_{\mathcal{D}} \mathrm{d}\mathbf{r} \; \omega\psi. \tag{4.2}$$

[2]Here, the term 'canonical' refers to Hamilton's equations of motion, as detailed in section 4.2. It qualifies a Hamiltonian system; the term we use in opposition is 'non-canonical'. It must be distinguished from the term 'canonical' used in the statistical physics context, when it qualifies a measure or a statistical ensemble (see footnote 4).

It is conserved, as the Hamiltonian dynamical system is autonomous.

The chapter is organized as follows: First, the dynamical invariants are identified, by working out the Hamiltonian structure of the 2D Euler equations. The specificity of this Hamiltonian system is to be non-canonical and infinite-dimensional. It has infinitely many dynamical invariants[3]. That is found in section 4.2. Second, the equivalent of a Liouville theorem is identified, so that a microcanonical measure can be expressed, at least formally: we start with a truncated version of the 2D Euler equations, where the phase-space variable is N-dimensional, and only the quadratic quantities are conserved. Namely, these quadratic invariants are the energy and the enstrophy (see later, expressions (4.2) and (4.11) for $k = 2$, respectively). The microcanonical measure of the actual full (finite-dimensional) system is obtained by taking the limit $N \to \infty$, and by possibly adding constraints, which correspond to other invariants. That is found in section 4.3. In fact, we call *microcanonical* any measure which accounts for the conservation of given quantities, even though it is not the infinity of invariants corresponding to the full system. This is consistent with usual thermodynamics terminology. For instance, we consider the *energy–enstrophy* microcanonical measure, corresponding to the above-mentioned conservation of quadratic invariants only. We discuss the reasons for such a restriction. In this framework, we compute explicitly the phase space volume. That is found in section 4.5. In section 4.4, we introduce the equilibrium statistical mechanics of 2D flows. The average vorticity $\bar{\omega}$ is a solution of a variational problem (it maximizes an entropy). In the energy–enstrophy ensemble[4], we show that the entropy computed from a mean-field approach is the same as the entropy computed directly from the energy–enstrophy microcanonical measure of section 4.5. Such a result is quite reassuring and amazing at the same time.

[3]Indeed, the 2D Euler equations simply *transport* the vorticity (see (4.1), page 63) so that the domain points which have a certain value of vorticity make up the same area at any time. It can be checked that, for any function $F(\omega)$,

$$\frac{\mathrm{d}}{\mathrm{d}t}\int_{\mathcal{D}} F(\omega) = \int_{\mathcal{D}} \frac{\partial}{\partial t}F(\omega) = \int_{\mathcal{D}} F'(\omega)\frac{\partial \omega}{\partial t} = -\int_{\mathcal{D}} F'(\omega)(\mathbf{u}\cdot\nabla\omega)$$
$$= -\int_{\mathcal{D}} (\mathbf{u}\cdot\nabla)F(\omega) = -\int_{\mathcal{D}} \nabla\cdot(F(\omega)\mathbf{u}) = -\int_{\partial\mathcal{D}} F(\omega)\mathbf{u}\cdot\mathbf{n} = 0.$$

Therefore, the number of dynamical invariants is infinite.

[4]The statistical *ensemble* is just the accessible part of phase space (set of microstates) corresponding to the measure of the same name (microcanonical or canonical, for given sets of invariants).

4.2 Hamiltonian structure and conservation laws

In a usual Hamiltonian problem, with N degrees of freedom, there is a finite set of generalized coordinates $\{q_i\}_{1\leq i\leq N}$ and conjugate momenta $\{p_i\}_{1\leq i\leq N}$. The phase space has then finite dimension $2N$. The 2D Euler equations do consist in a Hamiltonian system (whose structure will be explicited in the current section), but it is not canonical —there are no canonically conjugated pairs $\{q_i, p_i\}$— and it is infinite-dimensional. Indeed, the 2D Euler equations describe the time-evolution of the vorticity field $\omega(\mathbf{r})$: the phase space variable ω is continuous (infinite-dimensional), and the phase space is a function space. This section owes a lot to the enlightening review paper [Shepherd, 1990]. Please consider that we refer to it throughout the section, every time something is asserted with or without derivation.

We begin with a 'usual' (canonical finite-dimensional) Hamiltonian system, as mentioned above. Let us use the general notation x for the phase space variable. Here, $x = (q_1, \ldots, q_N, p_1, \ldots, p_N) =: (q, p)$. The *Hamiltonian function* $\mathcal{H}(x, t)$ quantifies the energy of the system. From Noether's theorem, to each symmetry of the Hamiltonian corresponds a conserved quantity, or *dynamical invariant*. If the Hamiltonian (function) has no explicit time-dependence[5] ($\partial_t \mathcal{H} = 0$), then the energy E is conserved ($\mathrm{d}_t E = 0$). A Hamiltonian system requires the specification of $\mathcal{H}$, and of a *Poisson bracket* operator $\{\cdot, \cdot\}$.

Starting with the canonical equations, i.e., the Hamilton equations,

$$\dot{p}_i = -\frac{\partial \mathcal{H}}{\partial q_i}, \quad \dot{q}_i = \frac{\partial \mathcal{H}}{\partial p_i}, \quad 1 \leq i \leq N, \tag{4.3}$$

the Poisson bracket is introduced, for functions $F(q, p, t)$ and $G(q, p, t)$:

$$\{F, G\} = \sum_{i=1}^{N} \left(\frac{\partial F}{\partial q_i}\frac{\partial G}{\partial p_i} - \frac{\partial F}{\partial p_i}\frac{\partial G}{\partial q_i} \right) \tag{4.4}$$

so that (4.3) can be rewritten

$$\dot{p}_i = \{p_i, \mathcal{H}\}, \quad \dot{q}_i = \{q_i, \mathcal{H}\}, \quad 1 \leq i \leq N. \tag{4.5}$$

For any function $F(x, t)$, we have

$$\frac{\mathrm{d}F}{\mathrm{d}t} = \{F, \mathcal{H}\} + \frac{\partial F}{\partial t}.$$

[5] For the sake of curiosity, such dynamical systems are said to be autonomous (the system is conservative).

So if $F(x,t) = F(x)$, it is a dynamical invariant ($\mathrm{d}_t F = 0$) as long as its Poisson bracket with $\mathcal{H}$ vanishes. The two objects $\mathcal{H}$ and $\{\cdot\,,\cdot\}$ are enough to characterize the Hamiltonian system in question. Note that $\{\cdot\,,\cdot\}$ can also be expressed in matrix form: (4.5) rewrites

$$\dot{x} = J\nabla\mathcal{H}, \quad \text{i.e.,} \quad \dot{x}_i = \sum_{j=1}^{2N} J_{ij}\frac{\partial\mathcal{H}}{\partial x_j}, \quad \text{for } i = 1,\dots,2N, \tag{4.6}$$

where J is the Poisson matrix:

$$J = \begin{pmatrix} 0_N & I_N \\ -I_N & 0_N \end{pmatrix}, \tag{4.7}$$

with 0_N denoting the null matrix, and I_N the identity matrix, both of them in dimension N. There is actually only one nonzero element of J in column j. Then, (4.6) reduces to

$$\dot{x}_i = J_{ij}\frac{\partial\mathcal{H}}{\partial x_j}, \quad \text{for } i = 1,\dots,2N. \tag{4.8}$$

Also, (4.4) rewrites

$$\{F,G\} = (\nabla F, J\nabla G) = \sum_{i,j=1}^{2N} \frac{\partial F}{\partial x_i} J_{ij} \frac{\partial G}{\partial x_j},$$

$(\cdot\,,\cdot)$ denoting the scalar product in the $2N$-dimensional phase space.

A Hamiltonian system is noncanonical if it cannot be brought into the *canonical form* (4.7–4.8). This is related to its J being singular. In addition to the invariants associated with symmetries of the Hamiltonian, non-canonical Hamiltonian systems possess so-called *Casimir invariants* $C(x)$, defined such that for all $i = 1,\dots,2N$,

$$\sum_{j=1}^{2N} J_{ij}\frac{\partial C}{\partial x_j} = J_{ij}\frac{\partial C}{\partial x_j} = 0 \tag{4.9}$$

or, equivalently, $J\nabla C = 0$. Such functions are dynamical invariants, since

$$\frac{\mathrm{d}C}{\mathrm{d}t} = (\nabla C, \dot{x}) = (\nabla C, J\nabla\mathcal{H}) = \{C,\mathcal{H}\} = -\{\mathcal{H},C\} = -(\nabla\mathcal{H}, J\nabla C) = 0.$$

In the canonical case, J is nonsingular, so there are no (nontrivial) Casimir invariants, as can be seen from (4.9). We see how the existence of Casimir invariants (or, for short, Casimirs) is related to the degeneracy of the kernel of the Poisson matrix. From (4.9), if this kernel has dimension k ($k \geq 1$), then there are k independent Casimirs.

Infinite dimension. Now that we have sketched what noncanonicality entails, let us give the extension of this formalism to the case of infinite dimension. Instead of a set of ordinary differential equations (4.6), we have partial differential equations (4.1). Functions are now functionals of the phase space variable ω:

$$\mathcal{F}[\omega] = \int_{\mathcal{D}} \mathrm{d}\mathbf{r}\ F(\omega(\mathbf{r},t)),$$

and the analogues of gradients ($\nabla\mathcal{H}$, ∇F, ...) are variational derivatives, of the form $\delta\mathcal{F}/\delta\omega$. Accordingly, the Poisson bracket reads

$$\{\mathcal{F},\mathcal{G}\} = \left(\frac{\delta\mathcal{F}}{\delta\omega}, J\frac{\delta\mathcal{G}}{\delta\omega}\right) = \int_{\mathcal{D}} \frac{\delta\mathcal{F}}{\delta\omega} J\frac{\delta\mathcal{G}}{\delta\omega},$$

where the scalar product $(\cdot\,,\cdot)$ is now defined on the infinite-dimensional phase space, and the operator J cannot be cast into a finite-dimensional matrix form any more. Explicitly, for the 2D Euler equations, $J = \partial(\cdot\,,\omega)$, where $\partial(\cdot\,,\cdot)$ denotes the Jacobian operator (viz., in Cartesian coordinates, $\partial(F,G) = \partial_x F\partial_y G - \partial_y F\partial_x G$). The Hamiltonian function(al) $\mathcal{H}[\omega]$ is identified with the kinetic energy (4.2). Then, (4.1) is equivalent to $\partial_t\omega = -\mathbf{u}\cdot\nabla\omega = -\partial(\psi,\omega) = \{\omega,\mathcal{H}\}$ provided[6]

$$\{\omega,\mathcal{H}\} = J\frac{\delta\mathcal{H}}{\delta\omega} = J(-\psi) = -\partial(\psi,\omega) = \partial(-\psi,\omega).$$

Therefore, the Casimirs $\mathcal{C}$ of the 2D Euler equations are defined by

$$J\frac{\delta\mathcal{C}}{\delta\omega} = \partial\left(\frac{\delta\mathcal{C}}{\delta\omega},\omega\right) = 0.$$

It can be checked that the family of functionals

$$\mathcal{C}[\omega] = \int_{\mathcal{D}} \mathrm{d}\mathbf{r}\ C(\omega(\mathbf{r},t)) \tag{4.10}$$

for arbitrary functions C are Casimirs of the 2D Euler equations. Therefore, we have an infinity of Casimirs. Because the functions $C(\omega)$ must be sufficiently regular, we consider that the conservation of the infinity of functionals of type (4.10) is equivalent to the conservation of the infinity of vorticity moments

$$\Gamma_k[\omega] = \int_{\mathcal{D}} \mathrm{d}\mathbf{r}\ \omega^k(\mathbf{r},t), \quad \text{for all } k \geq 1. \tag{4.11}$$

[6]We have $\delta\mathcal{H}/\delta\omega = -\psi$, since

$$\delta\mathcal{H} = \mathcal{H}[\omega+\delta\omega] - \mathcal{H}[\omega] + o(\delta\omega^2) = \int_{\mathcal{D}} -\psi\delta\omega + o(\delta\omega^2) = \left(\frac{\delta\mathcal{H}}{\delta\omega},\delta\omega\right) + o(\delta\omega^2).$$

4.3 Theoretical foundations of equilibrium statistical mechanics

The idea of statistical mechanics is that the state of a physical system with many degrees of freedom should be described by a probability measure on the phase space of the underlying dynamical system. Let us view the solution $\{(q(t), p(t))\}$ of (4.5) as a random vector. Say that it is given according to a probability measure $\mu(q, p, t)$, with density $f(q, p, t)$, verifying the normalization condition

$$\int \mathrm{d}q\mathrm{d}p \; f(q, p, t) = 1 \quad \text{for all } t \geq 0. \tag{4.12}$$

Again (see section 4.1), macroscopically, at time $t \geq 0$, a dynamical variable $F(q, p)$ takes the mean value

$$\bar{F}(t) = \int \mathrm{d}q\mathrm{d}p \; f(q, p, t) F(q, p).$$

From (4.3), the Hamiltonian flow, i.e., the flow in phase space, has nondivergent velocity $\dot{x} = (\dot{q}, \dot{p})$:

$$\sum_{i=1}^{N} \left(\frac{\partial \dot{q}_i}{\partial q_i} + \frac{\partial \dot{p}_i}{\partial p_i} \right) = 0. \tag{4.13}$$

This leads to Liouville's theorem, which states that the phase-space volume is invariant under the Hamiltonian flow, i.e., along trajectories. Indeed, the continuity equation for probability density f,

$$\frac{\partial f}{\partial t} + \sum_{i=1}^{N} \left(\frac{\partial (f \dot{q}_i)}{\partial q_i} + \frac{\partial (f \dot{p}_i)}{\partial p_i} \right) = 0,$$

reduces, through (4.13), to

$$\frac{\partial f}{\partial t} + \sum_{i=1}^{N} \left(\dot{q}_i \frac{\partial f}{\partial q_i} + \dot{p}_i \frac{\partial f}{\partial p_i} \right) = \frac{\partial f}{\partial t} + \{f, \mathcal{H}\} = \frac{\mathrm{d}f}{\mathrm{d}t} = 0. \tag{4.14}$$

So the most natural invariant measure to consider is the (properly normalized) measure with density constant and uniform, verifying the conservation of dynamical invariants. This measure is called the *microcanonical measure*. It has density

$$f(q, p) = \mathcal{N} \delta(E - \mathcal{H}(q, p)),$$

if energy E is the only dynamical invariant, $\mathcal{N}$ being a normalization constant so that (4.12) holds. If the system has conserved quantities in addition to

energy, the corresponding Dirac deltas have to be included. The measure given by the above density is uniform over the accessible part of phase space. Another way to get a grasp of 'why the microcanonical measure', is to see that the phase-space velocity $\dot{x}$ has the effect of stirring f (4.14). When the stationary state is reached in (4.14), the density has filamented so much that it is uniform [Diu et al., 1989].

The aim of equilibrium statistical mechanics is to determine the large-time (or final) state of a system, knowing its initial state: we are interested in the behaviour of a given trajectory in phase space. For an isolated system, all final states with the same value of energy (and other conserved quantities) as the initial state are accessible. Thus, the trajectory is constrained by the invariants of the dynamics. It is therefore natural to consider a measure that fulfills the conservation properties, i.e., that takes into account all the dynamical invariants. This justifies the use of the microcanonical measure.

If the system under consideration is not isolated, but coupled with an external bath of conserved quantities, other kinds of measures describe the system. If the energy of the system is not conserved, but rather its temperature is fixed, then *canonical measures* have to be used (see any textbook on statistical mechanics, for example [Diu et al., 1989]). It is sometimes argued that, in the limit of an infinite number of degrees of freedom, canonical and microcanonical measures are equivalent. Thus, as canonical measures are more easily handled, they are often preferred over microcanonical ones. However, while the equivalence of canonical and microcanonical ensembles is very natural and usually true in systems with short-range interactions (commonly found in condensed matter physics), it is often not actually so in systems with long-range interactions, such as the 2D Euler equations [Campa et al., 2009, Bouchet and Barré, 2005, Ellis et al., 2000]. That is why we work only with microcanonical measures in the following.

The 2D Euler equations form a Hamiltonian dynamical system, but of infinite dimension. In this paragraph, we generalize the notion of microcanonical measure to this system. Let us decompose the vorticity in an orthonormal basis $\{e_i\}_{i\geq 1}$,

$$\omega(\mathbf{r}, t) = \sum_{i=1}^{\infty} \omega_i(t) e_i(\mathbf{r}), \tag{4.15}$$

viewing $\{\omega_i\}_{i\geq 1}$ as the coordinates of a trajectory in phase space. Now, $x_i = \omega_i$ for $i \geq 1$. If the domain $\mathcal{D}$ is doubly periodic, it is natural to take $\{e_i\}_{i\geq 1}$ to be the Fourier basis. In the case (4.1) and in general, considering the expression of the Hamiltonian (see (4.2) or (4.21)), it is natural to take $\{e_i\}_{i\geq 1}$ to be the Laplacian eigenbasis.

In order to recover the usual relationship between Liouville's theorem and equilibrium statistical mechanics, with an explicit expression for the microcanonical measure, we first consider a truncation of (4.15) (at, say, $i = N$). We see $\{\omega_i\}_{1\leq i\leq N}$ as random variables which are statistically independent (see subsection 4.4.1). The dynamics read

$$\dot{\omega}_i = \sum_{j,k} A_{ijk}\omega_j\omega_k \quad \text{for all } i,j,k = 1,\dots,N. \tag{4.16}$$

The expression of $\{A_{ijk}\}$ need not be explicited for current purposes. It is enough to note that $A_{ijk} = 0$ whenever two of the indices are equal[7]. (4.16) is the equation for a trajectory in (N-dimensional) phase space. The phase-space velocity is then nondivergent:

$$\sum_{i=1}^{N} \frac{\partial \dot{\omega}_i}{\partial \omega_i} = 0 \tag{4.17}$$

and, what is more, $\partial\dot{\omega}_i/\partial\omega_i = 0$ for all $i = 1,\dots,N$. The latter relation is a detailed Liouville theorem. Let us denote the N-dimensional vector $(\omega_1,\dots,\omega_N)$ by ω^N. A certain ω^N defines a certain *microstate* of the system. Let $f(\omega^N)$ be the *probability density* of microstates in phase space:

$$\int_{\omega_1}^{\omega_1+\Delta\omega_1} \dots \int_{\omega_N}^{\omega_N+\Delta\omega_N} \prod_{i=1}^{N} \mathrm{d}\omega_i' \; f(\omega'^N)$$

is the *probability* that the system lies somewhere in phase space in $[\omega_1,\omega_1+\Delta\omega_1[\times\dots\times[\omega_N,\omega_N+\Delta\omega_N[$. We have the normalization condition $\int\prod_{i=1}^{N}\mathrm{d}\omega_i\; f(\omega^N) = 1$ (the integral is taken over the entire phase space, i.e., the space spanned by all possible vectors ω^N).

In his work, [Onsager, 1949] did not confront the difficulty of infinite dimension, as he studied the point-vortex model (N singular vortices free to move in 2D space). In this work, we start with finite-dimensional approximations, but we address the issue of infinite-dimensionality. Note that except for the point-vortex model, truncated systems do not conserve the infinity of invariants (4.11). A direct consequence of the detailed Liouville theorem is that any truncation of the Euler equations also verifies a Liouville theorem (4.17). Say that our N-dimensional system has (only) the following invariants: energy E and enstrophy Γ_2 (4.11). The probability density is then

$$\rho(\omega^N) = \mathcal{N}\delta(\mathcal{E}[\omega^N] - E)\delta(\mathit{\Gamma}_2[\omega^N] - \Gamma_2), \tag{4.18}$$

[7] See [Kraichnan and Montgomery, 1980, page 560].

where $\mathcal{N}$ is a normalization constant determined by $\int \mathrm{d}\omega^N \rho(\omega^N) = 1$; $\mathcal{N} = 1/\Omega^N(E, \Gamma_2)$, where $\Omega^N(E, \Gamma_2)$ is the density of states verifying $\mathcal{E}[\omega^N] = E$ and $\mathit{\Gamma}_2[\omega^N] = \Gamma_2$. In section 4.6, we discuss the relevance of keeping preferential invariants even for the actual (infinite-dimensional) dynamics.

Infinite dimension. The measure corresponding to the density (4.18) is given by

$$\mathrm{d}\mu^N_{m,Q} = \frac{1}{\Omega^N(E, \Gamma_2)} \prod_{i=1}^{N} \mathrm{d}\omega_i \; \delta(\mathcal{E}[\omega^N] - E)\delta(\mathit{\Gamma}_2[\omega^N] - \Gamma_2).$$

The subscript m stands for 'microcanonical', Q for 'quadratic', as only quadratic invariants are involved. We call microcanonical the measure

$$\mu_{m,Q}(E, \Gamma_2) = \lim_{N\to\infty} \mu^N_{m,Q}(E, \Gamma_2).$$

The proper rescaling for evaluating Ω^N is given in the appendix, page 81. The microcanonical measure corresponding to the infinite set of invariants $\{\Gamma_k\}_{k\geq 1}$ is defined by

$$\mu_m(E, \{\Gamma_k\}) = \lim_{n\to\infty} \lim_{N\to\infty} \mu^N_{m,n}(E, \Gamma_1, \ldots, \Gamma_n). \tag{4.19}$$

4.4 Equilibrium statistical mechanics of the 2D Euler equations

As introduced in chapter 1, an equilibrium statistical mechanics theory was proposed for the 2D Euler equations, by Miller, and by Robert and Sommeria [Miller, 1990, Robert and Sommeria, 1991]. We recall it in this section. This approach, based on the maximization of a mixing entropy, constrained by the conservation of the invariants, is a mean-field one: the use of a mean-field entropy is valid, since the correlation between vorticity values at different points can be neglected. The observables (energy, vorticity moments) can be computed from a coarse-grained vorticity field (average vorticity), which is a *macrostate* (i.e., consisting of many microstates). Before we write the variational problem which should be solved, we give a heuristic explanation of why a mean-field description is exact. The point is that the partial probability densities (of vorticity at different points) are independent: the probability measure is a product measure. The key implication is that the Gibbs entropy (related to the phase space volume) reduces to a coarse-grained entropy.

4.4.1 Validity of the mean field

We use the local probability density $\rho(\sigma, \mathbf{r})$, such that

$$\int_{\mathcal{B}} \mathrm{d}\mathbf{r} \int_{\sigma_1}^{\sigma_2} \mathrm{d}\sigma\ \rho(\sigma, \mathbf{r}) \tag{4.20}$$

is the probability to have $\sigma_1 \leq \omega(\mathbf{r}) < \sigma_2$ for $\mathbf{r} \in \mathcal{B} \subset \mathcal{D}$ (here, $\mathcal{B}$ has to be the ball of centre $\mathbf{r}$ and radius $\mathrm{d}\mathbf{r}$). Expressions are written somewhat more straightforwardly when considering discrete versions of the above. If we consider a truncated system where the spatial domain consists of a finite set of points, say $\{\mathbf{r}_j\}_{1\leq j\leq N}$, then the values $\{\sigma_j := \omega(\mathbf{r}_j)\}_{1\leq j\leq N}$ are statistically independent, as we explain in the following paragraphs. Equivalently, the measure is a product measure:

$$f(\sigma_1, \ldots, \sigma_N) \prod_{j=1}^{N} \mathrm{d}\sigma_j = \prod_{j=1}^{N} \mathrm{d}\sigma_j\ \rho(\sigma_j, \mathbf{r}_j).$$

Correlations between variables can appear only through the dynamical constraints: energy, Casimirs, and so on. For instance, the energy of the 2D Euler system can be expressed in a form where the interaction between vorticity values is explicit, using the Laplacian's Green function: for Dirichlet boundary conditions, we have

$$\mathcal{H}[\omega] = -\frac{1}{2} \int_{\mathcal{D}} \omega(\Delta^{-1}\omega) = \frac{1}{4\pi} \int_{\mathcal{D}} \int_{\mathcal{D}} \mathrm{d}\mathbf{r}\ \mathrm{d}\mathbf{r}'\ \omega(\mathbf{r})\omega(\mathbf{r}') \log|\mathbf{r} - \mathbf{r}'|. \tag{4.21}$$

The coupling between vorticity at point $\mathbf{r}$ and vorticity at point $\mathbf{r}'$ appears to be logarithmic, hence not integrable. Thus, $\omega(\mathbf{r})$ is coupled with the vorticity of any other point of the domain, not only of neighbouring points.

In systems where degrees of freedom are coupled with many others, it is usual to consider these degrees of freedom statistically independent at leading order in $1/N$, where N scales like the number of degrees of freedom. Then, a mean-field approach should be a valid approximation. For example, in systems with nearest-neighbour interactions, a mean-field approach becomes exact when the dimension tends to infinity (think of the Ising model). Indeed, when the number of coupled degrees of freedom tends to infinity, the interaction felt by one degree of freedom is no more sensitive to the fluctuations due to others, taken separately, but just to their average value. Then a mean-field treatment becomes exact, which is equivalent to saying that different degrees of freedom may be considered statistically independent.

4.4.2 Microcanonical variational problem

From the previous subsection, we have that the Gibbs entropy, formally denoted by

$$\mathcal{S}_G[f] = -\int \mathrm{d}\omega\ f(\omega)\log f(\omega),$$

reduces to the mean-field entropy

$$\mathcal{S}[\rho] = -\int_{\mathcal{D}} \mathrm{d}\mathbf{r} \int_{-\infty}^{+\infty} \mathrm{d}\sigma\ \rho(\sigma,\mathbf{r})\log\rho(\sigma,\mathbf{r}). \tag{4.22}$$

Here, the term 'mean-field' is understood with respect to the spatial coarse-graining. Note that we omit the Boltzmann constant as factor in the entropy definition. Then, the phase space volume (or, more accurately, the density of states) can be quantified from (4.22). Precisely, (4.22) can be proven to be proportional to the logarithm of the number of microstates corresponding to the macrostate ρ (Boltzmann's entropy formula) [Robert and Sommeria, 1991, and references therein].

We recall the variational problem, as derived in chapter 1. The average vorticity is given by

$$\bar{\omega}(\mathbf{r}) = \int_{-\infty}^{+\infty} \mathrm{d}\sigma\ \sigma\rho(\sigma,\mathbf{r}). \tag{4.23}$$

It is related to the average streamfunction $\bar{\psi}$ so that $\bar{\omega} = \Delta\bar{\psi}$. The vorticity distribution writes

$$\mathcal{A}[\rho](\sigma) = \int_{\mathcal{D}} \mathrm{d}\mathbf{r}\ \rho(\sigma,\mathbf{r}). \tag{4.24}$$

Since equations (4.1) express transport by an incompressible flow, the vorticity distribution is a dynamical invariant. Say, $\mathcal{A}[\rho](\sigma) = \gamma(\sigma)$, where $\gamma(\sigma)$ denotes a prescribed vorticity distribution. This conservation yields the conservation of all vorticity moments (4.11): domain-averaged vorticity Γ, enstrophy Γ_2, and higher-order moments. Note that if $\mathcal{D}$ is bounded, as in our example, Γ is also the circulation: $\Gamma = \int_{\partial\mathcal{D}} \mathbf{u}\cdot\mathrm{d}\mathbf{l}$. If $\mathcal{D}$ displays symmetries, the associated conservation laws (by Noether's theorem) have to be taken into account as well.

The local normalization condition has to be verified for all $\mathbf{r}\in\mathcal{D}$:

$$N[\rho](\mathbf{r}) = \int_{-\infty}^{+\infty} \mathrm{d}\sigma\ \rho(\sigma,\mathbf{r}) = 1. \tag{4.25}$$

Then, the mean-field entropy S of the system is given by the variational problem

$$S(E,\gamma) = \sup_{\{\rho\,|\,N[\rho]=1\}} \left\{\mathcal{S}[\rho]\ |\ \mathcal{E}[\bar{\omega}] = E,\ \mathcal{A}[\rho] = \gamma\right\}. \tag{MVP}$$

where $\mathcal{E}[\bar{\omega}]$ is the energy (4.2) of the average vorticity field $\bar{\omega}$. Indeed, the vanishing of correlations between vorticity values at different points implies that fluctuations about the average may be neglected when computing the energy of the system.

Up to constant terms (i.e., independent of the physical parameters), the mean-field entropy (MVP) is the same as the Boltzmann entropy defined from the rescaled logarithm of the density of states $\Omega = \lim_{N\to\infty} \Omega^N$ (of section 4.3). In the next section, we show that this is verified in the case of the energy–enstrophy measure, using explicit elementary computations.

4.5 The energy–enstrophy microcanonical measure

The energy–enstrophy microcanonical measure is defined by

$$\mathrm{d}\mu_{m,Q}(E,\Gamma_2) = \frac{1}{\Omega_Q(E,\Gamma_2)} \prod_{i=1}^{\infty} \mathrm{d}\omega_i \; \delta(\mathcal{E}[\omega] - E)\delta(\mathit{\Gamma}_2[\omega] - \Gamma_2), \tag{4.26}$$

as introduced on page 71. It is the microcanonical measure preserving the quadratic invariants. There is a priori no physical reason to exclude the other invariants; however, the energy–enstrophy microcanonical measure can be, in some cases, a good approximation of the complete microcanonical measure. Also, in numerical models, only finite-dimensional approximations of 2D Euler or other fluid motion equations can ever be considered. Except for the point-vortex model, these finite-dimensional approximations conserve precisely only the quadratic functionals, energy and enstrophy. The motivation to treat this case in detail is pedagogical: an elementary explicit computation proves the equivalence of the microcanonical measure introduced through Fourier mode decomposition (in section 4.3), with the solution to the microcanonical mean-field variational problem (of section 4.4).

We compute the entropy, as well as the probability density for each coordinate ω_i (partial densities). The computations are performed, on the one hand, directly from the definition of the energy–enstrophy measure (subsection 4.5.1), and on the other hand, from the mean-field variational problem (subsection 4.5.2). The two computations lead —fortunately— to the same results. The energy–enstrophy measure was discussed at length by many authors decades ago, including [Kraichnan and Montgomery, 1980]. However, their computations were performed in the canonical ensemble. The following discussion provides the first derivation in the microcanonical ensemble, bringing to light ensemble inequivalence for the energy–enstrophy ensembles

—microcanonical and canonical (see subsection 4.5.3). More precisely, it is an instance of partial inequivalence [Ellis et al., 2000].

4.5.1 Energy–enstrophy microcanonical measure from its finite-dimensional approximation

Following the discussion of section 4.3, the energy–enstrophy microcanonical measure is defined as the limit measure $\mu_{m,Q} = \lim_{N\to\infty} \mu^N_{m,Q}$, with

$$\mathrm{d}\mu^N_{m,Q} = \frac{1}{\Omega^N_Q(E,\Gamma_2)} \prod_{i=1}^{N} \mathrm{d}\omega_i \; \delta(\mathcal{E}[\omega^N] - E)\delta(\mathit{\Gamma}_2[\omega^N] - \Gamma_2), \tag{4.27}$$

where we use the same notation as in section 4.3. Let $\{\lambda_i\}_{i\geq 1}$ be the Laplacian eigenvalues associated with eigenmodes $\{e_i\}_{i\geq 1}$ (4.15), ordered so that $\lambda_1 < \lambda_2 < \ldots < \lambda_N$. We have $2\mathcal{E}[\omega^N] = \sum_{i=1}^N \omega_i^2/\lambda_i$ and $\mathit{\Gamma}_2[\omega^N] = \sum_{i=1}^N \omega_i^2$. Let us assume that the first eigenmode is non-degenerate ($\lambda_1 \neq \lambda_2$); this is not verified only in the case of a doubly periodic square domain. The main technical difficulty is to compute the phase space volume

$$\Omega^N_Q(E,\Gamma_2) = \int \mathrm{d}\mu^N_{m,Q} = \int \prod_{i=1}^{N} \mathrm{d}\omega_i \; \delta(\mathcal{E}[\omega^N] - E)\delta(\mathit{\Gamma}_2[\omega^N] - \Gamma_2), \tag{4.28}$$

and the entropy

$$S_Q(E,\Gamma_2) = \lim_{N\to\infty} \left(\frac{1}{N} \log \Omega^N_Q(E,\Gamma_2) - C_1(N, \{\lambda_i\}_{1\leq i\leq N}) \right), \tag{4.29}$$

where C_1 does not depend on the physical parameters, but only on geometric parameters. Then, it can be discarded, since the entropy is always defined up to an arbitrary constant.

The computation of Ω^N_Q and S_Q, using representation of the delta function as an integral in the complex plane, is given in the appendix, page 81. It yields the results (4.46) and (4.47), reproduced below:

$$\begin{aligned} \Omega^N_Q(E,\Gamma_2) &\underset{N\to\infty}{\sim} \frac{\exp(N S_Q(E,\Gamma_2))}{\sqrt{2E}}, \\ S_Q\,(E,\Gamma_2) &= \frac{1}{2}\log(\Gamma_2 - 2\lambda_1 E) + \frac{\log 2}{2}. \end{aligned} \tag{4.30}$$

Let us now evaluate the probability density for a microstate to have its (phase-space) coordinate ω_n known. Another way to say this is "for the mode e_n to have amplitude ω_n". This probability density has to be the ratio of the number of microstates with whichever values of $\{\omega_1, \ldots, \omega_{n-1}, \omega_{n+1}, \ldots, \omega_N\}$,

but given ω_n, over the total number of microstates Ω_Q^N. The energy contribution of e_n amounts to $E_n = \omega_n^2/2\lambda_n$, and its enstrophy contribution to ω_n^2. Let us introduce $\mathcal{E}_{\lambda_n}^{N-1} = \mathcal{E}[\omega^N] - \omega_n^2/2\lambda_n$ and $\Gamma_{2,\lambda_n}^{N-1} = \Gamma_2[\omega^N] - \omega_n^2$, which depend only on coordinates $\{\omega_i\}_{1\leq i\leq N, i\neq n}$. Therefore, the probability density for the mode e_n to have amplitude ω_n is

$$P_n^N(\omega_n) = \frac{\Omega_{Q,\lambda_n}^{N-1}(E - \omega_n^2/2\lambda_n, \Gamma_2 - \omega_n^2)}{\Omega_Q^N(E,\Gamma_2)}, \tag{4.31}$$

where

$$\Omega_{Q,\lambda_n}^{N-1}(E - \omega_n^2/2\lambda_n, \Gamma_2 - \omega_n^2) = \int_{\omega_n^2 \leq \min\{2\lambda_n E, \Gamma_2\}} \mathrm{d}\omega_1 \ldots \mathrm{d}\omega_{n-1}\mathrm{d}\omega_{n+1} \ldots \mathrm{d}\omega_N \\ \delta\big(\mathcal{E}_{\lambda_n}^{N-1} - (E - E_n)\big)\, \delta\big(\Gamma_{2,\lambda_n}^{N-1} - (\Gamma_2 - 2\lambda_n E_n)\big)\,.$$

The probability density of E_n is obtained through the change of variable $P_n^N(\omega_n)\mathrm{d}\omega_n = \hat{P}_n^N(E_n)\mathrm{d}E_n$. Using result (4.30) for both Ω_Q^N and $\Omega_{Q,\lambda_1}^{N-1}$ (then, λ_1 has to be replaced with λ_2), we obtain

$$\begin{aligned}
\hat{P}_1^N(E_1) &\underset{N\to\infty}{\sim} \frac{1}{2}\sqrt{\frac{\lambda_1 E}{E_1(E-E_1)}}\frac{(\Gamma_2 - 2\lambda_2 E + 2(\lambda_2-\lambda_1)E_1)^{(N-1)/2}}{(\Gamma_2 - 2\lambda_1 E)^{N/2}} \\
&\underset{N\to\infty}{\sim} \frac{1}{2}\sqrt{\frac{\lambda_1 E}{E_1(E-E_1)}}\left(\frac{\Gamma_2 - 2\lambda_2 E + 2(\lambda_2-\lambda_1)E_1}{\Gamma_2 - 2\lambda_1 E}\right)^{N/2} \\
&\underset{N\to\infty}{\sim} \frac{C_2}{\sqrt{E_1(E-E_1)}}\exp\left[\frac{N}{2}\log\left(\frac{\Gamma_2 - 2\lambda_2 E + 2(\lambda_2-\lambda_1)E_1}{\Gamma_2 - 2\lambda_1 E}\right)\right]
\end{aligned} \tag{4.32}$$

as long as $0 < E_1 < E$; C_2 does not depend on E_1. $\hat{P}_1^N(E_1)$ is exponentially peaked at $E_1 \to E$; indeed,

$$\sup_{E_1|0<E_1<E}\left\{\frac{1}{2}\log\left(\frac{\Gamma_2 - 2\lambda_2 E + 2(\lambda_2-\lambda_1)E_1}{\Gamma_2 - 2\lambda_1 E}\right)\right\} = 0$$

is obtained at $E_1 \to E$. (4.32) is a large-deviation result: we refer the reader to [Touchette, 2009, III. E. 7.] for details. E is the *most probable* value for the energy E_1. The asymptotic behaviour ($N \to \infty$) is

$$\hat{P}_1(E_1) = \delta(E - E_1).$$

Namely, all the energy condensates in the first mode for the energy–enstrophy microcanonical measure.

Likewise, for $n \geq 2$,

$$\hat{P}_n^N(E_n) \underset{N\to\infty}{\sim} \frac{C_3}{\sqrt{E_n(E-E_n)}} \exp\left[\frac{N}{2}\log\left(\frac{\Gamma_2 - 2\lambda_1 E + 2(\lambda_n - \lambda_1)E_n}{\Gamma_2 - 2\lambda_1 E}\right)\right]$$

as long as $0 < E_n < E$; C_3 does not depend on E_n. The asymptotic behaviour is now

$$\hat{P}_n(E_n) = \delta(E_n),$$

for all $n \geq 2$. For the energy–enstrophy microcanonical measure, modes $\{e_n\}_{n\geq 2}$ contain no energy, consistently with $\hat{P}_1(E_1) = \delta(E - E_1)$.

This condensation of energy in the first mode is the main physical prediction of the microcanonical energy–enstrophy ensemble.

4.5.2 Energy–enstrophy microcanonical measure from a mean-field approach

Let us compute the entropy in the (microcanonical) energy–enstrophy ensemble, now derived from the mean-field variational problem. The mean-field variational problem in the (microcanonical) energy–enstrophy ensemble is the equivalent of (MVP), page 73, but with only quadratic invariants taken into account:

$$S(E,\Gamma_2) = \sup_{\{\rho\,|\,N[\rho]=1\}} \left\{ \mathcal{S}[\rho] \mid \mathcal{E}[\bar{\omega}] = E,\ \int_{\mathcal{D}} \mathrm{d}\mathbf{r} \int \mathrm{d}\sigma\ \sigma^2 \rho(\sigma,\mathbf{r}) = \Gamma_2 \right\}. \tag{4.33}$$

Note that the functional to maximize should actually be the specific entropy $\mathcal{S}[\rho]/|\mathcal{D}|$, for this leads to the measure of rescaled phase-space volume (specific volume, volume per degree of freedom). It is customary, throughout the literature, to drop the $1/|\mathcal{D}|$ prefactor for convenience.

To compute the critical points of the variational problem, we introduce Lagrange multipliers, A, β, and α, associated with the conservation of N, $\mathcal{E}$, and Γ_2, respectively (see (4.25), (4.2), and (4.11) for $k = 2$, respectively, for the expression of these quantities). Critical points of (4.33) are such that

$$\frac{\delta\mathcal{S}}{|\mathcal{D}|} - \int_{\mathcal{D}} \mathrm{d}\mathbf{r}\ A(\mathbf{r})\delta N(\mathbf{r}) - \beta\delta\mathcal{E} - \alpha\delta\Gamma_2 = 0$$

for any $\delta\rho$. This is equivalent to

$$\rho(\sigma,\mathbf{r}) = \rho^*(\sigma,\mathbf{r}) := B(\mathbf{r}) \exp[|\mathcal{D}|(\beta\sigma\bar{\psi}(\mathbf{r}) - \alpha\sigma^2)],$$

where the prefactor $B(\mathbf{r}) := \exp(-1 - A(\mathbf{r})|\mathcal{D}|)$ is determined from the normalization constraint (4.25). Then,

$$\rho^*(\sigma,\mathbf{r}) = \sqrt{\frac{\alpha|\mathcal{D}|}{\pi}} \exp\left(-\alpha|\mathcal{D}|\left(\sigma - \frac{\beta\bar{\psi}(\mathbf{r})}{2\alpha}\right)^2\right). \tag{4.34}$$

Substituting (4.34) into (4.22) yields

$$\mathcal{S}[\rho^*] = -\frac{1}{2}\log\alpha \tag{4.35}$$

for the expression of the entropy (find computation in the appendix, page 85). We thus conclude that the maximum-entropy solution has minimal α.

We now compute E and Γ_2 as functions of β and α. First, the average vorticity is obtained by substituting (4.34) into (4.23):

$$\bar{\omega}(\mathbf{r}) = \int_{-\infty}^{+\infty} \mathrm{d}\sigma\ \sigma\rho^*(\sigma,\mathbf{r}) = \frac{\beta}{2\alpha}\bar{\psi}(\mathbf{r}). \tag{4.36}$$

Since $\bar{\omega}(\mathbf{r}) = \Delta\bar{\psi}(\mathbf{r}) = \beta\bar{\psi}(\mathbf{r})/(2\alpha)$, vorticity and streamfunction are both proportional to a Laplacian eigenmode: for some $n \geq 1$ and some $a \in \mathbb{R}$, $\bar{\omega}(\mathbf{r}) = ae_n(\mathbf{r})$ and $\bar{\psi}(\mathbf{r}) = -(a/\lambda_n)e_n(\mathbf{r})$, and we have $\beta = -2\lambda_n\alpha$. From $\mathcal{E}[\bar{\omega}] = E$, we have $E = a^2/(2\lambda_n)$. From $\int\sigma^2\rho^* = \Gamma_2$, we get $\Gamma_2 = 2\lambda_n E + 1/(2\alpha)$. Therefore,

$$\alpha = \frac{1}{2(\Gamma_2 - 2\lambda_n E)}$$

is minimal for $n = 1$ (recall $\lambda_1 < \lambda_2 < \ldots$).

To conclude, the entropy-maximizer mean field is $\bar{\omega}(\mathbf{r}) = \sqrt{2\lambda_1 E}\, e_1(\mathbf{r})$, so that the equilibrium entropy is

$$S_Q(E,\Gamma_2) = \frac{1}{2}\log(\Gamma_2 - 2\lambda_1 E) + \frac{\log 2}{2}. \tag{4.37}$$

This expression for the entropy is exactly the same as (4.30): we have shown that, in the energy–enstrophy ensemble, the mean-field variational problem yields the same result as the energy–enstrophy microcanonical measure, introduced through mode decomposition, where truncation at finite N is performed, and then limit $N \to \infty$ is taken. Note that finding $\bar{\omega} = \sqrt{2\lambda_1 E}\, e_1$ is equivalent to finding $\hat{P}_1(E_1) = \delta(E - E_1)$ and $\hat{P}_n(E_n) = \delta(E_n)$, as in the previous subsection.

4.5.3 Ensemble inequivalence

From the expression for the entropy (4.37), we can compute the inverse 'temperature' $\beta = \partial S_Q/\partial E = -\lambda_1/(\Gamma_2 - 2\lambda_1 E) < 0$ and the 'fugacity' $\alpha = \partial S_Q/\partial\Gamma_2 = 1/[2(\Gamma_2 - 2\lambda_1 E)] < 0$. Recall that these thermodynamical coefficients are related through $\beta = -2\lambda_1\alpha$ (subsection 4.5.2). This relation shows that some couples (β,α) —which a priori span a two-dimensional space— are not obtained in the energy–enstrophy microcanonical ensemble:

we are confined to the line $\{(\alpha, -2\lambda_1\alpha), \alpha > 0\}$. Besides, the determinant of the Hessian of S_Q, that is, $(\partial^2 S_Q/\partial E^2)(\partial^2 S_Q/\partial \Gamma_2^2) - (\partial^2 S_Q/\partial E \partial \Gamma_2)^2$ is zero: hence, S_Q is not strictly concave, unlike the entropy of short-range interacting systems. Both these properties reveal non-equivalence between microcanonical and canonical ensembles[8]: the two statistical ensembles give different predictions (see for instance [Bouchet and Barré, 2005, Ellis et al., 2000, Campa et al., 2009] and Chapter 2 of this thesis). This contrasts with the usual thermodynamics of condensed matter systems.

Note that a detailed discussion of ensemble inequivalence and related phase transitions, for statistical equilibria with a linear relation between vorticity and streamfunction (including the case of the energy–enstrophy ensemble), can be found in [Venaille and Bouchet, 2009]. The extension to slightly nonlinear relations between vorticity and streamfunction is found in chapter 2.

4.6 Open conclusion

Limitations of the energy–enstrophy approach. There is a priori no reason to take into account only quadratic invariants, except for being able to solve the mathematics easily. From the discussion of subsection 4.4.1, we know that a mean-field approach is exact (for 2D Euler equations); thus, any other microcanonical measure (corresponding to any set of invariants) could be considered. The reasons for favouring some invariants over others are phenomenological, ultimately. Different authors have argued for different interpretations [Chavanis and Sommeria, 1996, Ellis et al., 2002, Venaille and Bouchet, 2011, Naso et al., 2010], as recalled in chapter 1.

It was shown in previous works (see [Bouchet and Simonnet, 2009]) that, when taking into account all invariants, the energy is no longer confined to the first mode e_1. The energy–enstrophy measure may still be a good approximation in some cases: in the limit of small energy, for instance, most of the energy remains in the first few modes: the notion of condensation remains valid at a qualitative level. In contrast, in cases such as a doubly periodic domain with aspect ratio close to, but different from one [Bouchet and Simonnet, 2009], condensation is not verified at all.

Dynamical invariance. We have not discussed the invariance of the microcanonical measures per se. This invariance is verified a posteriori, by checking the time evolution of the statistics of the random field ω. Introducing

[8] This instance of ensemble inequivalence, for the energy–enstrophy ensembles, is actually a case of partial equivalence (see [Ellis et al., 2000] for a definition).

its characteristic functional, $F[l,t] = \langle \exp(\mathrm{i} \int \mathrm{d}\mathbf{r}\ l(\mathbf{r})\omega(\mathbf{r},t)) \rangle$, and cumulant-generating functional, $H[l,t] = \log F[l,t]$, makes it possible: in the exponential, you have all the vorticity moments (the average $\langle \cdot \rangle$ is taken with respect to the probability measure). Derivations rely on the fact that the measure is a product measure. We refer the interested reader to the journal paper [Bouchet and Corvellec, 2010, section 4] for details.

Towards non-equilibrium problems. It would be good to be able to extend this work to (slightly) non-equilibrium problems, such as the 2D Navier–Stokes equations with stochastic forces. For this non-conservative dynamical system, the *existing* invariant measures [Kuksin, 2004] have to bear fluxes of macroscopic quantities. Hopefully, the invariant measures described in the journal paper could be lowest-order solutions in an asymptotic expansion of (flux-permitting) invariant measures for dissipative systems. Indeed, in two-dimensional flows, the energy flux is thought to converge to zero in the limit of small forcing and dissipation, unlike in three-dimensional flows (where anomalous dissipation takes place). The limit of small forces and dissipation may then be well-behaved.

Also, in a statistical steady state, we have energy conservation 'on average' (over time averages). So, on average, the dissipation rate matches the energy input rate. This implies the relevance of microcanonical measures over canonical ones.

Appendix

In this appendix, we compute the entropy for the energy–enstrophy ensemble. Again (see (4.28), (4.29) and the related discussion), the entropy is defined by

$$S_Q(E,\Gamma_2) = \lim_{N\to\infty} \frac{1}{N} \log \Omega_Q^N(E,\Gamma_2),$$
$$\text{with} \quad \Omega_Q^N(E,\Gamma_2) = \int \prod_{i=1}^{N} \mathrm{d}\omega_i \; \delta(\mathcal{E}^N[\omega] - E)\delta(\Gamma_2^N[\omega] - \Gamma_2). \tag{4.38}$$

We start by relaxing the enstrophy constraint: the Dirac delta in enstrophy is replaced with a Boltzmann factor in the expression of Ω_Q^N. Thus, we compute, for $\alpha \geq 0$,

$$I_N(E,\alpha) = \int \prod_{i=1}^{N} \mathrm{d}\omega_i \; \delta(\mathcal{E}^N[\omega] - E) \exp(-N\alpha\omega_i^2). \tag{4.39}$$

The relation between $I_N(E,\alpha)$ and $\Omega_Q^N(E,\Gamma_2)$ will be discussed later in the appendix. Regarding the remaining Dirac delta (in energy), let us use a representation as an integral in the complex plane:

$$\begin{aligned}
I_N(E,\alpha) &= \int \prod_{i=1}^{N} \mathrm{d}\omega_i \; \delta\left(\sum_{i=1}^{N} \frac{\omega_i^2}{\lambda_i} - 2E\right) \exp(-N\alpha\omega_i^2) \\
&= \frac{1}{2\pi} \int_{-\infty}^{+\infty} \mathrm{d}k \;\; \exp(-2\mathrm{i}Ek) \prod_{i=1}^{N} \int \mathrm{d}\omega_i \;\; \exp\left(-\left(N\alpha - \frac{\mathrm{i}k}{\lambda_i}\right)\omega_i^2\right) \\
&= \frac{1}{2\pi} \int_{-\infty}^{+\infty} \mathrm{d}k \;\; \exp(-2\mathrm{i}Ek) \prod_{i=1}^{N} \sqrt{\frac{\pi}{N\alpha - \frac{\mathrm{i}k}{\lambda_i}}} \\
&= \frac{\pi^{(N/2)-1}}{2(N\alpha)^{N/2}} \int_{-\infty}^{+\infty} \mathrm{d}k \;\; \exp(-2\mathrm{i}Ek) \prod_{i=1}^{N} \left(1 - \frac{\mathrm{i}k}{N\alpha\lambda_i}\right)^{-1/2} \\
&= \frac{1}{2} \left(\frac{\pi}{N\alpha}\right)^{(N/2)-1} \int_{-\infty}^{+\infty} \mathrm{d}z \;\; \exp(-2\mathrm{i}EN\alpha z) \prod_{i=1}^{N} \left(1 - \frac{\mathrm{i}z}{\lambda_i}\right)^{-1/2},
\end{aligned} \tag{4.40}$$

where use has been made of Fubini's theorem (to swap product and integration in the variables $\{\omega_i\}_{1\leq i\leq N}$), and of the change of variable $z = k/(N\alpha)$.

Integrating complex-valued functions over the real axis is not trivial; for this purpose, we resort to path integration methods. Note that such techniques are commonly used in the physics community of phase transitions; let us mention [Loxley, 2008, appendix A] and [Campa et al., 2009, 4.4.4.]. We evaluate (4.40) in the framework of Langer's theory [Langer, 1967], as presented in [Schulman, 1981].

Analytic continuation in the complex plane

Let us evaluate the asymptotic behaviour (i.e., as $N \to \infty$) of the integral

$$J_N(E,\alpha) = \int_{-\infty}^{+\infty} \mathrm{d}z \ \exp(-2\mathrm{i}EN\alpha z) f_N(z)$$
$$\text{with} \quad f_N(z) = \prod_{j=1}^{N} \left(1 - \frac{\mathrm{i}z}{\lambda_j}\right)^{-1/2}. \tag{4.41}$$

Recall that $\{-\lambda_j\}_{1\le j\le N}$ are the first N eigenvalues of the Laplacian on $\mathcal{D}$, with order $\lambda_1 < \lambda_2 < \ldots < \lambda_N$. The trick is to change the integration contour from the real axis to the imaginary axis. We do not justify this here, but only apply the above-referenced path integration methods, detailing the various steps involved.

To begin with, let us investigate the asymptotic behaviour of f_N. So far, we have had $z \in \mathbb{R}$. Now let z take values in $\mathbb{C}$. $f_N(z)$ is singular at $z = -\mathrm{i}\lambda_j$, for $1 \le j \le N$. For $z \in \mathbb{C} \setminus \{-\mathrm{i}(\lambda_1 + x) : x \ge 0\}$, $f_N(z)$ is analytical, and so is $\log f_N(z)$. We show that $f_N(z) \sim N^{\mathrm{i}z|\mathcal{D}|/(8\pi)}$ as $N \to \infty$.

It is a classical result about Laplacian eigenvalue properties [Courant and Hilbert, 1953] that

$$\lambda_j \underset{j\to\infty}{\sim} \frac{4\pi}{|\mathcal{D}|} j.$$

Then, from the well-known equivalence for the harmonic series,

$$\sum_{j=1}^{N} \frac{1}{\lambda_j} \underset{N\to\infty}{\sim} \frac{|\mathcal{D}|}{4\pi} \log N. \tag{4.42}$$

Since $\log(1 + z/j) - z/j = o(1/j)$, we have

$$\log f_N(z) = -\frac{1}{2}\sum_{j=1}^{N} \log\left(1 - \frac{\mathrm{i}z}{\lambda_j}\right) = -\frac{1}{2}\sum_{j=1}^{N}\left[-\frac{\mathrm{i}z}{\lambda_j} + g_j(z)\right],$$

where $g_j(z) = o(1/\lambda_j)$. So $\sum_{j=1}^{N} g_j(z) = o(\log N)$, owing to (4.42). We are left with

$$\log f_N(z) \underset{N\to\infty}{\sim} \mathrm{i}z\frac{|\mathcal{D}|}{8\pi} \log N$$

and, hence,

$$f_N(z) \underset{N\to\infty}{\sim} N^{\mathrm{i}z\frac{|\mathcal{D}|}{8\pi}}. \ \blacksquare \tag{4.43}$$

As already mentioned, in (4.40), we take z to run from $-\mathrm{i}\infty$ to $+\mathrm{i}\infty$ instead of $-\infty$ to $+\infty$ (we boldly use the notation '$\pm\mathrm{i}\infty$' after [Schulman, 1981]). Actually, we take it to run from $-\mathrm{i}\infty$ to $-\mathrm{i}\lambda_1$, because there is no contribution

from the imaginary range $]-\lambda_1, +\infty[$ [Schulman, 1981, page 280]. Equivalently, making the change of variable $z = -\mathrm{i}(\lambda_1 + x)$, we take x to run from $+\infty$ to 0. Applying this procedure to (4.40) gives

$$\mathrm{i}\exp(-2EN\alpha\lambda_1)\int_0^{+\infty}\mathrm{d}x\ \exp(-2EN\alpha x)f_N(-\mathrm{i}(\lambda_1+x)),$$

whose imaginary part must be $J_N(E,\alpha)$. The main contribution to the integral comes from (the vicinity of) $x = 0$. Thus, we seek an expression for f_N which is more accurate than (4.43) in the vicinity of $z = -\mathrm{i}\lambda_1$. Introducing

$$h_N(z) = \left(1 - \frac{\mathrm{i}z}{\lambda_1}\right)^{1/2} f_N(z) = \prod_{j=2}^{N}\left(1 - \frac{\mathrm{i}z}{\lambda_j}\right)^{-1/2},$$

which is not singular at $z = -\mathrm{i}\lambda_1$, we have, similarly to (4.43),

$$h_N(z) \underset{N\to\infty}{\sim} N^{\mathrm{i}z\frac{|\mathcal{D}|}{8\pi}},$$

which yields

$$f_N(z) \underset{N\to\infty}{\sim} \frac{N^{\mathrm{i}z\frac{|\mathcal{D}|}{8\pi}}}{\left(1-\frac{\mathrm{i}z}{\lambda_1}\right)^{1/2}}.$$

Then,

$$\begin{aligned} J_N(E,\alpha) &\underset{N\to\infty}{\sim} N^{\lambda_1\frac{|\mathcal{D}|}{8\pi}}\sqrt{\lambda_1}\exp(-2EN\alpha\lambda_1)\int_0^{+\infty}\mathrm{d}x\ \exp(-2EN\alpha x)\frac{N^{x\frac{|\mathcal{D}|}{8\pi}}}{\sqrt{x}} \\ &\underset{N\to\infty}{\sim} N^{\lambda_1\frac{|\mathcal{D}|}{8\pi}}\sqrt{\lambda_1}\exp(-2EN\alpha\lambda_1)\int_0^{+\infty}\frac{\mathrm{d}x}{\sqrt{x}}\ \exp(-2EN\alpha x) \\ &= N^{\lambda_1\frac{|\mathcal{D}|}{8\pi}}\exp(-2EN\alpha\lambda_1)\sqrt{\frac{\pi\lambda_1}{2EN\alpha}}, \end{aligned}$$

where we have used the change of variable $y = \sqrt{2EN\alpha x}$. From (4.39), we conclude that

$$\begin{aligned} I_N(E,\alpha) &\underset{N\to\infty}{\sim} \frac{1}{2}\left(\frac{\pi}{N\alpha}\right)^{N/2} N^{\lambda_1\frac{|\mathcal{D}|}{8\pi}}\exp(-2EN\alpha\lambda_1)\sqrt{\frac{\lambda_1}{2E}} \\ &= \frac{1}{2}\left(\frac{\pi}{N}\right)^{N/2} N^{\lambda_1\frac{|\mathcal{D}|}{8\pi}}\sqrt{\frac{\lambda_1}{2E}}\exp\left(-N\left(2E\alpha\lambda_1 + \frac{\log\alpha}{2}\right)\right). \end{aligned} \quad (4.44)$$

Direct computation of the energy–enstrophy entropy

We now come back to the relationship between $\Omega_Q^N(E,\Gamma_2)$ (4.38) and $I_N(E,\alpha)$ (4.39). $\Omega_Q^N(E,\Gamma_2)$ is the density of states with energy E and enstrophy Γ_2;

$I_N(E,\alpha)$ is the density of states with energy E and *any* enstrophy $\Gamma_2 \geq 2\lambda_1 E$ [9], i.e., when the enstrophy constraint is *relaxed*; α is the variable dual to Γ_2. (4.39) rewrites

$$I_N(E,\alpha) = \int_{2\lambda_1 E}^{+\infty} \mathrm{d}\Gamma_2 \ \exp(-N\alpha\Gamma_2)\Omega_Q^N(E,\Gamma_2). \tag{4.45}$$

As has been done for I_N, analytic continuation in the complex plane can be performed for the computation of Ω_Q^N. It is just more tedious, as two auxiliary variables (analogous to k) have to come into play. Likewise, the asymptotic behaviour is

$$\Omega_Q^N(E,\Gamma_2) \underset{N\to\infty}{\sim} \frac{\exp(NS_Q(E,\Gamma_2))}{\sqrt{2E}}. \tag{4.46}$$

S_Q, the entropy, is the thermodynamic potential of the microcanonical ensemble. In (4.44), let $G(E,\alpha) := 2E\alpha\lambda_1 + \log\alpha/2$. This is the thermodynamic potential of the canonical (i.e., relaxed) ensemble. Therefore, it relates to the entropy as follows:

$$G(E,\alpha) = \inf_{\Gamma_2 \geq 2\lambda_1 E} \{-S_Q(E,\Gamma_2) + \alpha\Gamma_2\}.$$

To be precise, $G(E,\cdot)$ is the Legendre–Fenchel transform of $S_Q(E,\cdot)$. It is a classical result that if G is not singular, then S_Q can be computed from the inverse formula $S_Q(E,\Gamma_2) = \inf_{\alpha\geq 0}\{-G(E,\alpha) + \alpha\Gamma_2\}$ (see any textbook on convex analysis or [Bouchet, 2008]). Thus,

$$S_Q(E,\Gamma_2) = \big(-G(E,\alpha) + \alpha\Gamma_2\big)\big|_{\alpha=\frac{1}{2(\Gamma_2-2\lambda_1 E)}} = \frac{1}{2}\log\left(2(\Gamma_2 - 2\lambda_1 E)\right) + \frac{1}{2}.$$

Because the entropy, as a function of E and Γ_2, is defined up to an arbitrary constant, we keep the result

$$S_Q(E,\Gamma_2) = \frac{1}{2}\log\left(\Gamma_2 - 2\lambda_1 E\right) + \frac{\log 2}{2}, \tag{4.47}$$

because it is the same as that found in the mean-field approximation context. Note that the entropy diverges towards $-\infty$ for $\Gamma_2 = 2\lambda_1 E$, i.e., the minimal accessible enstrophy Γ_2 for a given energy E. As can be readily seen from the Poincaré inequality, only the two microscopic states $\omega = \pm\sqrt{2E}e_1$ correspond to the macrostate with the equality $\Gamma_2 = 2\lambda_1 E$. Then, the minimality in entropy was expected (hardly no uncertainty, hardly any 'lack of information').

[9] This condition is obtained straightforwardly from the expressions $\mathcal{E}[\omega] = \sum_i \omega_i^2/(2\lambda_i) = E$ and $\Gamma_2[\omega] = \sum_i \omega_i^2 = \Gamma_2$. It is an instance of Poincaré inequality.

Computation of the energy–enstrophy Boltzmann entropy

Substituting (4.34) into (4.22),

$$\begin{aligned}\mathcal{S}[\rho^*] &= -\sqrt{\frac{\alpha|\mathcal{D}|}{\pi}} \int_{\mathcal{D}} \mathrm{d}\mathbf{r} \int_{-\infty}^{+\infty} \mathrm{d}\sigma \; \mathrm{e}^{-\alpha|\mathcal{D}|\left(\sigma - \frac{\beta\bar{\psi}(\mathbf{r})}{2\alpha}\right)^2} \left[\log\left(\sqrt{\frac{\alpha|\mathcal{D}|}{\pi}}\right) - \alpha|\mathcal{D}|\left(\sigma - \frac{\beta\bar{\psi}(\mathbf{r})}{2\alpha}\right)^2\right] \\ &= -\sqrt{\frac{\alpha|\mathcal{D}|}{\pi}} \int_{\mathcal{D}} \mathrm{d}\mathbf{r} \int_{-\infty}^{+\infty} \mathrm{d}\sigma \; \mathrm{e}^{-\alpha|\mathcal{D}|\sigma^2} \left[\frac{1}{2}\log\left(\frac{\alpha|\mathcal{D}|}{\pi}\right) - \alpha|\mathcal{D}|\sigma^2\right] \\ &= -\frac{1}{2}\log\alpha - \frac{1}{2}\log\left(\frac{|\mathcal{D}|}{\pi}\right) + \frac{1}{2}.\end{aligned}$$

The last two terms of the r.h.s. being generic (for the entropy is defined up to a constant), we retain

$$\mathcal{S}[\rho^\star] = -\frac{1}{2}\log\alpha. \tag{4.48}$$

Appendix A

Derivation of the barotropic quasi-geostrophic model

We consider an Earth-like planet rotating at constant angular velocity Ω. The rotation axis is denoted by $\mathbf{e}_{axis}$. Let $\mathbf{v}$ be the three-dimensional velocity of our fluid, lying at the surface of the planet. The equation of motion for the fluid is given by the Navier–Stokes equations in the planet's rotating frame:

$$\frac{D\mathbf{v}}{Dt} + 2\Omega\mathbf{e}_{axis} \times \mathbf{v} = -\frac{\nabla p}{\rho} - \mathbf{g} + \nu\Delta\mathbf{v}, \tag{A.1}$$

where the first term of the lhs is the material derivative of the velocity, p is the pressure, ρ the density, $\mathbf{g}$ the gravitational field, and ν the viscosity. Note that a detailed derivation of the following is given in [Pedlosky, 1987, Chapters 2, 3, and 4].

We consider a local Cartesian coordinate system $(\mathbf{e}_x, \mathbf{e}_y, \mathbf{e}_z)$, at a given position in the fluid. $\mathbf{e}_x$ points eastward, $\mathbf{e}_y$ points northward, and $\mathbf{e}_z$ points upward. We are at latitude $\theta \in [-\pi/2, \pi/2]$. Then, $\mathbf{e}_{axis} = \cos\theta\mathbf{e}_y + \sin\theta\mathbf{e}_z$. The quantity $f = 2\Omega\sin\theta$, called the planetary vorticity, gives the strength of the Coriolis force as a function of latitude. It shows in the component formulation of (A.1). Now let us sketch the scale analysis relevant at large (horizontal) scale. This large scale is that of ocean basins, for instance. In meteorology, it is the synoptic scale, at which cyclones and anticyclones form. It is of order 10^6 m. Let us denote it by L. The thickness of the ocean layer (upper layer) which is in motion is of order 10^2 m. Let us denote it by H. Let U be a typical magnitude of the horizontal velocity. It is of the order of 1 m.s^{-1} in the atmosphere, 0.1 m.s^{-1} in the ocean.

From geometrical considerations, the ratio of vertical velocities to horizontal velocities is of order the aspect ratio $\delta := H/L \ll 1$. Let $\mathbf{u}$ be the two-dimensional velocity and w the vertical component of velocity. The quasi-geostrophic approximation arises from the smallness of the following nondimensional numbers:

– the Rossby number $Ro = U/(fL)$ compares the advective acceleration to the Coriolis acceleration;

– the (horizontal) Ekman number $Ek = \nu/(fL^2)$ compares the viscous frictional force to the Coriolis acceleration;

– and the aspect ratio $\delta = H/L$.

Note that for Ro to be small, we cannot be near the equator. The model is typically valid for mid-latitude flows. Another approximation is made to take into account the latitudinal extent of a given domain, in the local Cartesian coordinate system. It is the beta-plane approximation: the expression of f is linearized around the mean latitude θ_0 of the domain. We have

$$f \approx 2\Omega \sin\theta_0 + 2\Omega \cos\theta_0(\theta - \theta_0) \approx 2\Omega \sin\theta_0 + 2\Omega \cos\vartheta_0 \frac{y}{r_T} =: f_0 + \beta_C y,$$

where r_T is the planet's radius, and β_C is called the Coriolis parameter. We have another small parameter: $\beta_C L/f_0$. Note that f can take either sign (depending on the hemisphere), so we should write $|f|$ in the scale analysis. Say we are in the Northern Hemisphere and $f > 0$. The idea is to carry out an asymptotic expansion in the collective small parameter $\epsilon(\delta, Ro, Ek, \beta_C L/f_0, \ldots)$, which can depend on other small ratios. Velocity is expanded as $\mathbf{u} = \mathbf{u}_0 + \epsilon\mathbf{u}_1 + \ldots$ and the other fields likewise. At lowest (zeroth) order, the flow is geostrophic, i.e.,

$$f_0 \mathbf{e}_z \times \mathbf{u}_0 = -\frac{\nabla_{(x,y)} p_0}{\rho},$$

and hydrostatic, i.e.,

$$\frac{\partial p_0}{\partial z} = -\rho g,$$

where $\nabla_{(x,y)}$ is the horizontal gradient. The geostrophic and hydrostatic balances are valid in the interior of the fluid. The continuity equation,

$$\nabla \cdot \mathbf{u} = -\frac{\partial w}{\partial z},$$

yields, at lowest order,

$$\nabla \cdot \mathbf{u}_0 = 0,$$

which enables the introduction of a streamfunction, ψ, proportional to the pressure.

At next (first) order, we have

$$\frac{\partial \mathbf{u}_0}{\partial t} + \mathbf{u}_0 \cdot \nabla \mathbf{u}_0 + f_0 \mathbf{e}_z \times \mathbf{u}_1 + \beta_C y \mathbf{e}_z \times \mathbf{u}_0 = -\frac{\nabla p_1}{\rho} + \nu \Delta \mathbf{u}_0, \tag{A.2}$$

in dimensional form, and

$$\nabla \cdot \mathbf{u}_1 = -\frac{\partial w_1}{\partial z}. \tag{A.3}$$

After integration from bottom ($z = h_B$) to top ($z = h_T$), $\nabla \cdot \mathbf{u}_1 = -(w_1(h_T) - w_1(h_B))/(h_T - h_B) = (w_1(h_B) - w_1(h_T))/H$ + h.o.t. in ϵ.

For convenience, we introduce the notation $\operatorname{curl} \mathbf{a} := (\nabla \times \mathbf{a}) \cdot \mathbf{e}_z$. Since $\mathbf{u}$ is 2D, the vorticity $\boldsymbol{\omega} = \nabla \times \mathbf{u}$ has its horizontal components vanish. Let us note $\omega = \operatorname{curl} \mathbf{u}_0 = \Delta\psi$. Close to the bottom ($z = h_B$) and the top ($z = h_T$), we have boundary layers [Pedlosky, 1987, Chapter 4]. In the top and bottom boundary layers, the length scale is not H but δ_E, that is, the thickness of the Ekman layer: $\delta_E = \sqrt{\frac{2\nu}{f_0}}$. Boundary-layer analysis leads to

$$w_1(h_T) = \frac{\delta_E}{2} \left(\operatorname{curl} \mathbf{u}_T - \operatorname{curl} \mathbf{u}_0 \right), \tag{A.4}$$

where $\operatorname{curl} \mathbf{u}_T$ is the vorticity at $z = h_T$. We discard free surface variations so that $h_T = H$ (rigid-lid approximation). In the presence of topography, $h_B(x, y)$ is not uniform. Again, from boundary-layer analysis,

$$w_1(h_B) = \mathbf{u}_0 \cdot \nabla h_B + \frac{\delta_E}{2} \operatorname{curl} \mathbf{u}_0. \tag{A.5}$$

Applying the operator curl to (A.2) yields the barotropic quasi-geostrophic model; it is an equation in ω:

$$\begin{aligned} &\frac{\partial \omega}{\partial t} + \mathbf{u}_0 \cdot \nabla \left(\omega + \frac{f_0}{H} h_B + \beta_C y \right) = \\ &\nu \Delta \omega - \frac{\sqrt{2\nu f_0}}{H} \omega + \frac{\sqrt{2\nu f_0}}{H} \operatorname{curl} \mathbf{u}_T. \end{aligned} \tag{A.6}$$

The second term in the rhs, a linear friction, is usually interpreted as bottom drag. The last term is a forcing term: $\operatorname{curl} \mathbf{u}_T$, the vorticity field at $z = h_T$, corresponds to wind stress in the case of an ocean model. In the case of an experiment (rotating tank), $\mathbf{u}_T$ is the forcing velocity. The quantity

$$q = \frac{\omega + f}{h_T - h_B}$$

is the potential vorticity [Pedlosky, 1987, Chapter 3]. The planetary vorticity dominates the (relative) vorticity: $f \sim \Omega \sim 10^{-5}\ \mathrm{s}^{-1}$ and $\omega \sim U/L \sim 10^{-7}\ \mathrm{s}^{-1}$. Say $\omega/f \sim \epsilon$. The potential vorticity can then be expanded as $q = f_0/H_0 + \epsilon q_1 + \ldots$, to see that (A.6) expresses the transport of q_1. The term $\mathbf{u}_0 \cdot q_1$ is referred to, interchangeably, as the advection term, the nonlinear term, or the inertial term. For the large scales of atmospheric and oceanic motion, it

dominates the forcing and dissipation terms (rhs) [Pedlosky, 1987, page 179]. Therefore, we are led to consider the purely inertial limit:

$$\frac{\partial q_1}{\partial t} + \mathbf{u}_0 \cdot \nabla q_1 = 0,$$

where we have rescaled (A.6) and neglected the rhs.

Appendix B

Fold Bifurcation and Numerical Continuation

In this note, a quick overview of the pseudo-arclength continuation method is provided, along with a simple application, for the sake of illustration. The aim of this note is to show the interest of such a numerical method, when computing solution branches which display fold (saddle-node) bifurcations. Such solution branches are found in any system formally similar to the normal form of a saddle-node bifurcation, as known for dynamical systems ($\dot{x} = r + x^2$). The overview follows very closely [Kuznetsov, 2004].

B.1 Method

B.1.1 General Considerations

Let $F : \mathbb{R}^{n+1} \to \mathbb{R}^n$ and

$$M := \{y \in \mathbb{R}^{n+1} : \ F(y) = 0\}.$$

The numerical continuation problem consists in computing a sequence $\{y^j\}_{j=1}^{\infty}$ approximating M. We consider the case of a nonlinear equation in $u \in \mathbb{R}^n$, depending on a scalar parameter $\alpha \in \mathbb{R}$, so that $y = (u, \alpha)$. In the context of dynamical systems, i.e.,

$$u' = F(u, \alpha),$$

M is called the equilibrium curve. As α is varied, continuation methods come into play for the numerical analysis of bifurcations.

Assume an initial point $y^0 = (u^0, \alpha^0)$ is given —typically, for a certain value of $\alpha = \alpha^0$, the equilibrium $u = u^0$ can be found analytically. Numerical continuation is an iterative method, where the sequence $\{y^j\}_{j=1}^{\infty}$ satisfies the recurrence relation

$$y^{j+1} = y^j + \delta y^j \,, \quad j \geq 0. \tag{B.1}$$

Each iteration consists of two steps: i) prediction $y^j \mapsto \tilde{y}^{j+1}$, and ii) correction $\tilde{y}^{j+1} \mapsto y^{j+1}$.

Let ds be the step size.

B.1.2 Algorithm for Natural Continuation

i) Prediction

The step is taken in the parameter space, i.e.

$$\alpha^j \mapsto \alpha^{j+1} = \alpha^j + ds,$$

and the guess for u^{j+1} is taken to be the previous solution, i.e.,

$$u^j \mapsto \tilde{u}^{j+1} = u^j.$$

i) Correction

One has $\tilde{u}^{j+1}$ converge to u^{j+1} through a Newton-like method. Of course, convergence criteria must be specified: precision on $F(u^{j+1}) = 0$, etc.

B.1.3 Algorithm for Pseudo-Arclength Continuation

i) Prediction

The step is now taken in the space tangent to M. Say that y^j is the solution at iteration j. We may Taylor-expand

$$F(y^{j+1}) = F(y^j) + J^j \delta y^j + O(\|\delta y^j\|^2) = J^j \delta y^j + O(\|\delta y^j\|^2),$$

where J^j is the Jacobian of F evaluated at y^j. The guess $\tilde{y}^{j+1}$ is then given by

$$F(\tilde{y}^{j+1}) = J^j \delta y^j. \tag{B.2}$$

The Jacobian matrix is $n \times (n+1)$; it reads $J = [J_u \quad J_\alpha]$, with

$$J_u^j = \left[\frac{\partial F}{\partial u_b}(u_a^j, \alpha^j)\right]_{a,b=1,\dots,n}, \quad J_\alpha^j = \left[\frac{\partial F}{\partial \alpha}(u_a^j, \alpha^j)\right]_{a=1,\dots,n}.$$

Zeroing (B.2) amounts to solving

$$\begin{aligned} & J_u^j \delta u^j + J_\alpha^j \delta \alpha^j = 0 \\ \Leftrightarrow \quad & \delta u^j + (J_u^j)^{-1} J_\alpha^j \delta \alpha^j = 0 \end{aligned}$$

as long as J_u^j is invertible. The tangent vector being orthogonal to the gradient, it has to be along $(-(J_u^j)^{-1} J_\alpha^j, 1)$. Denoting the normalization factor by $N = \sqrt{\|(J_u^j)^{-1} J_\alpha^j\|^2 + 1}$,

$$v^j = \frac{1}{N} \begin{pmatrix} -(J_u^j)^{-1} J_\alpha^j \\ 1 \end{pmatrix} \tag{B.3}$$

is the unit vector tangent to M at point y^j. Thus, we take the following step:

$$y^j \mapsto \tilde{y}^{j+1} = y^j + ds\, v^j$$

The predicted point $\tilde{y}^{j+1}$ is close to the equilibrium curve, but it is not close enough in general. It must be corrected into y^{j+1} so that $F(y^{j+1}) = 0$ within desired accuracy.

i) Correction
In order to satisfy the constraint

$$\langle y^{j+1} - y^j, v^j \rangle = ds, \tag{B.4}$$

y^{j+1} is sought in a hyperplane orthogonal to v^j so that $\langle y^{j+1} - \tilde{y}^{j+1}, v^j \rangle = 0$. Indeed,

$$\begin{aligned} \text{(B.4)} &= \langle y^{j+1} - \tilde{y}^{j+1}, v^j \rangle + \langle \tilde{y}^{j+1} - y^j, v^j \rangle \\ &= \langle y^{j+1} - \tilde{y}^{j+1}, v^j \rangle + ds \langle v^j, v^j \rangle = ds. \end{aligned}$$

B.1.4 Branching Points

Branching points are the bifurcation points whenever the study is restricted to equilibria. A bifurcation is reached when J_u becomes singular. There, (B.3) is ill-defined. Therefore, we need to detect numerically the vanishing of $\det J_u$.

B.2 Simple Examples

B.2.1 Detection of a Fold Bifurcation

Let us start with a very simple low-dimensional ($n = 2$) system. Then, $u = (u_1, u_2)$. Say the mapping $F : \mathbb{R}^3 \to \mathbb{R}^2$ is given by

$$F(u, \lambda) = \begin{pmatrix} F_1(u_1, u_2, \lambda) = u_1^2 - \lambda \\ F_2(u_1, u_2, \lambda) = u_1 u_2 - \lambda \end{pmatrix}. \tag{B.5}$$

There is obviously no need for numerical tools to solve $F(u, \lambda) = 0$; we consider such a system for illustration purposes only. The equilibrium curve $M = \{(u_1, u_2, \lambda) \in \mathbb{R}^3 : u_1 = \pm\sqrt{\lambda}, u_2 = u_1, \lambda \geq 0\}$ is a smooth curve passing through the fold bifurcation point $(u, \lambda) = (0, 0)$, where the Jacobian $J(0, 0)$ has a simple eigenvalue.

The Jacobian, given by

$$J(u, \lambda) = \begin{pmatrix} 2u_1 & 0 & -1 \\ u_2 & u_1 & -1 \end{pmatrix} = \begin{pmatrix} \pm 2\sqrt{\lambda} & 0 & -1 \\ \pm\sqrt{\lambda} & \pm\sqrt{\lambda} & -1 \end{pmatrix} = \begin{bmatrix} J_u & J_\lambda \end{bmatrix},$$

is full-rank ($\operatorname{rank} J = n$) on $M \backslash \{(0,0)\}$.

Let us apply the algorithm of pseudo-arclength continuation to this trivial example. Take the initial point to be $(u_1^0 = \sqrt{\lambda^0}, u_2^0 = \sqrt{\lambda^0}, \lambda^0 > 0)$ and the continuation step to be $ds < 0$. Then, for $j \geq 0$, (u^{j+1}, λ^{j+1}) is approximated in tangent space by

$$\begin{cases} \tilde{u}^{j+1} = u^j + \dfrac{ds}{\sqrt{2(1+2\lambda^j)}} \begin{pmatrix} 1 \\ 1 \end{pmatrix} =: u^j + ds\, v_u^j, \\ \tilde{\lambda}^{j+1} = \lambda^j + ds \dfrac{\sqrt{\lambda^j}}{\sqrt{1+2\lambda^j}} =: \lambda^j + ds\, v_\lambda^j. \end{cases}$$

We have u_1, u_2, and λ decrease at each iteration. Up until a certain $j = K$, $\operatorname{sgn}(u^{j+1}) = \operatorname{sgn}(u^j)$ and $\operatorname{sgn}(\lambda^{j+1}) = \operatorname{sgn}(\lambda^j)$. Afterwards, we reach the negative 'half-space' of $\mathbb{R}^3$. To follow M, we want to keep moving towards negative values of (u_1, u_2), but λ values have to increase again (towards $+\infty$).

Keeping $ds < 0$, we have to do $v_\lambda^{K+2} \mapsto -v_\lambda^{K+2}$. If we do not, we will see $(\tilde{u}^{K+2}, \tilde{\lambda}^{K+2})$ converge to (u^{K+2}, λ^{K+2}) at the correction step (provided the fold is not *too* sharp), but then $(\tilde{u}^{K+3}, \tilde{\lambda}^{K+3})$ will find itself back in the positive 'half-space', in the vicinity of $(\tilde{u}^{K+1}, \tilde{\lambda}^{K+1})$. The vanishing of $\det J_u \geq 0$ will then be detected from this oscillation around the fold-bifurcation point, here $(0,0)$.

Appendix C

Towards a numerical computation of equilibria in a channel/annulus

C.1 Computation of $\lambda_* = -\beta_*$

λ_* is the smallest value of $-\beta$ such that (2.20). The series $\hat{f}(x)$ converges pointwise for all $x \in \mathbb{R}\backslash\{-\lambda_{0,n}\}_{n\geq 1}$. Because $\{e_{0,n}(r)\}$ are just the azimuthally invariant eigenfunctions of the Laplacian in polar coordinates, with specific boundary conditions, we can say that $\lambda_{0,n}$ scales like n^2 and $\lambda_{0,n}\langle e_{0,n}\rangle^2$ scales like 1. Indeed, in Cartesian geometry, we would take the domain to be a channel of length L_x along the x-axis, of width L_y along the y axis, and with L_x-periodicity in x. Then, the x-invariant orthonormalized eigenfunctions are $\{u_n(y) = \sqrt{\frac{2}{L_x L_y}} \sin\left(n\frac{\pi}{2}\frac{y}{L_y}\right)\}_{n=2p+1,\, p\in\mathbb{N}}$, associated with the set of eigenvalues $\{-\sigma_n = -\left(\frac{n\pi}{2L_y}\right)^2\}$, so $\langle u_n\rangle = \frac{2\sqrt{2L_xL_y}}{n\pi}$. The summand can then be expressed explicitly as a function of n:

$$-\frac{\sigma_n\langle u_n\rangle^2}{\sigma_n + x} = -\frac{L_x}{L_y}\frac{2}{\left(\frac{n\pi}{2L_y}\right)^2 + x},$$

so that the series $f^{\text{cart}}(x) = -\sum_{n\geq 1}\frac{\sigma_n\langle u_n\rangle^2}{\sigma_n+x}$ as well as its partial sums can be evaluated using mathematical software.

For all $n \in \mathbb{N}^*$, we have $\hat{f}(x \underset{>}{\overset{<}{\to}} -\lambda_{0,n}) \to \pm\infty$ and $\hat{f}(x)$ decreasing on the interval $]-\lambda_{0,n+1}, -\lambda_{0,n}[$. So $\lambda_* \in]\lambda_{0,1}, \lambda_{0,2}[$. Unlike in Cartesian geometry, we do not have explicit expressions for $\{\lambda_{0,n}\}$ and $\{e_{0,n}\}$ (we evaluate these as detailed earlier in this part). In practice, it is costly to compute them for $n = 1, \ldots, N$ when $N \gtrsim 5$. Let us denote by λ_{*N} the value such that $f_N(-\lambda_{*N}) = 0$ (up to numerical precision), where $f_N(x)$ is the N^{th} partial sum of $\hat{f}(x)$. We notice that for $N = 3, \ldots, 6$ the sequence $\{\lambda_{*N}\}$ is monotonically decreasing with N. Also, the sequence of absolute or relative increases ($\{\lambda_{*N} - \lambda_{*N-1}\}$ or $\{(\lambda_{*N} - \lambda_{*N-1})/\lambda_{*N}\}$) decreases (in absolute value) with N, in such a way that it is well fitted and bounded by C/N^2, C being a constant. Because the range of N is so small, such a fit is not that reliable. But we find the same behavior for the zeroes of the partial sums of $f^{\text{cart}}(x)$, where N can be taken

very large. Since the integrand of f has the same order (in n) as that of f^{cart}, we consider this a countercheck for our C/N^2 fit. Since

$$\sum_{N=k+1}^{+\infty} \frac{1}{N^2} = \frac{1}{k} - \frac{1}{2k^2} + o(\frac{1}{k^3}),$$

we conclude that $\lambda^* \approx \lambda_6^* - C\left(\frac{1}{6} - \frac{1}{72}\right)$, when C is the fitting coefficient for $|\lambda_{*N} - \lambda_{*N-1}| = C/N^2$, determined with precision c. We determined $C \pm c$ by ourself, since fitting tools from software are not of great help when dealing with only four points. At the end of the day,

$$\lambda^* = \lambda_6^* - C\left(\frac{1}{6} - \frac{1}{72}\right) \pm \left(\frac{C+c}{216} + c(\frac{1}{6} - \frac{1}{72})\right).$$

For $r_i = 0.25$, we estimate that $C = 9.5 \pm 0.5$ (see Figure C.2), leading to $\lambda_*(r_i = 0.25) = 19.4 \pm 0.1$; since $\lambda_{1,1}(r_i = 0.25) = 19.780306$, $\min\{\lambda_{1,1}, \lambda_*\} = \lambda_*$.

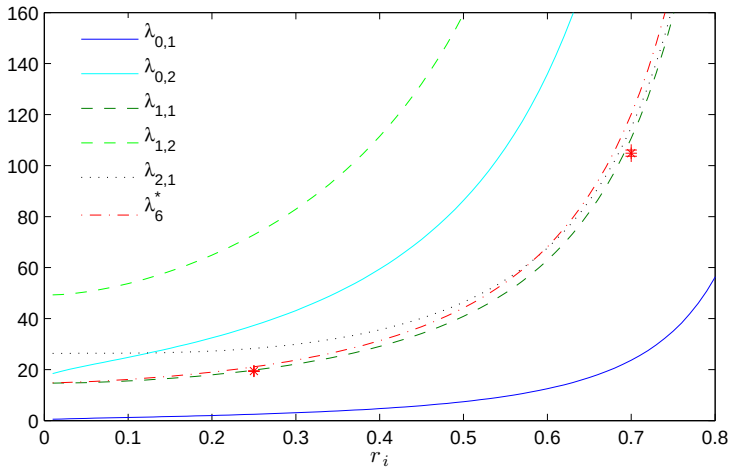

Figure C.1: First (lowest) eigenvalues and λ_{*6}, for $r_i \in]0, 0.8]$. We can see that $\lambda_{*6} > \lambda_{1,1}$ on the entire range of equivalent aspect ratios. But the estimated λ_* (red star) falls below $\lambda_{1,1}$ for $r_i = 0.25$ and $r_i = 0.7$; the vertical red crosses are the uncertainty bounds on this estimated quantity.

We estimated $\lambda_*(r_i = 0.7)$ in the same fashion (see Figure C.2), and also found that it was less than $\lambda_{1,1}(r_i = 0.7)$. We believe that $\lambda_* < \lambda_{1,1}$ on the entire range of equivalent aspect ratios. In this respect, the annular domain is not analogous to the rectangular domain: **no matter how thin it is, the annulus is never "elongated" so as to allow for a dipole structure**. The canonical problem has a unique solution if $\beta > -\lambda_*$.

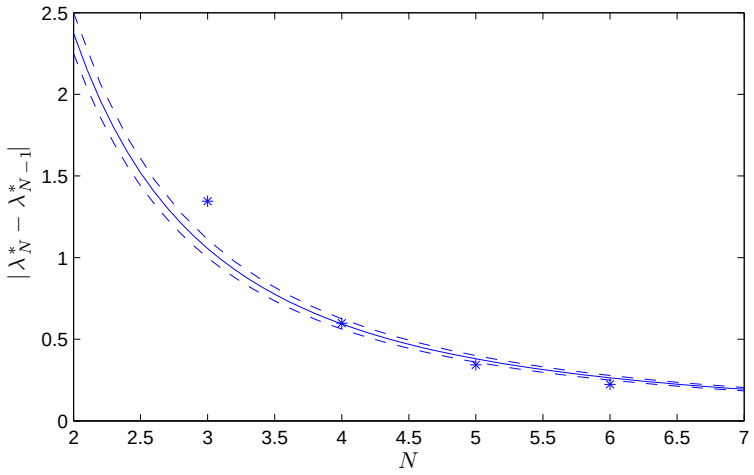

Figure C.2: Absolute increase of the zero of partial sums $\{f_N(x)\}$ as a function of N, for only a few (accessible) values of N. We fitted these points privileging the last three. The solid line is $9.5/N^2$; the dashed line above (resp. below) it is $10/N^2$ (resp. $9/N^2$).

C.2 Numerical computation of the equilibria

We want to solve numerically

$$F(\psi') = 0 = \Delta\psi' + h - f\left(\psi' + \frac{y}{L_x}\left[\Gamma_e - \int_{\mathcal{D}_e^+} \frac{\partial\psi'}{\partial n}\right]\right) \tag{C.1}$$

in ψ' with Dirichlet boundary conditions. All we need to do is discretize the expressions for F, for its derivatives with respect to ψ' and with respect to the continuation parameters (the Jacobian consisting of these derivatives). We have

$$\begin{cases} y = i \times \delta y \quad \text{with } i = 1, \dots, N\,,\ \delta y = L_y/(N+1)\,, \\ x = j \times \delta x \quad \text{with } j = 1, \dots, M\,,\ \delta x = L_x/(M+1)\,, \end{cases}$$

$(i = 0)$ is the inner boundary, $(i = N+1)$ is the outer boundary and for all i, periodicity in x gives $\psi'(i, M) = \psi'(i, 0)$ and $\psi'(i, M+1) = \psi'(i, 1)$. From the boundary conditions, we have for all j : $\psi'(0, j) = \psi'(N+1, 0) = 0$. For instance, the term

$$\frac{y}{L_x}\int_{\mathcal{D}_e^+} \frac{\partial\psi'}{\partial n} \;\mapsto\; \frac{-i}{M+1}\sum_{j=0}^{M} \psi'(N, j)\,.$$

We consider the nonlinear form $f(\psi) = -\tanh(\sigma\psi + \gamma)$, where σ and γ

are continuation parameters, so that

$$F(\psi') = \Delta\psi' + h + \tanh\left(\sigma\psi' + \gamma + \frac{\sigma y}{L_x}\Gamma_e - \frac{\sigma y}{L_x}\int_{\mathcal{D}_e^+}\frac{\partial\psi'}{\partial n}\right).$$

The discretized equivalent of the above reads

$$F(i,j) := F(\psi'(i,j)) = \frac{\psi'(i,j+1)+\psi'(i,j-1)-2\psi'(i,j)}{\delta x^2} + \tag{C.2}$$

$$+\frac{\psi'(i+1,j)+\psi'(i-1,j)-2\psi'(i,j)}{\delta y^2} + h(i,j) + \tag{C.3}$$

$$+\tanh\left(\sigma\psi'(i,j)+\gamma+\sigma\Gamma_e\frac{i}{L_x}\delta y + \sigma\frac{i}{M+1}\sum_{k=1}^{M}\psi'(N,k)\right). \tag{C.4}$$

The expression for the $NM \times NM$ Jacobian matrix is given below:

$$J = \left\{\frac{\partial F(i,j)}{\partial\psi'(l,k)}\right\}_{(i,j),(l,k)\in[\![1,N]\!]\times[\![1,M]\!]} =$$

$$\begin{bmatrix}
d_1 & \frac{1}{\delta x^2} & 0 & \dots & 0 & \frac{1}{\delta y^2} & 0 & \dots & 0 & b_1 & \dots & \dots \\
\frac{1}{\delta x^2} & d_2 & \frac{1}{\delta x^2} & 0 & \dots & 0 & \frac{1}{\delta y^2} & 0 & \vdots & b_2 & \dots & \dots \\
0 & \frac{1}{\delta x^2} & \ddots & \ddots & \ddots & \ddots & \ddots & \ddots & 0 & \vdots & \dots & \dots \\
\frac{1}{\delta y^2} & \ddots & & \frac{1}{\delta x^2} & d_{M+1} & \frac{1}{\delta x^2} & \ddots & \frac{1}{\delta y^2} & \vdots & b_{M+1} & \dots & \dots \\
 & & \ddots & & & & & & \frac{1}{\delta y^2} & b_{(N-2)M} & \dots & \dots \\
 & & \ddots & \frac{1}{\delta x^2} & d_{(N-2)M+1} & \frac{1}{\delta x^2} & 0 & \dots & 0 & b_{(N-2)M+1}+\frac{1}{\delta y^2} & b_{(N-2)M+1} & \dots \\
\vdots & & & & \ddots & \ddots & & & \vdots & b_{(N-2)M+2} & b_{(N-2)M+2}+\frac{1}{\delta y^2} & \dots \\
 & & & & & \ddots & \ddots & & \frac{1}{\delta x^2} & \vdots & \dots & \ddots \\
 & & & \frac{1}{\delta y^2} & & & & \frac{1}{\delta x^2} & d_{(N-1)M} & b_{(N-1)M}+\frac{1}{\delta x^2} & \dots & \dots \\
 & & & \ddots & & & & & \frac{1}{\delta x^2} & b_{(N-1)M+1}+d_{(N-1)M+1} & b_{(N-1)M+1}+\frac{1}{\delta x^2} & \dots \\
 & & & & & & \ddots & & \vdots & & & \\
 & & & & & & & \frac{1}{\delta y^2} & 0 & b_{NM-1} & \dots & b_{NM-1}+d_{NM-1} \\
 & & & & & & & & \frac{1}{\delta y^2} & b_{NM} & \dots & b_{NM}+\frac{1}{\delta x^2}
\end{bmatrix}$$

where

$$d_{p(i,j)} = -2\left(\frac{1}{\delta x^2} + \frac{1}{\delta y^2}\right) + \quad \text{(C.5)}$$

$$+\sigma\left[1 - \tanh^2\left(\sigma\psi'(i,j) + \gamma + \sigma\Gamma_e\frac{i}{L_x}\delta y + \sigma\frac{i}{M+1}\sum_{k=1}^{M}\psi'(N,k)\right)\right], \quad \text{(C.6)}$$

the global index p running over $[\![1, N]\!] \times [\![1, M]\!]$. The $NM \times M$ submatrix $B = \{b_p\}_{p\in[\![1,NM]\!]}$ is a line matrix (it consists of M identical columns):

$$b_{p(i,j)} = \sigma\frac{i}{M+1}\left[1 - \tanh^2\left(\sigma\psi'(i,j) + \gamma + \sigma\Gamma_e\frac{i}{L_x}\delta y + \sigma\frac{i}{M+1}\sum_{k=1}^{M}\psi'(N,k)\right)\right]$$

It can be seen that there are $4M - 1$ coefficients of J which are a sum of a $B-$term and a (sub)diagonal term. A d_p is referred to as a diagonal term, while δx^{-2} and δy^{-2} are referred to as subdiagonal terms (the δx^{-2} (resp. δy^{-2}) terms align on the two subdiagonals located 1 (resp. M) rank(s) from the diagonal).

Bibliography

[Ahlers, 2006] Ahlers, G. (2006). Experiments with Rayleigh-Bénard convection. In Mutabazi, I., Wesfreid, J. E., and Guyon, E., editors, *Dynamics of Spatio-Temporal Cellular Structures, Henri Bénard Centenary Review*, volume 207, chapter 4, pages 67–94. Springer, New York. (Cited on page 2.)

[Arnol'd, 1966] Arnol'd, V. I. (1966). On an A Priori Estimate in the Theory of Hydrodynamical Stability. *Izv. Vyssh. Uchebn. Zaved. Matematika*, 54(5):3–5. (Cited on page 24.)

[Berhanu et al., 2009] Berhanu, M., Gallet, B., Monchaux, R., Bourgoin, M., Odier, P., Pinton, J.-F., Plihon, N., Volk, R., Fauve, S., Mordant, N., Pétrélis, F., Aumaître, S., Chiffaudel, A., Daviaud, F., Dubrulle, B., and Ravelet, F. (2009). Bistability between a stationary and an oscillatory dynamo in a turbulent flow of liquid sodium. *Journal of Fluid Mechanics*, 641:217–+. (Cited on page 3.)

[Berhanu et al., 2007] Berhanu, M., Monchaux, R., Fauve, S., Mordant, N., Pétrélis, F., Chiffaudel, A., Daviaud, F., Dubrulle, B., Marié, L., Ravelet, F., Bourgoin, M., Odier, P., Pinton, J.-F., and Volk, R. (2007). Magnetic field reversals in an experimental turbulent dynamo. *Europhysics Letters*, 775:59001–+. (Cited on pages iv, 1, 2, and 3.)

[Bouchet, 2008] Bouchet, F. (2008). Simpler variational problems for statistical equilibria of the 2D Euler equation and other systems with long range interactions. *Physica D Nonlinear Phenomena*, 237:1976–1981. (Cited on pages 16, 23, 24, and 84.)

[Bouchet and Barré, 2005] Bouchet, F. and Barré, J. (2005). Classification of Phase Transitions and Ensemble Inequivalence, in Systems with Long Range Interactions. *Journal of Statistical Physics*, 118:1073–1105. (Cited on pages vi, 18, 27, 29, 30, 31, 32, 41, 62, 69, and 79.)

[Bouchet and Corvellec, 2010] Bouchet, F. and Corvellec, M. (2010). Invariant measures of the 2D Euler and Vlasov equations. *Journal of Statistical Mechanics: Theory and Experiment*, 8:21–+. (Cited on pages vi, 18, 62, and 80.)

[Bouchet and Simonnet, 2009] Bouchet, F. and Simonnet, E. (2009). Random Changes of Flow Topology in Two-Dimensional and Geophysical Turbulence. *Physical Review Letters*, 102(9):094504–+. (Cited on pages 11, 23, 27, and 79.)

[Campa et al., 2009] Campa, A., Dauxois, T., and Ruffo, S. (2009). Statistical mechanics and dynamics of solvable models with long-range interactions. Phys. Rep., 480(3-6):57–159. (Cited on pages 62, 69, 79, and 81.)

[Chandra and Verma, 2011] Chandra, M. and Verma, M. K. (2011). Dynamics and symmetries of flow reversals in turbulent convection. Phys. Rev. E, 83(6):067303–+. (Cited on pages iv and 1.)

[Charney and Flierl, 1981] Charney, J. G. and Flierl, G. R. (1981). Oceanic analogues of large-scale atmospheric motions. In Wunsch, C. and Warren, B. A., editors, *Evolution of Physical Oceanography*, chapter 18, pages 539–43. The MIT Press, Cambridge, Massachusetts. (Cited on page 7.)

[Chavanis, 2009] Chavanis, P. H. (2009). Dynamical and thermodynamical stability of two-dimensional flows: variational principles and relaxation equations. *European Physical Journal B*, 70:73–105. (Cited on page 16.)

[Chavanis and Sommeria, 1996] Chavanis, P. H. and Sommeria, J. (1996). Classification of self-organized vortices in two-dimensional turbulence: the case of a bounded domain. *J. Fluid Mech.*, 314:267–297. (Cited on pages v, 16, 18, 22, 39, and 79.)

[Chillá et al., 2004] Chillá, F., Rastello, M., Chaumat, S., and Castaing, B. (2004). Long relaxation times and tilt sensitivity in Rayleigh Bénard turbulence. *European Physical Journal B*, 40:223–+. (Cited on page 2.)

[Chow and Hale, 1982] Chow, S. N. and Hale, J. K. (1982). *Methods of bifurcation theory*. Grundlehren der mathematischen Wissenschaften. Springer-Verlag. (Cited on page 47.)

[Cortet et al., 2010] Cortet, P.-P., Chiffaudel, A., Daviaud, F., and Dubrulle, B. (2010). Experimental Evidence of a Phase Transition in a Closed Turbulent Flow. *Physical Review Letters*, 105(21):214501–+. (Cited on page 3.)

[Corvellec and Bouchet, 2011a] Corvellec, M. and Bouchet, F. (2011a). A complete theory of low-energy phase diagrams for two-dimensional turbulence steady states and equilibria. *preprint*. (Cited on pages vi and 18.)

[Corvellec and Bouchet, 2011b] Corvellec, M. and Bouchet, F. (2011b). Continuous and discontinuous transitions in geophysical turbulence. In *Advances in Turbulence XIII*, Journal of Physics: Conference Series. Euromech. (Cited on pages vi and 18.)

[Courant and Hilbert, 1953] Courant, R. and Hilbert, D. (1953). *Methods of Mathematical Physics*, volume 1. Wiley-Interscience, New York. (Cited on pages 54 and 82.)

[Diu et al., 1989] Diu, R., Guthmann, C., Lederer, D., and Roulet, B. (1989). *Éléments de physique statistique*. Hermann, éditeurs des sciences et des arts. (Cited on page 69.)

[Ellis et al., 2000] Ellis, R. S., Haven, K., and Turkington, B. (2000). Large Deviation Principles and Complete Equivalence and Nonequivalence Results for Pure and Mixed Ensembles. *J. Stat. Phys.*, 101:999. (Cited on pages 69, 75, and 79.)

[Ellis et al., 2002] Ellis, R. S., Haven, K., and Turkington, B. (2002). Nonequivalent statistical equilibrium ensembles and refined stability theorems for most probable flows. *Nonlinearity*, 15:239–255. (Cited on pages 23 and 79.)

[Gallet et al., 2011] Gallet, B., Herault, J., Laroche, C., Pétrélis, F., and Fauve, S. (2011). Reversals of a large scale field generated over a turbulent background. *ArXiv e-prints*. (Cited on pages iv, 1, and 10.)

[Graef and Müller, 1996] Graef, F. and Müller, P. (1996). Uniqueness of solutions and conservation laws for the quasigeostrophic model. *Dynamics of Atmospheres and Oceans*, 25:109–132. (Cited on page 53.)

[Kimoto and Ghil, 1993] Kimoto, M. and Ghil, M. (1993). Multiple Flow Regimes in the Northern Hemisphere Winter. Part I: Methodology and Hemispheric Regimes. *Journal of Atmospheric Sciences*, 50:2625–2644. (Cited on pages iv and 2.)

[Kraichnan, 1967] Kraichnan, R. H. (1967). Inertial Ranges in Two-Dimensional Turbulence. *Physics of Fluids*, 10:1417–1423. (Cited on page 22.)

[Kraichnan and Montgomery, 1980] Kraichnan, R. H. and Montgomery, D. (1980). Two-dimensional turbulence. *Reports on Progress in Physics*, 43:547–619. (Cited on pages 12, 70, and 74.)

[Kuksin, 2004] Kuksin, S. B. (2004). The Eulerian Limit for 2D Statistical Hydrodynamics. *Journal of Statistical Physics*, 115:469–492. (Cited on page 80.)

[Kuznetsov, 2004] Kuznetsov, Y. A. (2004). Numerical Analysis of Bifurcations. In *Elements of Applied Bifurcation Theory*, number 112 in Applied Mathematical Sciences, chapter 10, pages 505–+. Springer-Verlag, New York, Third edition. (Cited on page 91.)

[Langer, 1967] Langer, J. S. (1967). Theory of the condensation point. *Annals of Physics*, 41:108–157. (Cited on page 81.)

[Leprovost et al., 2006] Leprovost, N., Dubrulle, B., and Chavanis, P.-H. (2006). Dynamics and thermodynamics of axisymmetric flows: Theory. Phys. Rev. E, 73(4):046308–+. (Cited on page 4.)

[Loxley, 2008] Loxley, P. N. (2008). Rate of magnetization reversal due to nucleation of soliton-antisoliton pairs at point-like defects. Phys. Rev. B, 77(14):144424–+. (Cited on page 81.)

[Majda and Wang, 2006] Majda, A. J. and Wang, X. (2006). *Nonlinear Dynamics and Statistical Theories for Basic Geophysical Flows*. Cambridge University Press. (Cited on pages 15 and 16.)

[McWilliams, 1977] McWilliams, J. (1977). A note on a consistent quasi-geostrophic model in a multiply connected domain. *Dynamics of Atmospheres and Oceans*, 1:427–441. (Cited on page 51.)

[Michel and Robert, 1994] Michel, J. and Robert, R. (1994). Statistical Mechanical Theory of the Great Red Spot of Jupiter. *Journal of Statistical Physics*, 77:645–666. 10.1007/BF02179454. (Cited on page 26.)

[Miller, 1990] Miller, J. (1990). Statistical mechanics of Euler equations in two dimensions. *Phys. Rev. Lett.*, 65(17):2137–2140. (Cited on pages 12 and 71.)

[Monchaux et al., 2006] Monchaux, R., Ravelet, F., Dubrulle, B., Chiffaudel, A., and Daviaud, F. (2006). Properties of Steady States in Turbulent Axisymmetric Flows. *Physical Review Letters*, 96(12):124502–+. (Cited on page 4.)

[Mujica and Lathrop, 2005] Mujica, N. and Lathrop, D. P. (2005). Bistability and hysteresis in a highly turbulent swirling flow. *Physica A Statistical Mechanics and its Applications*, 356:162–166. (Cited on page 2.)

[Naso et al., 2010] Naso, A., Chavanis, P. H., and Dubrulle, B. (2010). Statistical mechanics of two-dimensional Euler flows and minimum enstrophy states. *European Physical Journal B*, 77:187–212. (Cited on pages 22 and 79.)

[Niemela et al., 2001] Niemela, J. J., Skrbek, L., Sreenivasan, K. R., and Donnelly, R. J. (2001). The wind in confined thermal convection. *Journal of Fluid Mechanics*, 449:169–178. (Cited on pages iv and 1.)

[Onsager, 1949] Onsager, L. (1949). Statistical hydrodynamics. *Nuovo Cimento*, 6 (No. 2 (Suppl.)):249–286. (Cited on pages 12, 63, and 70.)

[Pedlosky, 1987] Pedlosky, J. (1987). *Geophysical Fluid Dynamics*. Springer-Verlag, New York, Second edition. (Cited on pages 21, 54, 87, 89, and 90.)

[Qiu and Miao, 2000] Qiu, B. and Miao, W. (2000). Kuroshio Path Variations South of Japan: Bimodality as a Self-Sustained Internal Oscillation. *Journal of Physical Oceanography*, 30:2124–2137. (Cited on pages 7 and 8.)

[Ravelet et al., 2008] Ravelet, F., Chiffaudel, A., and Daviaud, F. (2008). Supercritical transition to turbulence in an inertially driven von Kármán closed flow. *Journal of Fluid Mechanics*, 601:339–364. (Cited on pages iv and 2.)

[Ravelet et al., 2004] Ravelet, F., Marié, L., Chiffaudel, A., and Daviaud, F. (2004). Multistability and Memory Effect in a Highly Turbulent Flow: Experimental Evidence for a Global Bifurcation. *Physical Review Letters*, 93(16):164501–+. (Cited on pages iv, 2, 3, and 4.)

[Robert, 1990] Robert, R. (1990). Etats d'équilibre statistique pour l'écoulement bidimensionnel d'un fluide parfait. *C. R. Acad. Sci.*, 311(9):575–578. (Cited on page 12.)

[Robert, 1991] Robert, R. (1991). A maximum-entropy principle for two-dimensional perfect fluid dynamics. *J. Stat. Phys.*, 65:531–553. (Cited on page 12.)

[Robert and Sommeria, 1991] Robert, R. and Sommeria, J. (1991). Statistical equilibrium states for two-dimensional flows. *J. Fluid Mech.*, 229:291–310. (Cited on pages 12, 13, 16, 71, and 73.)

[Rose and Marshall, 2009] Rose, B. E. J. and Marshall, J. (2009). Ocean Heat Transport, Sea Ice, and Multiple Climate States: Insights from Energy Balance Models. *Journal of Atmospheric Sciences*, 66:2828–+. (Cited on page 8.)

[Schmeits and Dijkstra, 2001] Schmeits, M. J. and Dijkstra, H. A. (2001). Bimodal Behavior of the Kuroshio and the Gulf Stream. *Journal of Physical Oceanography*, 31:3435–3456. (Cited on page 7.)

[Schulman, 1981] Schulman, L. S. (1981). *Techniques and Applications of Path Integration*. John Wiley & Sons. (Cited on pages 81, 82, and 83.)

[Shepherd, 1990] Shepherd, T. G. (1990). Symmetries, conservation laws, and Hamiltonian structure in geophysical fluid dynamics. *Advances in Geophysics*, 32:287–339. (Cited on page 65.)

[Sommeria, 1986] Sommeria, J. (1986). Experimental study of the two-dimensional inverse energy cascade in a square box. *Journal of Fluid Mechanics*, 170:139–168. (Cited on pages iv and 1.)

[Tian et al., 2001] Tian, Y., Weeks, E. R., Ide, K., Urbach, J. S., Baroud, C. N., Ghil, M., and Swinney, H. L. (2001). Experimental and numerical studies of an eastward jet over topography. *J. Fluid Mech.*, 438:129–157. (Cited on pages iv, 2, 4, and 51.)

[Touchette, 2009] Touchette, H. (2009). The large deviation approach to statistical mechanics. Phys. Rep., 478(1-3):1–69. (Cited on page 76.)

[Venaille and Bouchet, 2009] Venaille, A. and Bouchet, F. (2009). Statistical Ensemble Inequivalence and Bicritical Points for Two-Dimensional Flows and Geophysical Flows. *Physical Review Letters*, 102(10):104501–+. (Cited on pages v, vi, 11, 17, 18, 22, 38, 39, 52, 56, 58, 59, and 79.)

[Venaille and Bouchet, 2011] Venaille, A. and Bouchet, F. (2011). Solvable Phase Diagrams and Ensemble Inequivalence for Two-Dimensional and Geophysical Turbulent Flows. *Journal of Statistical Physics*, 143:346–380. (Cited on page 79.)

[Weeks et al., 1997] Weeks, E. R., Tian, Y., Urbach, J. S., Ide, K., Swinney, H. L., and Ghil, M. (1997). Transitions between blocked and zonal flows in a rotating annulus with topography. *Science*, 278(November):1598–1601. (Cited on page 4.)